March 6, 1961 (NASA TMX ---; MTP-AERO-61-16)

N63-86268 *
Code 5

THE EFFECT OF PROPELLANT SLOSHING ON THE STABILITY OF AN ACCELEROMETER CONTROLLED RIGID SPACE VEHICLE

By

Helmut F. Bauer 6 mar. 1961 reger

CA - next p.

Flutter and Vibration Section
DYNAMICS ANALYSIS BRANCH
AEROBALLISTICS DIVISION

Arranged and Processed
by
TECHNICAL PUBLICATIONS SECTION
SPACE SYSTEMS INFORMATION BRANCH

RKT/747

NASA - GEORGE C. MARSHALL SPACE FLIGHT CENTER

MTP-AERO-61-16

THE EFFECT OF PROPELLANT SLOSHING ON THE STABILITY OF AN ACCELEROMETER CONTROLLED RIGID SPACE VEHICLE

By Helmut F. Bauer

ABSTRACT

The danger of unstable modes for spacecraft resulting from propellant sloshing is well known. Additional artificial stabilization through the control system can enhance the stability behavior of the vehicle if the gain values and sensor characteristics are properly chosen. Very useful results can be obtained from a simplified stability investigation of an accelerometer controlled rigid space vehicle with respect to propellant sloshing. In this parametric study the liquid was simulated by an equivalent mechanical model, consisting either of mass-spring-damper-systems or pendulum-damper-systems for each sloshing mode and a nonsloshing mass with a moment of inertia. For simplification, only the propellant sloshing in one tank was considered. The influence of various parameters, such as ratio of sloshing propellant mass to total vehicle mass, natural slosh frequency, control frequency, control damping, gain factors of the attitude control system, accelerometer gain, its natural frequency, damping and location were investigated. The effect of elastic deformations, aerodynamic forces and the inertia of the swivel engines was not considered. Half of the thrust was available for control purposes. Only the dominant first sloshing mode was considered, since higher mode mass ratios are considerably smaller than for the first sloshing mode, (except in four quarter tanks, where the mass of one other sloshing mode is of considerable amount compared with that of the first sloshing mode).

The stability boundary was determined in terms of the amount of damping of the propellant in the tank required for various tank locations (slosh mass location).

The potential hazard in control due to propellant sloshing in space vehicles can be eliminated by proper choice of tank form (slosh mass ratio decrease and slosh frequency increase), proper selection of characteristics, location and gain value of the accelerometer, and as a last resort by baffles in the propellant tanks.

March 6, 1961 MTP-AERO-61-16

THE EFFECT OF PROPELLANT SLOSHING ON THE STABILITY OF AN ACCELEROMETER CONTROLLED RIGID SPACE VEHICLE

By

Helmut F. Bauer

Flutter and Vibration Section
DYNAMICS ANALYSIS BRANCH
AEROBALLISTICS DIVISION

Arranged and Processed
by
TECHNICAL PUBLICATIONS SECTION
SPACE SYSTEMS INFORMATION BRANCH

TABLE OF CONTENTS

	Page
SUMMARY	1
I. INTRODUCTION	1
II. EQUATIONS OF MOTION AND CONTROL EQUATIONS	3
III. STABILITY POLYNOMIAL	7
1. Stability Analysis of Accelerometer Controlled Craft Including the Effect of Sloshing and Employing a Real Accelerometer	7
2. Stability Analysis of an Accelerometer Controlled Vehicle Including the Effect of Sloshing and Employing an Ideal Accelerometer	13
3. Stability Analysis with Real Accelerometer Control (Sloshing Not Included)	16
4. Stability Analysis with Ideal Accelerometer Control (Sloshing Not Included)	18
IV. APPLICATION	20
V. CONCLUSION	30
VI. APPENDIX: Mechanical Model	37
REFERENCES	38
FIGURES	39-85

LIST OF ILLUSTRATIONS

Figure		Page
1.	Mechanical Model for Propellant Sloshing	39
2.	Natural Frequency f_n for Liquid in a Circular Cylindrical Tank	40
2a.	Natural Frequency f_n for Liquid in a Cylindrical Tank with Annular Cross Section	41
3.	Natural Frequency f_n for a Liquid in a Cylindrical Quarter Tank	42
4.	Sloshing Mass $\frac{m_n}{\zeta a^3}$ for Liquid in a Circular Cylindrical Tank	43
5.	Sloshing Mass $\frac{m_n}{\zeta a^3}$ for Liquid in a Circular Cylindrical Tank with Annular Cross Section (k=0.5)	44
6.	Sloshing Mass $\frac{m_n}{\zeta a^3}$ for Four Quarter Tanks	45
7a.	Stability Boundary for Rigid Accelerometer Controlled Space Vehicle (Sloshing Suppressed) Varying Accelerometer Frequency	46
7b.	Stability Boundary for Rigid Accelerometer Controlled Space Vehicle (Sloshing Suppressed) Varying Accelerometer Damping for ω_a = 55 rad/sec	47
7c.	Stability Boundary for Rigid Accelerometer Controlled Space Vehicle (Sloshing Suppressed) Varying Accelerometer Damping for ω_a = 12 rad/sec	48
7d.	Stability Boundary for Rigid Accelerometer Controlled Space Vehicle (Sloshing Suppressed) Varying Control Frequency for ω_a = 55 rad/sec	49
7e.	Stability Boundary for Rigid Accelerometer Controlled Space Vehicle (Sloshing Suppressed) Varying Control Frequency for ω_a = 12 rad/sec	50
7f.	Stability Boundary for Rigid Accelerometer Controlled Space Vehicle (Sloshing Suppressed) Varying Control Damping for ω_a = 55 rad/sec	51
7g.	Stability Boundary for Rigid Accelerometer Controlled Space Vehicle (Sloshing Suppressed) Varying Control Damping for ω_a = 12 rad/sec	52

LIST OF ILLUSTRATIONS (Cont)

Figure		Page
8a.	Stability Boundary for Rigid Spacecraft. Varying Slosh Mass Ratio	53
8b.	Stability Boundary for Rigid Spacecraft. Varying Control Frequency	54
8c.	Stability Boundary for Rigid Spacecraft. Varying Control Damping	55
8d.	Stability Boundary for Rigid Spacecraft. Varying Slosh Frequency	56
8e.	Stability Boundary for Rigid Spacecraft. Varying Attitude Gain Value a_o	57
9a.	Stability Boundary for Rigid Spacecraft with Ideal Accelerometer Control. Varying Slosh Mass Ratio	58
9b.	Stability Boundary for Rigid Spacecraft with Ideal Accelerometer Control. Varying Control Frequency	59
9c.	Stability Boundary for Rigid Spacecraft with Ideal Accelerometer Control. Varying Control Damping	60
9d.	Stability Boundary for Rigid Spacecraft with Ideal Accelerometer Control. Varying Slosh Frequency	61
9e.	Stability Boundary for Rigid Spacecraft with Ideal Accelerometer Control. Varying Attitude Gain Value a_o	62
9f.	Stability Boundary for Rigid Spacecraft with Ideal Accelerometer Control. Varying Accelerometer Gain	63
9g.	Stability Boundary for Rigid Spacecraft with Ideal Accelerometer Control. Varying Accelerometer Location	64
9h.	Stability Boundary for Rigid Spacecraft with Ideal Accelerometer Control. Varying Accelerometer Location	65
10a.	Stability Boundary for Rigid Spacecraft with a Real Accelerometer Control. Varying Sloshing Mass Ratio with Accelerometer Frequency of 55 rad/sec and Gain Value $\lambda = 1.0$	66
10b.	Stability Boundary for Rigid Spacecraft with a Real Accelerometer Control. Varying Sloshing Mass Ratio with Accelerometer Frequency of 55 rad/sec and Gain Value $\lambda = 1.5$	67

LIST OF ILLUSTRATIONS (Cont)

Figure		Page
10c.	Stability Boundary for Rigid Spacecraft with a Real Accelerometer Control. Varying Sloshing Mass Ratio with Accelerometer Frequency of 12 rad/sec and Gain Value $\lambda = 1.0$	68
10d.	Stability Boundary for Rigid Spacecraft with a Real Accelerometer Control. Varing Control Frequency with Accelerometer Frequency of 55 rad/sec and Gain Value $\lambda = 1.0$	69
10e.	Stability Boundary for Rigid Spacecraft with a Real Accelerometer Control. Varying Control Frequency with Accelerometer Frequency of 12.0 rad/sec and Gain Value $\lambda = 1.0$	
10f.	Stability Boundary for Rigid Spacecraft with a Real Accelerometer Control. Varying Control Damping with Accelerometer Frequency of 55 rad /sec and Gain Value $\lambda = 1$	70
10g.	Stability Boundary for Rigid Spacecraft with a Real Accelerometer Control. Varying Control Damping with Accelerometer Frequency of 12 rad/sec and Gain Value $\lambda = 1$	71
10h.	Stability Boundary for Rigid Spacecraft with Real Accelerometer Control. Varying Slosh Frequency with Accelerometer Frequency of 55 rad/sec and Gain Value $\lambda = 1$	72
10i.	Stability Boundary for Rigid Spacecraft with Real Accelerometer Control. Varying Slosh Frequency with Accelerometer Frequency of 12 rad/sec and Gain Value $\lambda = 1$	73
10j.	Stability Boundary for Rigid Spacecraft with Real Accelerometer Control. Varying Attitude Gain Value with Accelerometer Frequency of 55 rad/sec and Gain Value $\lambda = 1$	74
10k.	Stability Boundary for Rigid Spacecraft with Real Accelerometer Control. Varying Attitude Gain Value with Accelerometer Frequency of 12 rad/sec and Gain Value $\lambda = 1$	75

LIST OF ILLUSTRATIONS (Cont)

Figure		Page
10l.	Stability Boundary for Rigid Spacecraft with Real Accelerometer Control. Varying Accelerometer Gain with Accelerometer Frequency of 55 rad/sec.	77
10m.	Stability Boundary for Rigid Spacecraft with Real Accelerometer Control. Varying Accelerometer Gain with Accelerometer Frequency of 12 rad/sec	78
10n.	Stability Boundary for Rigid Spacecraft with Real Accelerometer Control. Varying Accelerometer Frequency .	79
10o.	Stability Boundary for Rigid Spacecraft with Real Accelerometer Control. Varying Control Damping with Accelerometer Frequency of 55 rad/sec and Gain Value $\lambda = 1$	80
10p.	Stability Boundary for Rigid Spacecraft with Real Accelerometer Control. Varying Control Damping with Accelerometer Frequency of 12 rad/sec and Gain Value $\lambda = 1$	81
10q.	Stability Boundary for Rigid Spacecraft with Real Accelerometer Control. Varying Control Damping with Accelerometer Frequency of 12 rad/sec and Gain Value $\lambda = 1$	82
10r.	Stability Boundary for Rigid Spacecraft with Real Accelerometer Control. Varying Tank Radius with Accelerometer Frequency of 55 rad/sec	83
10s.	Stability Boundary for Rigid Spacecraft with Real Accelerometer Control. Varying Tank Radius with Accelerometer Frequency of 12 rad/sec	84
10t.	Stability Boundary for Rigid Spacecraft with Real Accelerometer Control. Varying Acceleration Location with Accelerometer Frequency of 12 rad/sec	85

DEFINITION OF SYMBOLS

m	mass of space vehicle
m_s	sloshing mass
y	lateral translation of rigid vehicle
ξ_s	displacement of sloshing mass relative to the centerline of the tank
F	thrust
φ	angle of rotation of rigid vehicle relative to inertial space
β	gimbal angle of engines against centerline of the vehicle
x_E	coordinate of gimbal point (measured positive from center of gravity towards tail of the vehicle)
g	longitudinal acceleration of the vehicle
x_s	slosh mass location
I_{eff}	moment of inertia of the vehicle about the center of gravity
γ_s	slosh damping (twice the amount of critical damping)
k^2	square of the radius of gyration
k_s	spring constant of slosh model
ω_s	natural circular sloshing frequency
a	tank radius
h	liquid height
a_0, a_1	gain values of attitude control system
g_2	gain value of accelerometer control system
A_i	indicated acceleration perpendicular to spacecraft axis

DEFINITION OF SYMBOLS (Continued)

ω_a	accelerometer frequency (radians/sec)
ζ_a	accelerometer damping (amount of critical damping of accelerometer)
x_a	accelerometer location
μ	ratio of sloshing mass to total vehicle mass
$\lambda = gg_2$	gain parameter of accelerometer
ω_c	control frequency (radians/sec)
ζ_c	control damping
x_{CR}	location of center of instantaneous rotation

GEORGE C. MARSHALL SPACE FLIGHT CENTER

MTP-AERO-61-16

THE EFFECT OF PROPELLANT SLOSHING ON THE STABILITY OF AN ACCELEROMETER CONTROLLED RIGID SPACE VEHICLE

By Helmut F. Bauer

SUMMARY

Due to the danger of unstable modes for spacecraft resulting from propellant sloshing, and since additional artificial stabilization through the control system can enhance the stability behavior of the vehicle, a simplified stability investigation was made of an accelerometer controlled rigid space vehicle with respect to propellant sloshing.

In this parametric study, the liquid was simulated by an equivalent mechanical model consisting of mass-spring-damper-systems, or by pendulum-damper-systems for each sloshing mode and a nonsloshing mass with a moment of inertia. Only the propellant sloshing in one tank was considered, and the influence of various parameters was investigated. Half of the thrust was available for control purposes. Only the dominant first sloshing mode was considered.

The stability boundary was determined in terms of the amount of damping of the propellant in the tank required for various tank locations.

The potential hazard in control due to propellant sloshing can be eliminated by proper choice of tank form, proper selection of characteristics, location and gain value of the accelerometer, and as a last resort by baffles in the propellant tanks.

I. INTRODUCTION

The dynamic response of the liquid propellant in the tanks of a spacecraft may lead to saturation of the control system. The alleviation of this influence can be achieved in many ways: proper choice of tank form, tank location, gain settings of the control system and, finally, as a last resort, by the introduction of baffles. Additional artificial

stabilization with angle-of-attack meter or accelerometer, which is used to alleviate the required control deflections of the gimbal engines, also has a strong influence on the stability of the craft due to sloshing. Very useful results can be obtained from a simplified stability investigation of an accelerometer controlled rigid space vehicle. The location and gain of an accelerometer and its vibrational characteristics, such as its natural frequency and damping, may enhance the stability character of the vehicle. In order to obtain a general knowledge of the influence of tank and accelerometer location, the interaction between the translation, pitching, and propellant sloshing is investigated. The forces and moments of the oscillating propellant in the tank are described by an equivalent mechanical model, consisting of a mass-point attached to a spring and damper for each sloshing mode and a fixed mass with a moment of inertia (Fig. 1). Since the effect of higher modes is very small, only the first mode of sloshing is considered in the analysis. This is justified by the fact that, in a circular cylindrical tank, the ratio of the sloshing mass to the propellant mass for the second sloshing mode is already smaller than three percent of the first sloshing mode. In a cylindrical tank with annular cross section, the second sloshing mode mass is, in the most unfavorable case of a diameter ratio of inner to outer diameter, less than 12 percent. In the quarter tank, however, the mass of the second sloshing mode is about 43 percent of that of the first mode. In this case, the second sloshing mode will have some influence and thus cannot be neglected. This case and the treatment of two-tank sloshing at various tank locations will be treated in another paper.

For further simplification, forces and torques due to aerodynamic or elastic deformations of the spacecraft were neglected. The inertial effects of the swivel engines were not considered. The parameters affecting the stability are: the ratio of oscillating propellant mass to the total mass of the space vehicle, the natural slosh frequency, the control frequency, the control damping, the gain factors of the attitude control and accelerometer control sensor and the location, the natural frequency and damping of the accelerometer. The stability boundary was determined in terms of the amount of damping of the propellant in the tank required for various tank locations (slosh mass location).

The effect of a real accelerometer was also investigated. In the cases where sloshing was suppressed, the stability of the system was represented by the gain value of the accelerometer versus its location.

As an illustration of these effects on the stability, a vehicle was chosen whose dimensions are similar to the Saturn space vehicle. Four cases were treated:

1. Stability analysis of an accelerometer controlled rigid spacecraft including the effect of sloshing and considering a real accelerometer with certain vibrational characteristics.

2. Stability analysis of an accelerometer controlled rigid spacecraft including the effect of propellant sloshing and considering the accelerometer to be ideal.

3. Stability analysis of a rigid spacecraft with real accelerometer control (no sloshing included).

4. Stability analysis of a rigid spacecraft with ideal accelerometer control (no sloshing included).

II. EQUATIONS OF MOTION AND CONTROL EQUATION

In the following investigation, all effects due to aerodynamics, structural deformations, and propellant flow through the tanks and pipelines (Coriolis effects) are neglected. Furthermore, the inertial effects of the swiveling engines are not considered. A rigid space vehicle is treated, where the propellant in one tank is free to oscillate. The coordinate system has its origin in the center of gravity of the undisturbed spacecraft. The accelerated coordinate system is replaced by an inertial system so that the vehicle is considered in an equivalent gravitational field. The x-coordinate of this inertial coordinate system is tangent to the standard flight path.

The curvature of the standard flight trajectory is neglected. Roll motion is neglected and the investigation is restricted to the interactions of translational and pitching motion and the propellant oscillations. For the sake of simplicity, the "disc motion", which describes the motion of the propellant in a completely filled and closed tank (solidified free propellant surface), and the compliance of the gimbal engines are neglected. Furthermore, it is assumed that half of the thrust is available for control purposes. The equations of motion are then:

1. <u>Equation of Lateral Translation</u>

$$m\ddot{y} + m_s \ddot{\xi}_s = F(\varphi + \tfrac{1}{2}\beta) \tag{1}$$

where m represents the total mass of the spacecraft, m_s the sloshing mass of the first propellant mode and F the total thrust. The factor $\frac{1}{2}$ on the right hand side of Equation (1) is due to the fact that only half of the thrust is available to be gimballed. The displacement of the sloshing mass m_s relative to the centerline of the tank is represented by ξ_s and the engine deflection by β.

2. Equation of Pitching Motion

$$I_{eff}\,\ddot{\varphi} + \frac{Fx_E}{2}\,\beta - m_s\,x_s\,\ddot{\xi}_s - gm_s\,\xi_s = 0 \qquad (2)$$

I_{eff} represents the effective moment of inertia of the vehicle about its center of gravity. It can be written as:

$$I_{eff} = \int x^2\,m_A'\,dx + \int I_o'\,dx + m_o\,x_o^2 + I_o + m_s\,x_s^2 \equiv mk^2 \qquad (2a)$$

The distance of the swivel point of the gimbal engine from the origin is represented by x_E, m_A' is the mass per unit length of the air frame, I_o' its geometric moment of inertia, m_o the fixed (nonsloshing) mass of the propellant, which is located at the station x_o, I_o is its moment of inertia about its center of gravity and x_s is the location at which the sloshing propellant mass point is placed. The radius of gyration of the vehicle is represented by k.

3. Equation of Propellant Motion

$$m_s\ddot{\xi}_s + \omega_s\,\gamma_s\,m_s\,\dot{\xi}_s + k_s\,\xi_s - m_s\,x_s\,\ddot{\varphi} - gm_s\,\varphi + m_s\,\ddot{y} = 0 \qquad (3)$$

ω_s is the natural circular frequency of the first propellant mode, γ_s is the damping factor of the propellant and k_s is the spring constant of the equivalent mechanical model, describing the fluid motion in the tank $\left(\frac{k_s}{m_s} = \omega_s^2\right)$. For a cylindrical tank of circular cross section, the natural frequencies are

$$Fn = \frac{\omega_n}{2\pi} = \frac{1}{2\pi}\sqrt{\frac{g\epsilon_n}{a}\tanh\left(\epsilon_n\frac{h}{a}\right)} \qquad (n = 1,2,3----) \qquad (3a)$$

where the radius of the tank is a, h is the propellant height and g is the longitudinal acceleration of the vehicle, ϵ_n are the roots of the first derivative of the Bessel function of first order and first kind ($J_1'(\epsilon_n) = 0$) (Fig. 2). The mass m_s of the sloshing propellant is obtained from:

$$m_n = m_p\,\frac{2\tanh\left(\epsilon_n\frac{h}{a}\right)}{\left(\epsilon_n\frac{h}{a}\right)\left(\epsilon_n^2 - 1\right)} \qquad (n = 1,2,3----) \qquad (3b)$$

where m_p is the mass of the propellant in the tank (Fig. 4).

For a cylindrical tank with annular cross section and diameter ratio k of inner-to-outer tank, the natural frequencies of the propellant are (Fig. 2a)

$$f_{n-1} = \frac{1}{2\pi} \sqrt{\frac{g\,\xi_{n-1}}{a} \tanh\left(\xi_{n-1}\frac{h}{a}\right)} \qquad (n = 1,2,3----)$$

where ξ_{n-1} are the roots of the determinant

$$\begin{vmatrix} J_1'(\xi) & y_1'(\xi) \\ J_1'(k\xi) & y_1'(k\xi) \end{vmatrix} = 0$$

The mass m_s of the sloshing propellant is obtained from (Fig. 5)

$$m_{n-1} = m_p \frac{\bar{A}_{n-1}\left[\frac{2}{\pi\,\xi_{n-1}} - k\,C_1(k\,\xi_{n-1})\right] \tanh\left(\xi_{n-1}\frac{h}{a}\right)}{\left(1 - k^2\right)\left(\xi_{n-1}\frac{h}{a}\right)}$$

for n = 1 where m_p is the mass of the propellant in the tank and

$$\bar{A}_{n-1} = 2\,\frac{\left[\frac{2}{\pi\,\xi_{n-1}} - k\,C_1(k\,\xi_{n-1})\right]}{\frac{4}{\pi^2}\left(1 - \frac{1}{\xi_{n-1}^2}\right) + C_1^2(k\,\xi_{n-1})\,(1 - k^2\,\xi_{n-1}^2)}$$

and

$$C_1(k\,\xi_{n-1}) = \begin{vmatrix} J_1(k\,\xi_{n-1}) & y_1(k\,\xi_{n-1}) \\ J_1'(\xi_{n-1}) & y_1'(\xi_{n-1}) \end{vmatrix}$$

For four cylindrical quarter tanks with radius a and filled with liquid to a height h, the natural frequencies of the propellant are: (Fig. 3)

$$f_{nm} \equiv \frac{1}{2\pi} \sqrt{\frac{g\,\epsilon_{nm}}{a} \tanh\left(\epsilon_{nm}\frac{h}{a}\right)} \qquad \begin{matrix}(n = 1,2,3----)\\(m = 0,1,2----)\end{matrix}$$

where ϵ_{nm} are the roots of $J_{2m}'(\epsilon_{nm}) = 0$. The mass of the sloshing propellant is obtained from

$$m_{nm} = m_p \frac{64\ \epsilon_{nm} \tanh\left(\epsilon_{nm} \frac{h}{a}\right)}{\pi^2 \left(\epsilon_{nm}^2 - 4m^2\right) J_{2m}^2 \left(\epsilon_{nm}\right) \left(\epsilon_{nm} \frac{h}{a}\right)} \cdot \sum_{\mu=0}^{\infty} \frac{J_{2m+2\mu+1}\left(\epsilon_{nm}\right)}{(2m+2\mu-1)\ (2m+2\mu+3)} \cdot$$

$$\left\{ \frac{J_{2m}\left(\epsilon_{nm}\right)}{(4m^2-1)} + \frac{2}{\epsilon_{nm}} \sum_{\mu=0}^{\infty} J_{2m+2\mu+1}\left(\epsilon_{nm}\right) \right\} \qquad \begin{matrix}(n = 1,2,3\text{----}) \\ (m = 0,1,2\text{----})\end{matrix}$$

for $n = m = 1$ where m_p is the mass of the propellant in the tank. It can be seen that other modes cannot be neglected, (Fig. 6) because $m_{10} \approx 0.43\ m_{11}$.

4. Control Equation

$$\beta = a_0\ \varphi + a_1\ \dot{\varphi} + g_2\ A_i \tag{4}$$

This equation represents the idealized control equation, relating the attitude angle φ and the indicated acceleration A_i of the accelerometer perpendicular to the spacecraft axis. Derivatives of β which produce increasing phase lags with increasing frequency have been neglected and are not important for the basic argument. The gain value of the accelerometer is represented by g_2.

5. Accelerometer Equation

$$\frac{\ddot{A}_i}{\omega_a^2} + \frac{2\zeta_a}{\omega_a} \dot{A}_i + A_i = \ddot{y} - x_a\ \ddot{\varphi} - g\varphi = 0 \tag{5}$$

where ω_a is the natural circular frequency of the accelerometer, ζ_a is the damping of the accelerometer and x_a is its location. If the accelerometer is considered ideal ($\omega_a \gg 1$) its equation reads

$$A_i = \ddot{y} - x_a\ \ddot{\varphi} - g\varphi \tag{5a}$$

By substitution of the control deflection β and the accelerometer equation into the equations of motion, the following set of linear homogeneous differential equations is obtained.

$$\ddot{y} - \frac{g}{2}\left(a_0\ \varphi + a_1\ \dot{\varphi}\right) - g\varphi + \mu\ \ddot{\xi}_s - \frac{\lambda}{2} A_i = 0 \tag{6}$$

$$\ddot{\varphi} + \frac{g x_E}{2k^2}\left(a_0\ \varphi + a_1\ \dot{\varphi}\right) - \frac{\mu}{k^2} x_s\ \ddot{\xi}_s - \frac{\mu}{k^2} g\ \xi_s + \frac{\lambda x_E}{2k^2} A_i = 0 \tag{7}$$

$$\ddot{y} - x_s\ \ddot{\varphi} - g\varphi + \ddot{\xi}_s + \omega_s\ \gamma_s\ \dot{\xi}_s + \omega_s^2\ \xi_s = 0 \tag{8}$$

$$\frac{\ddot{A}_i}{\omega_a^2} + \frac{2\zeta_a}{\omega_a} \dot{A}_i + A_i - \ddot{y} + x_a\ \ddot{\varphi} + g\varphi = 0 \tag{9}$$

where

$g = \frac{F}{m}$ is the longitudinal acceleration

$\mu = \frac{m_s}{m}$ is the ratio of the sloshing mass to the total vehicle mass

x_E is the distance of the swivel engine gimbal point to the center of gravity of the vehicle (origin)

$\lambda = gg_2$ is a gain parameter of the accelerometer.

III. STABILITY POLYNOMIAL

Assuming solutions of the differential Equations 6, 7, 8, and 9 with the time dependency e^{st}, where s is a complex number, the stability polynomial can be obtained. The above differential equations are transformed into a set of linear homogenous algebraic equations, of which the determinant of coefficients must be zero in order to have other than trivial solutions, i.e.

$$\begin{vmatrix} s^2 & -g - \frac{g}{2}(a_0 + a_1 s) & \mu s^2 & -\frac{\lambda}{2} \\ 0 & s^2 + \frac{gx_E}{2k^2}(a_0 + sa_1) & -\frac{\mu}{k^2}(x_s s^2 + g) & \frac{\lambda x_E}{2k^2} \\ s^2 & -(x_s s^2 + g) & s^2 + \omega_s \gamma_s s + \omega_s^2 & 0 \\ -s^2 & x_a s^2 + g & 0 & \frac{s^2}{\omega_a^2} + \frac{2\zeta_a s}{\omega_a} + 1 \end{vmatrix} = 0 \qquad (10)$$

1. Stability Analysis of Accelerometer Controlled Craft Including the Effect of Sloshing and Employing a Real Accelerometer

Employing a real accelerometer with a natural circular frequency ω_a and a damping factor ζ_a results in the determinant (10). The evaluation of this determinant leads to a sixth degree polynomial.

$$A_6 s^6 + A_5 s^5 + A_4 s^4 + A_3 s^3 + A_2 s^2 + A_1 s + A_0 = 0 \qquad (11)$$

of which the coefficients A_λ ($\lambda = 0,1,2,\ldots.6$) can be written with

$$\omega_c^2 = \frac{g x_E \, a_o}{2k^2\left(1 - \frac{\lambda}{2} - \frac{\lambda x_E \, x_a}{2k^2}\right)} \tag{12}$$

as the square of the circular control frequency (frequency of the pitch mode) and

$$a_1 = \frac{2\zeta_c \, a_o}{\omega_c} \tag{13a}$$

$$\frac{g x_E \, a_1}{2k^2} = 2\zeta_c \, \omega_c \left(1 - \frac{\lambda}{2} - \frac{\lambda x_E \, x_a}{2k^2}\right) \tag{13b}$$

where ζ_c is the control damping and x_a is the accelerometer location.

$$A_6 = k_{17} + k_{18} \, x_s^2 \tag{14a}$$

$$A_5 = k_{13} + k_{14} \, \gamma_s + k_{15} \, x_s + k_{16} \, x_s^2 \tag{14b}$$

$$A_4 = k_9 + k_{10} \, \gamma_s + k_{11} \, x_s + k_{12} \, x_s^2 \tag{14c}$$

$$A_3 = k_6 + k_7 \, \gamma_s + k_8 \, x_s \tag{14d}$$

$$A_2 = k_3 + k_4 \, \gamma_s + k_5 \, x_s \tag{14e}$$

$$A_1 = k_1 + k_2 \, \gamma_s \tag{14f}$$

$$A_o = k_o \tag{14g}$$

where the abbreviations k_λ ($\lambda = 0,1,\ldots 18$) are functions of the slosh mass ratio, the control frequency, the control damping, the accelerometer gain value, its location and its vibrational characteristics, the slosh frequency the attitude gain values, the distance from the gimbal point to the center of gravity of the vehicle and the radius of gyration of the spacecraft. **Their respective values are:**

$$k_o = \omega_c^2 \, \omega_s^2\left(1 - \frac{\lambda}{2} - \frac{\lambda x_E \, x_a}{2k^2}\right) + \frac{2\mu \, \omega_c^4 \, k^2}{a_o \, x_E^2}\left(1 - \frac{\lambda}{2} - \frac{\lambda x_E \, x_a}{2k^2}\right)^2$$

$$k_1 = \frac{4\mu \, k^2 \, \zeta_a \, \omega_c^4}{a_o \, x_E^2 \, \omega_a}\left(1 - \frac{\lambda}{2} - \frac{\lambda x_E \, x_a}{2k^2}\right)^2 + 2\omega_s^2 \, \omega_c \, \zeta_c \left(1 - \frac{\lambda}{2} - \frac{\lambda x_E \, x_a}{2k^2}\right)$$

$$+ 4\mu \, \zeta_c \, k^2 \, \omega_c^3 \left(1 - \frac{\lambda}{2} - \frac{\lambda x_E \, x_a}{2k^2}\right)^2 + \frac{2\zeta_a \, \omega_c^2 \, \omega_s^2}{\omega_a}\left(1 - \frac{\lambda}{2} - \frac{\lambda x_E \, x_a}{2k^2}\right)$$

$$k_2 = \omega_c^2 \, \omega_s \left(1 - \frac{\lambda}{2} - \frac{\lambda x_E \, x_a}{2k^2}\right)$$

$$k_3 = \frac{2k^2 \, \mu \, \omega_c^4}{x_E^2 \, a_o \, \omega_a^2}\left(1 - \frac{\lambda}{2} - \frac{\lambda x_E \, x_a}{2k^2}\right)^2 + \frac{8\mu \, \zeta_a \, \zeta_c \, k^2 \, \omega_c^3}{a_o \, x_E^2 \, \omega_a}\left(1 - \frac{\lambda}{2} - \frac{\lambda x_E \, x_a}{2k^2}\right)^2$$

$$+ (1 - \mu) \, \omega_c^2 \left(1 - \frac{\lambda}{2} - \frac{\lambda x_E \, x_a}{2k^2}\right) + \frac{\omega_s^2 \, \omega_c^2}{\omega_a^2}\left(1 - \frac{\lambda}{2} - \frac{\lambda x_E \, x_a}{2k^2}\right)$$

$$+ \omega_s^2 \left(1 - \frac{\lambda}{2} - \frac{\lambda x_E \, x_a}{2k^2}\right) + 4\zeta_a \, \zeta_c \, \omega_s^2 \, \omega_c \left(1 - \frac{\lambda}{2} - \frac{\lambda x_E \, x_a}{2k^2}\right)$$

$$- \frac{\mu \, \lambda x_a \, \omega_c^2}{a_o \, x_E}\left(1 - \frac{\lambda}{2} - \frac{\lambda x_E \, x_a}{2k^2}\right)$$

$$k_4 = 2\zeta_a \frac{\omega_s \, \omega_c^2}{\omega_a}\left(1 - \frac{\lambda}{2} - \frac{\lambda x_E \, x_a}{2k^2}\right) + 2\omega_s \, \omega_c \, \zeta_a \left(1 - \frac{\lambda}{2} - \frac{\lambda x_E \, x_a}{2k^2}\right)$$

$$k_5 = \frac{\mu\omega_c^2}{x_E}\left(1 - \frac{\lambda}{2} - \frac{\lambda x_E \, x_a}{2k^2}\right) - \frac{(2 - \lambda) \, \mu\omega_c^2}{x_E \, a_o}\left(1 - \frac{\lambda}{2} - \frac{\lambda x_E \, x_a}{2k^2}\right)$$

$$+ 2\zeta_c \, \omega_c \left(1 - \mu + \frac{\omega_s^2}{\omega_c^2}\right)\left(1 - \frac{\lambda}{2} - \frac{\lambda x_E \, x_a}{2k^2}\right) + \frac{2\zeta_a \, \omega_s^2}{\omega_a^2}$$

$$k_6 = \frac{4\mu \, \zeta_c \, \omega_c^3 \, k^2}{x_E^2 \, a_o \, \omega_a^2}\left(1 - \frac{\lambda}{2} - \frac{\lambda x_E \, x_a}{2k^2}\right)^2 + \frac{2 \, (1 - \mu) \, \zeta_a \, \omega_c^2}{\omega_a}\left(1 - \frac{\lambda}{2} - \frac{\lambda x_E \, x_a}{2k^2}\right)$$

$$2\zeta_c \, \omega_c \left(1 - \mu + \frac{\omega_s^2}{\omega_c^2}\right)\left(1 - \frac{\lambda}{2} - \frac{\lambda x_E \, x_a}{2k^2}\right) + \frac{2\zeta_a \, \omega_s^2}{\omega_a^2}$$

$$k_7 = \omega_s \left(1 - \frac{\lambda}{2} - \frac{\lambda x_E\, x_a}{2k^2}\right) + \frac{4\zeta_a\, \zeta_c\, \omega_s\, \omega_c}{\omega_a}\left(1 - \frac{\lambda}{2} - \frac{\lambda x_E\, x_a}{2k^2}\right)$$

$$+ \frac{\omega_s\, \omega_c^2}{\omega_a^2}\left(1 - \frac{\lambda}{2} - \frac{\lambda x_E\, x_a}{2k^2}\right)$$

$$k_8 = \frac{2\mu\, \zeta_c\, \omega_c}{x_E}\left(1 - \frac{\lambda}{2} - \frac{\lambda x_E\, x_a}{2k^2}\right) - \frac{4\mu\, \zeta_a\, \omega_c^2}{x_E\, a_o\, \omega_a}\left(1 - \frac{\lambda}{2} - \frac{\lambda x_E\, x_a}{2k^2}\right)$$

$$+ \frac{2\mu\, \zeta_a\, \omega_c^2}{x_E\, \omega_a}\left(1 - \frac{\lambda}{2} - \frac{\lambda x_E\, x_a}{2k^2}\right)$$

$$k_9 = \frac{\omega_c^2}{\omega_a^2}\left(1 - \frac{\lambda}{2} - \frac{\lambda x_E\, x_a}{2k^2}\right)(1 - \mu) + \frac{4\zeta_c\, \zeta_a\, \omega_c}{\omega_a}\left(1 - \frac{\lambda}{2} - \frac{\lambda x_E\, x_a}{2k^2}\right)(1 - \mu)$$

$$+ 1 - \mu - \frac{\lambda}{2} + \frac{\omega_s^2}{\omega_a^2} - \frac{\lambda x_a\, x_E}{2k^2}(1 - \mu)$$

$$k_{10} = \frac{2\zeta_c\, \omega_c\, \omega_s}{\omega_a^2}\left(1 - \frac{\lambda}{2} - \frac{\lambda x_a\, x_E}{2k^2}\right) + \frac{2\zeta_a\, \omega_s}{\omega_a}$$

$$k_{11} = \frac{\mu\omega_c^2}{x_E\, \omega_a^2}\left(1 - \frac{\lambda}{2} - \frac{\lambda x_a\, x_E}{2k^2}\right) + \frac{4\mu\, \zeta_a\, \zeta_c\, \omega_c}{x_E\, \omega_a}\left(1 - \frac{\lambda}{2} - \frac{\lambda x_E\, x_a}{2k^2}\right)$$

$$- \frac{\mu\lambda\,(x_E + x_a)}{2k^2} - \frac{2\mu\, \omega_c^2}{\omega_a^2\, a_o\, x_E}\left(1 - \frac{\lambda}{2} - \frac{\lambda x_E\, x_a}{2k^2}\right)$$

$$k_{12} = \frac{\mu\,(\lambda - 2)}{2k^2}$$

$$k_{13} = \frac{2\zeta_c\, \omega_c}{\omega_o^2}\left(1 - \frac{\lambda}{2} - \frac{\lambda x_E\, x_a}{2k^2}\right)(1 - \mu) + \frac{2\zeta_a}{\omega_a}(1 - \mu)$$

$$k_{14} = \frac{\omega_s}{\omega_a^2}$$

$$k_{15} = \frac{2\mu\, s_c\, \omega_c}{x_E\, \omega_a^2} \left(1 - \frac{\lambda}{2} - \frac{\lambda x_E\, x_a}{2k^2}\right)$$

$$k_{16} = - \frac{2\mu\, \zeta_a}{\omega_a\, k^2}$$

$$k_{17} = \frac{1 - \mu}{\omega_a^2}$$

$$k_{18} = - \frac{\mu}{k^2\, \omega_a^2}$$

The coefficients of the sixth degree polynomial (n = 6) are real. The necessary and sufficient conditions for stability are (Ref. 6):

1. The coefficients A_n, A_{n-1}, $A_{n-3} \ldots > 0$

$$\left\{\begin{matrix} A_1,\ A_0 > 0 \text{ if n is even} \\ A_0 > 0 \qquad \text{if n is odd} \end{matrix}\right\}$$

2. The Hurwitz determinants

$$H_{n-1},\ H_{n-3} \ldots\ldots > 0 \qquad \left\{\begin{matrix} H_3 > 0 \text{ if n is even} \\ H_2 > 0 \text{ if n is odd} \end{matrix}\right\}$$

This is for a sixth degree polynomial (n = 6)

$$A_6,\ A_5,\ A_3,\ A_1,\ A_0 > 0 \tag{15}$$

$$H_5,\ H_3 > 0 \tag{16}$$

which is

$$H_5 = \begin{vmatrix} A_5 & A_3 & A_1 & 0 & 0 \\ A_6 & A_4 & A_2 & A_0 & 0 \\ 0 & A_5 & A_3 & A_1 & 0 \\ 0 & A_6 & A_4 & A_2 & A_0 \\ 0 & 0 & A_5 & A_3 & A_1 \end{vmatrix}$$

$$H_3 = \begin{vmatrix} A_5 & A_3 & A_1 \\ A_6 & A_4 & A_2 \\ 0 & A_5 & A_3 \end{vmatrix}$$

This means that all roots $s = \sigma + i\omega$ have a negative real part. The conditions $\sigma = 0$ represent the dividing boundary between stability (damped oscillation) and instability (diverging oscillations). The boundary of the stability region is, therefore,

$$H_5 = 0,\ A_6 = 0 \quad \text{(dynamic stability)} \tag{17}$$

$$(A_0 = 0 \quad \text{static stability})$$

It can be seen, that $A_6 = 0$ $\left(x_s = \pm\sqrt{k_{17}/k_{18}}\right)$ represents in the $(x_s \gamma_s)$ plane straight boundaries parallel to the γ_s-axis. It is $x_s = \pm k\sqrt{\frac{1-\mu}{\mu}}$. The Hurwitz determinant $H_5 = 0$ can be represented in form of

$$c_0(x_s) + c_1(x_s)\ \gamma_s + c_2(x_s)\ \gamma_s^2 + c_3(x_s)\ \gamma_s^3 + c_4(x_s)\ \gamma_s^4 + c_5(x_s)\ \gamma_s^5 = 0$$

and the $c_\lambda(x_s)$ $(\lambda = 0,1,\ldots.5)$ are polynomials in x_s. From Equation 18 the intersection points with the x_s-axis of the stability boundary curve can be obtained by taking $(\gamma_s = 0)$ and solving the equation for x_s:

$$c_0(x_s) = 0$$

Stability is achieved for all points $(x_s\ \gamma_s)$ above the boundary curve. The stability boundary breaks off at the left and right due to the results of $A_6 = 0$. Therefore, stability is only exhibited inside these boundaries, i.e., above the stability curve, left of the right boundary of $A_6 = 0$ and right of its left boundary. Sometimes these

latter boundaries are outside the spacecraft and are, therefore, due to the physical insignificance not indicated.

2. Stability Analysis of an Accelerometer Controlled Vehicle Including the Effect of Sloshing and Employing an Ideal Accelerometer

The employment of an ideal accelerometer ($\omega_a^2 \gg 1$) instead of a real one with certain vibrational characteristics, results with Equations 1, 2, 3, 4, and 5a in a fourth degree polynomial

$$\bar{A}_4 s^4 + \bar{A}_3 s^3 + \bar{A}_2 s^2 + \bar{A}_1 s + \bar{A}_0 = 0 \tag{19}$$

of which the coefficients $\bar{A}_\lambda$ ($\lambda = 0, 1, 2, 3, 4$) can be written with Equation 12 and 13

$$\bar{A}_0 = \bar{k}_0 \tag{20a}$$

$$\bar{A}_1 = \bar{k}_1 + \bar{k}_2 \gamma_s \tag{20b}$$

$$\bar{A}_2 = \bar{k}_3 + \bar{k}_4 \gamma_s + \bar{k}_5 x_s \tag{20c}$$

$$\bar{A}_3 = \bar{k}_6 + \bar{k}_7 \gamma_s + \bar{k}_8 x_s \tag{20d}$$

$$\bar{A}_4 = \bar{k}_9 + \bar{k}_{10} x_s + \bar{k}_{11} x_s^2 \tag{20e}$$

where

$$\bar{k}_0 = \omega_s^2 \omega_c^2 \left(1 - \frac{\lambda}{2} - \frac{\lambda x_E x_a}{2k^2}\right) + \frac{2\omega_s^2 \lambda^2 k^2}{x_E^2 a_0} \left(1 - \frac{\lambda}{2} - \frac{\lambda x_E x_a}{2k^2}\right)^2$$

$$\bar{k}_1 = 2\zeta_c \omega_c \omega_s^2 \left(1 - \frac{\lambda}{2} - \frac{\lambda x_E x_a}{2k^2}\right) + \frac{4\mu \zeta_c \omega_c^3 k^2}{a_0 x_E^2} \left(1 - \frac{\lambda}{2} - \frac{\lambda x_E x_a}{2k^2}\right)^2$$

$$\bar{k}_2 = \omega_c^2 \omega_s \left(1 - \frac{\lambda}{2} - \frac{\lambda x_E x_a}{2k^2}\right)$$

$$\bar{k}_3 = (1 - \mu) \omega_c^2 \left(1 - \frac{\lambda}{2} - \frac{\lambda x_E x_a}{2k^2}\right) + \omega_s^2 \left(1 - \frac{\lambda}{2} - \frac{\lambda x_a x_E}{2k^2}\right)$$

$$- \frac{\lambda\mu x_a \omega_c^2}{x_E a_0} \left(1 - \frac{\lambda}{2} - \frac{\lambda x_E x_a}{2k^2}\right)$$

$$\bar{k}_4 = 2\zeta_c\ \omega_c\ \omega_s \left(1 - \frac{\lambda}{2} - \frac{\lambda x_E\ x_a}{2k^2}\right)$$

$$\bar{k}_5 = \frac{\mu}{x_E}\ \omega_c^2 \left(1 - \frac{\lambda}{2} - \frac{\lambda x_E\ x_a}{2k^2}\right) - \frac{(2 - \lambda)\ \mu\ \omega_c^2}{x_E\ a_o} \left(1 - \frac{\lambda}{2} - \frac{\lambda x_E\ x_a}{2k^2}\right)$$

$$\bar{k}_6 = 2\zeta_c\ \omega_c\ (1 - \mu) \left(1 - \frac{\lambda}{2} - \frac{\lambda x_E\ x_a}{2k^2}\right)$$

$$\bar{k}_7 = \omega_s \left(1 - \frac{\lambda}{2} - \frac{\lambda x_E\ x_a}{2k^2}\right)$$

$$\bar{k}_8 = \frac{2\mu\ \zeta_c\ \omega_c}{x_E} \left(1 - \frac{\lambda}{2} - \frac{\lambda x_E\ x_a}{2k^2}\right)$$

$$\bar{k}_9 = 1 - \mu - \frac{\lambda}{2} - \frac{\lambda x_E\ x_a}{2k^2}\ (1 - \mu)$$

$$\bar{k}_{10} = -\ \frac{\mu\lambda}{2k^2}\ (x_a + x_E)$$

$$\bar{k}_{11} = \frac{\mu}{2k^2}\ (\lambda - 2)$$

The necessary and sufficient conditions for stability (n = 4) are that

1. $\bar{A}_4,\ \bar{A}_2,\ \bar{A}_o > 0$
2. $H_3 > 0$

which is

$$H_3 = \begin{vmatrix} \bar{A}_3 & \bar{A}_1 & 0 \\ \bar{A}_4 & \bar{A}_2 & \bar{A}_o \\ 0 & \bar{A}_3 & \bar{A}_1 \end{vmatrix} = \bar{A}_1\bar{A}_2\bar{A}_3 - \bar{A}_o\bar{A}_3^2 - \bar{A}_1^2\ \bar{A}_4$$

The stability boundary is obtained from $H_3 = 0$

$$\bar{A}_4 = 0 \tag{21}$$

$$\bar{A}_1\bar{A}_2\bar{A}_3 = \bar{A}_0\bar{A}_3^2 + \bar{A}_4\bar{A}_1^2 \tag{22}$$

which is (because the results are presented in the (x_s, γ_s) plane)

$$(k_1 + k_2 x_s + k_3 x_s^2) + (k_4 + k_5 x_s + k_6 x_s^2)\ \gamma_s + \gamma_s^2\ (k_7 + k_8 x_s + k_9 x_s^2) + \gamma_s^3 = 0 \tag{23}$$

with

$$k_1 = \bar{k}_1 \bar{k}_3 \bar{k}_6 - \bar{k}_1^2 \bar{k}_9 - \bar{k}_0 \bar{k}_6^2$$

$$k_2 = \bar{k}_1 \bar{k}_5 \bar{k}_6 + \bar{k}_1 \bar{k}_3 \bar{k}_8 - 2\bar{k}_0 \bar{k}_6 \bar{k}_8 - \bar{k}_1^2 \bar{k}_{10}$$

$$k_3 = \bar{k}_1 \bar{k}_5 \bar{k}_8 - \bar{k}_0 \bar{k}_8^2 - \bar{k}_1^2 \bar{k}_{11}$$

$$k_4 = \bar{k}_1 \bar{k}_4 \bar{k}_6 + \bar{k}_2 \bar{k}_3 \bar{k}_6 + \bar{k}_1 \bar{k}_3 \bar{k}_9 - 2\bar{k}_0 \bar{k}_6 \bar{k}_7 - 2\bar{k}_1 \bar{k}_2 \bar{k}_9$$

$$k_5 = \bar{k}_2 \bar{k}_5 \bar{k}_6 + \bar{k}_1 \bar{k}_5 \bar{k}_7 + \bar{k}_1 \bar{k}_4 \bar{k}_8 + \bar{k}_2 \bar{k}_3 \bar{k}_8 - 2\bar{k}_0 \bar{k}_7 \bar{k}_8 - 2\bar{k}_1 \bar{k}_2 \bar{k}_{10}$$

$$k_6 = \bar{k}_2 \bar{k}_5 \bar{k}_8 - 2\bar{k}_1 \bar{k}_2 \bar{k}_{11}$$

$$k_7 = \bar{k}_2 \bar{k}_4 \bar{k}_6 + \bar{k}_1 \bar{k}_4 \bar{k}_7 + \bar{k}_2 \bar{k}_3 \bar{k}_7 - \bar{k}_0 \bar{k}_7^2 - \bar{k}_2^2 \bar{k}_9$$

$$k_8 = \bar{k}_2 \bar{k}_5 \bar{k}_7 + \bar{k}_2 \bar{k}_4 \bar{k}_8 - \bar{k}_2^2 \bar{k}_{10}$$

$$k_9 = \bar{k}_2^2 \bar{k}_{11}$$

$$k_{10} = \bar{k}_2 \bar{k}_4 \bar{k}_7$$

It can be seen that $\bar{A}_4 = 0$ represents straight boundaries parallel to the γ_s-axis. These straight boundary lines are represented by the equations

$$x_s = \frac{1}{2\mu(\lambda - 2)} \left\{ \mu\lambda(x_a + x_E) \pm \sqrt{\mu^2\lambda^2(x_a + x_E)^2 - 16\left[k^2\mu\left(\lambda - 1 - \frac{\lambda^2}{6}\right) + k^2\mu^2\left(1 - \frac{\lambda}{2}\right) + \frac{\lambda x_E x_a}{2}\mu\left(1 - \frac{\lambda}{2} - \mu\right)\right]} \right\}$$

From Equation 13 the intersection points of the stability boundary curve can be obtained by taking $\gamma_s = 0$ and solving the quadratic equation in x_s.

$$k_1 + k_2 x_s + k_3 x_s^2 = 0 \tag{24}$$

Stability is achieved for all points (γ_s, x_s) above the boundary curve. The stability boundary breaks off at the left and right due to the results of relation 21. Therefore, stability is only achieved inside these boundaries, i.e., above the stability boundary due to Equation 23 and left of the right boundary of Equation 21 and right to the left boundary of Equation 21. Sometimes the boundaries of Equation 21 are outside the spacecraft and are, therefore, not indicated.

3. Stability Analysis with Real Accelerometer Control (Sloshing Not Included)

The employment of a real accelerometer with the natural circular frequency ω_a and the damping factor ζ_a results in the equations

$$\ddot{y} - g\varphi - \frac{g}{2}\beta = 0 \tag{25}$$

$$\ddot{\varphi} + \frac{gx_E}{2k^2}\beta = 0 \tag{26}$$

$$\beta = a_o\,\varphi + a_1\,\dot{\varphi} + g_2 A_i \tag{27}$$

$$\frac{\ddot{A}_i}{\omega_a^2} + \frac{2\zeta_a \dot{A}_i}{\omega_a} + A_i = \ddot{y} - x_a\,\ddot{\varphi} - g\varphi \tag{28}$$

which are, with the introduction of the control Equation 27,

$$\ddot{y} - g\varphi - \frac{g}{2}(a_o\,\varphi + a_1\,\dot{\varphi}) - \frac{\lambda}{2}A_i = 0 \tag{29}$$

$$\ddot{\varphi} + \frac{gx_E}{2k^2}(a_o\,\varphi + a_1\,\dot{\varphi}) + \frac{\lambda x_E}{2k^2}A_i = 0 \tag{30}$$

$$\frac{\ddot{A}_i}{\omega_a^2} + \frac{2\zeta_a}{\omega_a}\dot{A}_i + A_i - \ddot{y} + x_a\,\ddot{\varphi} + g\varphi = 0 \tag{31}$$

They can be obtained from Equations 6, 7 and 9 by setting the sloshing mass ratio $\mu = 0$ and leaving out the slosh Equation 8.

Assuming again solutions of the form e^{st}, where $s = \sigma + i\omega$ is a complex number, the stability polynomial can be obtained from the determinant.

$$\begin{vmatrix} s^2 & -\frac{g}{2}(2 + a_o + a_1 s) & -\frac{\lambda}{2} \\ 0 & s^2 + \frac{g x_E (a_o + a_1 s)}{2k^2} & \frac{\lambda x_E}{2k^2} \\ -s^2 & x_a s^2 + g & \frac{s^2}{\omega_a^2} + \frac{2\zeta_a}{\omega_a} s + 1 \end{vmatrix} = 0$$

and is of the fourth degree.

$$\bar{\bar{A}}_4 s^4 + \bar{\bar{A}}_3 s^3 + \bar{\bar{A}}_2 s^2 + \bar{\bar{A}}_1 s + \bar{\bar{A}}_o = 0 \tag{32}$$

The stability boundary is presented such that the magnitude of gain of the accelerometer is determined versus the accelerometer location. Writing

$$\frac{x_a}{|x_{CR}|} = \alpha \tag{33}$$

where $|x_{CR}|$ is the distance of the center of instantaneous rotation to the center of gravity of the spacecraft. The coefficients $\bar{\bar{A}}_\lambda$ ($\lambda = 0, 1, 2, 3, 4$) are then:

$$\bar{\bar{A}}_o = \bar{\bar{k}}_o + \bar{\bar{k}}_1 \lambda (1 + \alpha) \tag{34a}$$

$$\bar{\bar{A}}_1 = \bar{\bar{k}}_2 + \bar{\bar{k}}_3 \lambda (1 + \alpha) \tag{34b}$$

$$\bar{\bar{A}}_2 = \bar{\bar{k}}_4 + \bar{\bar{k}}_5 \lambda (1 + \alpha) \tag{34c}$$

$$\bar{\bar{A}}_3 = \bar{\bar{k}}_6 + \bar{\bar{k}}_7 \lambda (1 + \alpha) \tag{34d}$$

$$\bar{\bar{A}}_4 = \frac{1}{\omega_a^2} \tag{34e}$$

where the abbreviations $\bar{\bar{k}}_\lambda$ are the functions of the control frequency, the control damping and the vibration characteristics of the accelerometer.

$$\bar{\bar{k}}_o = \omega_c^2$$

$$\bar{\bar{k}}_1 = -\frac{\omega_c^2}{2}$$

$$\bar{\bar{k}}_2 = \frac{2\zeta_a \omega_c^2}{\omega_a} + 2\zeta_c \omega_c$$

$$\bar{\bar{k}}_3 = -\frac{\zeta_a \omega_c^2}{\omega_a} - \zeta_c \omega_c$$

$$\bar{\bar{k}}_4 = 1 + \frac{\omega_c^2}{\omega_a^2} + \frac{4\zeta_a \zeta_c \omega_c}{\omega_a}$$

$$\bar{\bar{k}}_5 = -\frac{1}{2} - \frac{\omega_c^2}{2\omega_a^2} - \frac{2\zeta_a \zeta_c \omega_c}{\omega_a}$$

$$\bar{\bar{k}}_6 = \frac{2\zeta_c \omega_c}{\omega_a^2} + \frac{2\zeta_a}{\omega_a}$$

$$\bar{\bar{k}}_7 = -\frac{\zeta_c \omega_c}{\omega_a^2}$$

The stability boundary can finally be expressed in (λ, α) plane by the equation

$$k_o + \lambda k_1 (1 + \alpha) + \lambda^2 k_2 (1 + \alpha)^2 + \lambda^3 k_3 (1 + \alpha)^3 = 0 \qquad (35)$$

where

$$k_o = \bar{\bar{k}}_2 \bar{\bar{k}}_4 \bar{\bar{k}}_6 - \bar{\bar{k}}_o \bar{\bar{k}}_6^2 - \frac{\bar{\bar{k}}_2^2}{\omega_a^2}$$

$$k_1 = \bar{\bar{k}}_3 \bar{\bar{k}}_4 \bar{\bar{k}}_6 + \bar{\bar{k}}_2 \bar{\bar{k}}_5 \bar{\bar{k}}_6 + \bar{\bar{k}}_2 \bar{\bar{k}}_4 \bar{\bar{k}}_7 - \frac{2\bar{\bar{k}}_2 \bar{\bar{k}}_3}{\omega_a^2} - 2\bar{\bar{k}}_o \bar{\bar{k}}_6 \bar{\bar{k}}_7 - \bar{\bar{k}}_1 \bar{\bar{k}}_6^2$$

$$k_2 = \bar{\bar{k}}_3 \bar{\bar{k}}_5 \bar{\bar{k}}_6 + \bar{\bar{k}}_3 \bar{\bar{k}}_4 \bar{\bar{k}}_7 + \bar{\bar{k}}_2 \bar{\bar{k}}_5 \bar{\bar{k}}_7 - \frac{\bar{\bar{k}}_3^2}{\omega_a^2} - \bar{\bar{k}}_o \bar{\bar{k}}_7^2 - 2\bar{\bar{k}}_1 \bar{\bar{k}}_6 \bar{\bar{k}}_7$$

$$k_3 = \bar{\bar{k}}_3 \bar{\bar{k}}_5 \bar{\bar{k}}_7 - \bar{\bar{k}}_1 \bar{\bar{k}}_7^2$$

It can be seen from k_o that the α-axis $(\lambda = 0)$ is in the stable region.

4. <u>Stability Analysis with Ideal Accelerometer Control (Sloshing Not Included)</u>

The case treating the stability with an ideal accelerometer can be obtained either by the Equations 25, 26, 27, and 5a or by working $\frac{1}{\omega_a} = 0$ in the previous case. The stability polynomial is of second degree

$$A_2 s^2 + A_1 s + A_o = 0 \qquad (36)$$

with

$$A_0 = k_0 + k_1 \lambda (1 + \alpha) \tag{37a}$$

$$A_1 = k_2 + k_3 \lambda (1 + \alpha) \tag{37b}$$

$$A_2 = 1 - \frac{\lambda}{2} (1 + \alpha) \tag{37c}$$

The stability boundary curve is obtained from $A_1 = 0$ and reads

$$\lambda = \frac{-k_2}{k_3} \frac{1}{1 + \alpha}$$

and represents a hyperbola.

The values $k\lambda$ are

$$k_0 = \omega_c^2$$

$$k_1 = -\frac{\omega_c^2}{2}$$

$$k_2 = 2\zeta_c \omega_c$$

$$k_3 = -\zeta_c \omega_c$$

with these values the stability boundaries $A_1 = A_2 = 0$ are seen to be identical

$$\lambda = \frac{2}{1 + \alpha} \tag{38}$$

The α-axis ($\lambda = 0$) lies in the stable region.

IV. APPLICATION

The influence of the various physical parameters on the stability behavior of the vehicle is treated numerically by considering a Saturn type vehicle with the dimensions $x_E = 500$ inches and a square of the radius of gyration of $k^2 = 2.513 \times 10^5 (\text{inch})^2$. The length of the vehicle was taken to be 2300 inches with the center of gravity (origin of coordinate system) being 500 inches from the base of the craft. In those cases, where the accelerometer location was not changed it was chosen to be at $x_a = -240$ inches, which is 240 inches forward of the center of gravity of the space vehicle.

The parameters are:

1. $\mu = \frac{m_s}{m}$ ratio of sloshing mass to total mass of the vehicle.
2. x_E distance of swivel point from the center of gravity of the spacecraft.
3. k radius of gyration of the vehicle.
4. ω_c undamped circular control frequency.
5. ζ_c control damping ratio.
6. ω_s first natural undamped circular slosh frequency.
7. γ_s damping factor of propellant.
8. ω_a circular undamped frequency of the accelerometer.
9. ζ_a accelerometer damping ratio
10. $\lambda = g\, g_2$ product of longitudinal vehicle acceleration times accelerometer gain value g_2.
11. x_a location of accelerometer measured from the center of gravity of the vehicle $\left(\alpha = \frac{x_a}{|x_{cr}|}\right)$ (x_{cr} is the center of instantaneous rotation).
12. x_s distance of the first sloshing mass from the center of gravity of the vehicle.
13. a_o gain value of the attitude control system.

Case A:

The stability boundary of an accelerometer controlled vehicle with real or ideal accelerometer can be seen in this case. The motion of the propellant is suppressed. For an ideal accelerometer $1/\omega_a \approx 0$ ($\omega_a \gg 1$) the stability is represented by the hyperbola

$$\lambda = \frac{2}{1 + \alpha}$$

where $\alpha = \frac{x_a}{|x_{cr}|}$ is the ratio of the accelerometer location to the absolute value of the center of instantaneous rotation. For real accelerometers, the stability boundary is not changing considerably, except to the amount that the stability region is slightly decreased, i.e., the gain values $\lambda = g.g_2$ experience only stable values for smaller values than in the ideal accelerometer case.

The magnitude of range of the parameters in Case A is given in the following Table I.

TABLE I

ω_a	ζ_a	ω_c	ζ_c	Figures
changes	0.7	2.0	0.7	Figure 7a
55	varies	2.0	0.7	Figure 7b
12	varies	2.0	0.7	Figure 7c
55	0.7	varies	0.7	Figure 7d
12	0.7	varies	0.7	Figure 7e
55	0.7	2.0	varies	Figure 7f
12	0.7	2.0	varies	Figure 7g

It can be seen in Figure 7a that the ideal accelerometer is hardly different from the case of a real accelerometer with a circular natural frequency of 60 radians/sec. A decrease in the natural frequency of the accelerometer causes a slight shift of the stability boundary, thus decreasing the stable area slightly. Increase of the accelerometer damping factor ζ_a from subcritical to high supercritical damping also decreases the stability area in the same sense as above, (Figure 7b) for large accelerometer frequency ($\omega_a = 55$). For small accelerometer frequency ($\omega_a = 12.0$) increasing accelerometer damping first increases the stability region slightly for very low damping values (until $\zeta_a = 0.2$) then decreases the region again slightly with increasing damping ζ_a (Figure 7c). Increasing control frequency exhibits decreasing stability region for large and small accelerometer frequency, (Figures 7d, e). For small accelerometer frequency, the decrease of the stability region

is slightly more pronounced, since for small control frequency, in this case the stability boundary it is already below the one with large accelerometer frequency. For changing control damping, the stability exhibits the same trends for both low and high accelerometer frequency. With increasing control damping, the stability region is slightly enlarged, especially noticeable in the case of small accelerometer frequency. Thus the control damping has the strongest effect on the stability, especially for low accelerometer frequency.

It may be noted, however, that due to other effects, such as bending, the accelerometer should be located before the bending loop (where $y' < 0$). In a rigid space vehicle the λ value is also restricted to a certain range if aerodynamic forces are included in the treatment and the drift-minimum principle is considered. Without aerodynamic forces or for a neutrally stable rigid vehicle the drift-minimum principle is satisfied for $\lambda = a_o$. This would mean in our case $\lambda = a_o = 3.5$. For smaller a_o values, a kind of load minimum ($a_o = 0$) would be approached. (This effect of loads reduction, however, is only valid for quasi-steady states.) Due to the drift-minimum consideration, the accelerometer is best located in the vicinity of the center of instantaneous rotation, thus having a larger range of values available.

Case B:

In the following Case B, the stability boundary with respect to propellant sloshing is treated for no accelerometer control. For ideal accelerometer ($\omega_a \gg 1$), the stability equation was obtained in Section III, paragraph 2. If no accelerometer control is employed ($\lambda = 0$), and only an attitude control system is used, the equations reduce to

$$A_4 s^4 + A_3 s^3 + A_2 s^2 + A_1 s + A_o = 0$$

where the coefficients A_λ can be obtained from the equations 20a....e and the k_λ from the $\bar{k}_\lambda$ by substituting for $\lambda = 0$. The boundaries due to $A_4 = 0$ are

$$x_s = \pm \sqrt{-\frac{k_9}{k_{11}}}$$

which results in

$$x_s = \pm k \sqrt{\frac{1 - \mu}{\mu}}$$

The stability boundary intersects the x_s-axis in the values obtained from equation 23 for $\gamma_s = 0$ and $\lambda = 0$ and are for $\frac{\omega_c^2}{a_o \omega_s^2} < 1$

$$X_1 \approx - |x_{cr}| + \left(1 - \frac{|x_{cr}|}{x_E}\right) \cdot \frac{\omega_c^2}{a_o \omega_s^2} \cdot \mu \cdot |x_{cr}|$$

$$X_2 \approx \frac{\omega_c^2}{a_o \omega_s^2} \cdot (1 - \mu) \cdot |x_{cr}|$$

For very small values of $\frac{\omega_c^2}{a_o \omega_s^2}$ the stability boundary intersects the x_s-axis close to the center of gravity (origin) and close to the center of instantaneous rotation. Due to the fact that the $x_{1,2}$ values are proportional to the mass ratio μ and $(1 - \mu)$ respectively the value x_2 is more sensitive to changes of ω_s, ω_c and a_o. Since $|x_{cr}|$ is of the same magnitude as x_E (in this type of vehicle $x_E = 500$ inches and $|x_{cr}| = 502.6$) the change of x_1 is significant.

The magnitude of range of the parameters in Case B is given by Table II.

If no accelerometer control is employed ($\lambda = 0$), and only an attitude control system is employed, it can be seen that propellant sloshing has quite some effect on the stability of a rigid space vehicle. Figure 8a exhibits the danger zone of a rigid spacecraft for small values of $\frac{\omega_c^2}{a_o \omega_s^2}$. It is approximately between the center of instantaneous rotation and the center of gravity. With increasing slosh mass ratio μ, the stability is decreasing in this region, i.e., more baffling has to be employed in the tank in order to maintain stability. Considering only the wall friction of an unbaffled tank as contributing to the damping ($\gamma_s = 0.02$), the vehicle is always stable for a slosh mass ratio of $\mu < 0.15$. In Figure 8b the influence of an increase in the circular control frequency indicates a rather strong increase of the danger zone towards the tail of the craft. The sloshing mass ratio was considered to be $\mu = 0.1$. The increase in the control frequency demands more baffling in the danger zone. For a control frequency of about twice the magnitude of the nominal control frequency of 0.3 cycles/sec, about three times as much damping has to be introduced in the tank in order to maintain stability. The case of $\omega_c > \omega_s$ is very unfavorable since it demands even more baffling and exhibits a larger danger zone. Keeping the control frequency a considerable

TABLE II

	μ	ω_c	ξ_c	ω_s	a_o	λ	ω_a	ξ_a	x_a	Figure
CASE B	changes	2.0	0.7	5.0	3.5	0	-	-	-	8a
	0.1	changes	0.7	5.0	3.5	0	-	-	-	8b
	0.1	2.0	changes	5.0	3.5	0	-	-	-	8c
	0.1	2.0	0.7	changes	3.5	0	-	-	-	8d
	0.1	2.0	0.7	5.0	changes	0	-	-	-	8e
CASE C	changes	2.17	0.7	5.0	3.5	1.0	-	0	-240	9a
	0.1	changes	0.7	5.0	3.5	1.0	-	0	-240	9b
	0.1	2.17	changes	5.0	3.5	1.0	-	0	-240	9c
	0.1	2.17	0.7	changes	3.5	1.0	-	0	-240	9d
	0.1	2.17	0.7	5.0	changes	1.0	-	0	-240	9e
	0.1	2.17	0.7	5.0	3.5	changes	-	0	-240	9f
	0.1	2.17	0.7	5.0	3.5	1.0	-	0	changes	9g
CASE D	changes	2.0	0.7	5.0	3.5	1.0	55	0.7	-240	10a
	changes	2.0	0.7	5.0	3.5	1.0	12	0.7	-240	10c
	0.1	changes	0.7	5.0	3.5	1.0	55	0.7	-240	10d
	0.1	changes	0.7	5.0	3.5	1.0	12	0.7	-240	10e
	0.1	2.0	changes	5.0	3.5	1.0	55	0.7	-240	10f
	0.1	2.0	changes	5.0	3.5	1.0	12	0.7	-240	10g
	0.1	2.0	0.7	changes	3.5	1.0	55	0.7	-240	10h
	0.1	2.0	0.7	changes	3.5	1.0	12	0.7	-240	10i
	0.1	2.0	0.7	5.0	changes	1.0	55	0.7	-240	10j
	0.1	2.0	0.7	5.0	changes	1.0	12	0.7	-240	10k
	0.1	2.0	0.7	5.0	3.5	changes	55	0.7	-240	10l
	0.1	2.0	0.7	5.0	3.5	changes	12	0.7	-240	10m
	0.1	2.0	0.7	5.0	3.5	1.0	changes	0.7	-240	10n
	0.1	2.0	0.7	5.0	3.5	1.0	55	changes	-240	10o
	0.1	2.0	0.7	5.0	3.5	1.0	12	changes	-240	10p&q
	0.1	2.0	0.7	5.0	3.5	1.0	55	0.7	change	10r
	0.1	2.0	0.7	5.0	3.5	1.0	12	0.7	change	10s&t

amount below the first sloshing mode frequency with relatively low damping in the tank avoids instability, and keeps the danger zone restricted to the approximate region between the center of gravity and the center of instantaneous rotation. For a sloshing mass ratio of 10%, the wall friction is sufficient to maintain stability as long as the control frequency is below 0.3 cycles. The change of the control damping ζ_c can be seen in Figure 8c. It exhibits the following trend: for increasing subcritical control damping ($\zeta_c < 1$), the stability is decreasing in the danger zone, i.e., more damping has to be introduced to maintain stability. The danger zone is unchanged by the change of the control damping. For increasing supercritical control damping($\zeta_c > 1$) the stability is increasing, i.e., less damping is required in tank locations in the danger zone. No baffling is required for a sloshing mass of $\mu = 0.1$ in the danger zone, if the control damping $\zeta_c \leq 0.5$ or if $\zeta_c \geq 2.5$ This means that for the parameters considered ($\omega_s = 5.0$, $\omega_c = 2$, $a_o = 3.5$, simple attitude control system with lead net work), the wall friction in the tank is sufficient to maintain stability for a rigid space vehicle of the Saturn type. A further question that always presents itself to the design engineer is the problem of tank design. Tanks with large diameters exhibit low sloshing frequencies which are in many cases too close to the control frequency of the vehicle. Providing partitions in the tank or clustering the tanks increases not only the sloshing frequency but also reduces the sloshing mass considerably. In Figure 8d the effect of the change of the sloshing frequency is shown. The danger zone increases toward the aft of the craft for decreasing slosh frequency which decreases the stability considerably. An increase of the slosh frequency enhances the stability, i.e., decreases the danger zone and reduces the amount of baffling necessary to maintain stability. For the treated case of a rigid space craft with a sloshing mass ratio of $\mu = 0.1$, the wall friction will be sufficient to maintain stability at any tank location if the natural sloshing frequency is above 3.0 cycles/sec.

The control factor a_o of the attitude control systems exhibits a slight decrease of the danger zone toward the base of the craft and a slight decrease in stability for decreasing values (Figure 8e).

<u>Case C:</u>

The stability boundaries with respect to propellant sloshing is treated for an accelerometer controlled space craft employing an ideal accelerometer ($\omega_a \gg 1$) in addition to the control system of the previous Case B. The boundaries due to $A_6 = 0$ are given by equation 23a.

$$X_{1;2} = \frac{1}{\alpha \mu (\lambda - 2)} \left\{ \mu \lambda (X_a + X_E) \pm \left[\mu^2 \lambda^2 (X_a - X_E)^2 - 1\, b(b^2 \mu (\lambda - 1 - \frac{\lambda^2}{4}) + k^2 \mu^2 (1 - \frac{\lambda}{2}) + \frac{\lambda X_E X_a \mu}{2} (1 - \frac{\lambda}{2} - \mu) \right]^{\frac{1}{2}} \right\}$$

From this it can be seen that the left and right boundaries depend strongly on the accelerometer locations x_a and the accelerometer gain values λ. The mass ratio is also of some importance, especially for the left boundary, i.e., for the negative sign in front of the square root. For most of the treated cases these boundaries are beyond the spacecraft and therefore not indicated.

Figure 9a exhibits the influence of increasing slosh mass ratio. The most favorable gain value $\lambda = 1.0$ for an ideal accelerometer controlled space vehicle was employed. The danger area is decreased considerably to a very short zone below the center of instantaneous rotation where wall friction for the liquid in the tanks already is sufficient to maintain stability. The increase of the control frequency above the slosh frequency results in a decrease in stability and an increase of the danger zone towards the base of the craft. Due to ideal accelerometer control, however, the damping necessary to obtain stability for sloshing mass of 10% of the vehicle mass is very small, even in the case when the control frequency is twice the sloshing frequency. For $\omega_s = 5.0$ radians/sec and $\omega_c = 10.0$ radians/sec the necessary damping $\gamma_s = 0.01$, (Figure 9b). The change of the control damping exhibits the same behavior as in the previous Case . It decreases the stability for increasing subcritical damping and increases the stability for increasing supercritical damping. The effect in the already small danger zone is hardly recognized, (Figure 9c). If the slosh frequency is below the control frequency $\omega_s < \omega_c$, the danger zone is large and covers nearly the complete region behind the center of instantaneous rotation. Small damping, however, already guarantees stability (Figure 9d). For increasing slosh frequency, a considerable decrease in the danger zone is noticed and an increase in stability is obtained. Figure 9c shows that no appreciable stability is encountered by change of the attitude control value a_o. The accelerometer gain value $\lambda = g_2 g$ has a very pronounced influence on the stability behavior of the vehicle. In Figure 9f it can be seen that, for $\lambda < 1$, the danger zone is behind the center of instantaneous rotation and is increasing towards a value slightly behind the center of gravity as λ approaches the value zero. A loss in stability takes place in the danger zone while λ is decreasing. For increasing $\lambda > 1$, the danger zone shifts forward of the center of instantaneous rotation and increases the magnitude of the zone and the required damping for tanks in this location. From a certain value $\lambda > 1.5$ on, propellant motion in all tanks in front of the center of instantaneous rotation leads to instabilities while, for tanks behind the center of instantaneous rotation, the motion of the propellant is stable. The value $\lambda = 1$ is the most favorable gain for which all other parameter changes were performed. In Figure 9g, the influence of the location of the accelerometer upon the stability can be seen. For the most favorable gain value $\lambda = 1$, the change of the location of the accelerometer did

not lead to instabilities. For other gain values, however, the location of the accelerometer definitely has an influence on the stability. For gain values λ larger than 1.5, the fluid motion in all tanks behind the center of instantaneous rotation exhibits strong instabilities for accelerometer locations behind the center of gravity. The propellant motion in tanks in front of the center of instantaneous rotation shows instabilites if the accelerometer is located in front of the center of gravity (Figure 9h). For gain values λ smaller than unity, the behavior of the stability boundary is similar to that one without accelerometer control. The previous results are only valid for an ideal accelerometer, which means for an accelerometer frequency of large value ($\omega_a \gg 1$). For an accelerometer with vibrational characteristics ω_a and ζ_a (noted as a real accelerometer) the stability behavior is quite different from that of an ideal accelerometer depending, of course, mainly on the value of its natural frequency. The range of parameter changes, can be depicted from Table II. Two circular frequencies for the accelerometer were treated $\omega_a = 12$ and 55 radians/sec. In Figure 10a, the influence of increasing slosh mass ratio can be seen for a spacecraft with additional accelerometer control, where the accelerometer had a circular natural frequency of $\omega_a = 55$ radians/sec and a subcritical damping of $\zeta_a = 0.7$. With increasing slosh mass ratio, the danger zone incrases aft of the center of instantaneous rotation and the stability decreases. That is, in the danger zone more damping is needed to maintain stability. It can be noted, however, that for wall friction only ($\gamma_s = 0.25$), the vehicle is stable for sloshing mass ratio $\mu < 0.30$. Increasing the gain value to $\lambda = 1.5$ (an optimal value for stability) with an accelerometer of circular natural frequency of $\omega_a = 55$ radians/sec, no instabilities are obtained for slosh mass ratios of $\mu < 0.21$ (Figure 10b). For larger slosh mass ratios the vehicle becomes very strongly instable. It may be noted that the stability curve breaks off at the left at the indicated values, thus pointing out the instability beyond this point. For low accelerometer frequency ($\omega_a = 12$ radians/sec), the stability situation is becoming very hopeless from the standpoint of sloshing (Figure 10c). Sloshing is even excited by the accelerometer control and creates a situation which is worse than in a craft with simple attitude control only. The danger zone is increased and continues to increase with increasing slosh mass ratio. Very high baffling would be necessary in order to maintain stability. The damping required in this case is about three to four times larger than in the case without accelerometer control. From this we can conclude that the accelerometer frequency should be well apart from the slosh control frequency. With increasing gain value λ, this situation is becoming even more unfavorable, i.e., the danger zone is increasing over almost the entire vehicle and stability requires tremendous damping values. Figure 10d exhibits the effect of the change of the control frequency for a vehicle with an accelerometer frequency of $\omega_a = 55$ radians/sec. An

increase of the control frequency below the slosh frequency decreases the danger zone slightly, while an increase of the control frequency above the slosh frequency increases the danger zone towards the aft of the craft. The damping during the increase of the control frequency remains comparatively small (γ_s = 0.01 and less). For an accelerometer frequency of ω_a = 12 radians/sec, the stability behavior can be seen in Figure 10c. Increase of the control frequency results in a decrease of the danger zone and an increase in stability. The effect is more pronounced than in the previous case and the vehicle is less stable for equal control frequencies in comparison with the case of ω_a = 55 radians/sec. Figure 10f exhibits the influence of control damping. Increasing control damping decreases the danger zone and increases the stability. For the use of the low accelerometer frequency ω_a = 12 radians/sec, the stability behavior can be seen in Figure 10g, which exhibits, for increasing subcritical damping, decreasing danger zone and increasing stability, while for increasing supercritical damping increase of the danger zone and loss of stability area are encountered. Low subcritical damping, however, seems unfavorable in both accelerometer frequency cases; especially in the low accelerometer frequency case more baffling has to be applied in order to maintain stability. The effect of changes in the sloshing frequency is shown in Figure 10h and 10i. Slosh frequencies below the control frequency exhibit a large danger zone from a value slightly in front of the center of instantaneous rotation almost to the base of the spacecraft. For low accelerometer frequency (ω_a = 12 radians/sec), this is even more pronounced. Increasing slosh frequency shows a decrease in the danger zone and an increase in stability. Increasing slosh frequency above the control frequency $\omega_s > \omega_c$ decreases the stability and increases the danger zone towards the base of the craft again. For low accelerometer frequencies, these effects are more magnified. For a slosh frequency in the vicinity of the accelerometer frequency, the stability is decreased and the danger zone is increased. The gain value a_o of the attitude control system has only very small influence upon the stability boundary for an accelerometer frequency ω_a = 55 radians/sec which is large compared to the control frequency ω_c = 2 radians/sec (Figure 10j) The danger zone is only a short length behind the center of instantaneous rotation. With the wall friction damping value (γ_s = 0.02), the vehicle is already stable for the given parameters. For small accelerometer frequency (ω_a = 12 radians/sec) a small effect can be observed. The danger zone and stability region, however, are unfavorable (Figure 10k).

Figure 10 l and 10 m exhibit the influence of the change of the accelerometer gain value $\lambda = g_2 g$. For an accelerometer frequency of ω_a = 55 radians/sec, an increase of the gain value to about λ = 1.5 enhances the stability and decreases the danger zone to a very small region between center of instantaneous rotation and the center of gravity. Further increase of λ extends the danger zone in front of the

center of instantaneous rotation. The larger λ becomes, the more baffling is required. If the accelerometer frequency is only $\omega_a = 12$ radians/sec, the situation is quite different. For increasing gain value, the danger zone increases from the center of instantaneous rotation to the aft of the craft. Very strong damping in the tanks has to be introduced in order to maintain stability. Further increases decrease the stability region again, but still require a large zone to be baffled very strongly. While in the case of a large accelerometer, low damping is already sufficient for stability. A damping twenty to thirty times larger is required for the case of low accelerometer frequency. Again we can conclude that large accelerometer frequency eliminates the greatest part of the problem. To obtain the influence of the very important parameter, the natural frequency of the accelerometer, Figure 10n, shows that for increasing accelerometer frequency, the danger zone enlarges and requires more damping. Above the slosh frequency for $\frac{\omega_a}{\omega_s} > 2$, a decrease of the danger zone and an increase in the stability area are noticed. The larger the ratio $\frac{\omega_a}{\omega_s}$ the less damping is required in order to obtain stability.

The increase of the damping of the accelerometer exhibits an increase of the danger zone and requires more damping in the tanks. This effect is more magnified for small accelerometer frequencies (Figures 10 o, 10 p, and 10q). It can be noticed that from twice the critical damping on, for small accelerometer frequency $\omega_a = 12$ radians/sec, a further increase of the accelerometer damping slightly decreases the danger zone and slightly enhances the stability. A very important parameter in the design of a control system is the location of an accelerometer as indicated in Figure 10r, 10s, and 10t. A location of the accelerometer behind the center of gravity must be avoided. For a natural frequency of $\omega_a = 55$ radians/sec of the accelerometer, any location in front of the center of gravity requires low damping only for stability in a small danger zone. For an accelerometer frequency $\omega_a = 12$ radians/sec, a location of an accelerometer behind the center of gravity requires high baffling in the tanks between the base and the center of instantaneous rotation. Further shifting of the accelerometer towards the nose of the vehicle enhances the stability and decreases the danger zone. All these results are valid for a rigid spacecraft. It should, however, be noted that bending in an accelerometer-controlled craft plays an important role. Gain factor λ, location of the accelerometer and the ratio of the bending frequency to the accelerometer frequency as well as to the control frequency have some definite influence. If the bending and control frequency are sufficiently apart, only negative bending displacements are permissible. This indicates that for the control of the first two bending modes a location in front of the center of gravity, where both bending modes exhibit negative deflection, is favorable. This location also would remedy the sloshing problems with little

baffling, but since it exhibits limitations in magnitude due to rigid body control (Case A), it must be treated with care with respect to the gain value λ of the accelerometer.

V. CONCLUSION

For spacecraft of increasing size, the influence of propellant sloshing upon the stability becomes more pronounced. Aerodynamically unstable spacecraft create loads and require control torques, which can be a potential hazard to the flight performance of the vehicle. Therefore, artificial stabilization such as angle-of-attack meter and/or accelerometer control is employed. This helps to alleviate the required control deflections of the gimbal engines, jet vanes, or air vanes. For a given configuration, the control requirements are strongly dependent upon the gain settings of the control system (attitude and accelerometer control). Sloshing propellant requires additional control torques. In order to minimize this effect, proper choice of the control values, tank forms, tank location, and, as a last resort, baffles will enhance the stability situation. The amount of sloshing mass is determined by the tank geometry, the mass density of the propellant, and the liquid height. The tank location, i.e., slosh mass location, plays an important role. The conclusions drawn from the results of a rigid space vehicle with additional ideal accelerometer control lead to optimistic results concerning the baffling of the tanks in order to maintain stability. An actual accelerometer has its own natural frequency; therefore, the relation of control, sloshing and accelerometer frequency are of utmost importance. Without consideration of propellant sloshing, rigid body stability can be obtained for any location of the accelerometer along the vehicle. Drift minimum requirements, however, demand certain values for the gain $\lambda = (g_2 . g)$, which can only be obtained in front of the instantaneous center of rotation. It should be noted, however, that for bending mode stability, the accelerometer should be located between the front nodal point and the center of instantaneous rotation for bending frequency of at least three to five times the control frequency. In most cases, a simple control system such as that considered here in the rigid body analysis cannot be employed in bending feedback analysis without additional phase shaping in the network.

For $\omega_c < \omega_s << \omega_a$ the amount of damping required in the tanks in order to maintain stability decreases considerably. One further advantage of an accelerometer controlled vehicle is the decrease of the danger zone, i.e., the zone where, for a sloshing mass being located, a baffle of appropriate damping characteristic has to be introduced to obtain stability. This danger zone was for values $\frac{\omega_c^2}{\omega_s^2 \, a_o} < 1$ for a rigid vehicle with simple attitude control

system with lead network approximately between the center of gravity and the center of instantaneous rotation. With additional accelerometer control, this danger zone can be decreased if the accelerometer frequency is large enough ($\omega_a >> \omega_c$). For small accelerometer frequency ($\omega_a \approx 5$ to $10 \cdot \omega_c$) the danger zone is enlarged for decreasing ω_a .

In the following the effect of the various parameters will be summarized:

1. Slosh Mass Ratio μ

a. Without accelerometer control: increasing slosh mass ratio decreases the stability and requires more baffling. The danger zone is for values $\frac{\omega_c^2}{a_o \omega_s^2} < 1$ approximately between the center of gravity and the center of instantaneous rotation (Figure 8a).

b. With Accelerometer Control

1) ω_a = 55 radians/sec: increasing slosh mass ratio decreases the stability and requires more baffling. The damping required to maintain stability is only two-fifths of that of a rigid vehicle without accelerometer control. The danger zone is decreased to three-fifths of the danger zone for a vehicle without accelerometer control (starting at the center of instantaneous rotation toward the aft of the craft, Figure 10a).

2) ω_a = 12 radians/sec: increasing slosh mass ratio decreases the stability and requires more baffling. Ten times as much damping is needed in the tanks compared with the case of accelerometer frequency ω_a = 55 radians/sec. Even five times as much damping has to be introduced in the tanks compared with the results of a space vehicle without accelerometer control. Thus it can be concluded that no accelerometer control should be employed rather than one with too low a natural accelerometer frequency. The danger zone is even larger than for a system without accelerometer control and increases towards the aft of the craft for increasing slosh mass ratio (Figure 10c).

3) Ideal accelerometer: an ideal accelerometer eliminates the danger zone almost completely except for a small region at the center of instantaneous rotation, where wall friction is already sufficient to maintain stability.

2. Control Frequency ω_c

a. Without accelerometer control: increase of the control frequency decreases the stability and increases the danger zone toward the aft of the vehicle. Furthermore it requires stronger baffling. The situation becomes worse for control frequencies larger than the slosh frequencies (Figure 8b).

b. With Accelerometer Control

1) ω_a = 55 radians/sec: increasing control frequency decreases the stability slightly and increases the danger zone toward the base of the craft. The baffle requirements are very low compared to the case without accelerometer. Figure 10d shows that wall friction is already sufficient to maintain stability.

2) ω_a = 12 radians/sec: decrease of the control frequency decreases the stability and also increases the danger zone toward the aft of the vehicle (Figure 10e).

3) Ideal accelerometer: increase of the control frequency decreases the stability and increases the danger zone toward the base of the vehicle (Figure 9b). Again as in the cases 1) and 2), the baffle requirements are smaller than in the case without accelerometer control. Except for a control frequency of a ω_a = 12 radians/sec, the same baffling is required in the case without accelerometer control for ω_c = 10 radians/sec.

3. Control Damping ζ_c

a. Without accelerometer control: increasing subcritical control damping decreases stability whereas increasing supercritical damping increases the stability. Supercritical control damping requires less baffling (Figure 8c).

b. With Accelerometer Control

1) ω_a = 55 radians/sec: increasing subcritical damping increases the stability and decreases the danger zone. Increasing supercritical damping increases the danger zone and decreases the stability slightly. The baffling required in the tanks is very small for all control damping values. It is of the same magnitude as in the case without accelerometer control (Figure 10f).

2) ω_a = 12 radians/sec: increasing subcritical control damping increases the stability and decreases the danger zone. An increase in supercritical damping first increases the stability and decreases the danger zone, but around the propellant sloshing frequency,

it decreases the stability and increases the danger zone toward the aft of the vehicle. The damping values required for stability are at least two to three times larger than those of the two previous cases (Figure 10g).

3) Ideal accelerometer: for the particular gain value of $\lambda = 1$ the change of control damping ζ_c has practically no influence. The trend, however, is the same as in the case with no accelerometer control (Figure 9c).

4. Sloshing Frequency ω_s

a. Without accelerometer control: increasing slosh frequency enhances the stability and decreases the danger zone. For slosh frequencies below the control frequency the danger zone is the entire length behind the center of instantaneous rotation and requires considerably more damping in order to maintain stability (Figure 8d).

b. With Accelerometer Control

1) $\omega_a = 55$ radians/sec: for the slosh frequency below the control frequency, the danger zone is enlarged and the stability is decreased. For increasing slosh frequency, the danger zone first decreases and the stability increases slightly. Further increase in the sloshing frequency toward the accelerometer frequency decreases the stability and increases the danger zone (Figure 10h).

2) $\omega_a = 12$ radians/sec: this case exhibits the same behavior (Figure 10) except for about three times larger damping being required to maintain stability.

3) Ideal accelerometer: increasing the sloshing frequency slightly decreases stability. Sloshing frequency below the control frequency increases the danger zone and decreases the stability (Figure 9d).

5. Gain Value a_o of the Attitude Control System

a. Without accelerometer control: a decrease in the gain value a_o decreases the stability and increases the danger zone. It is, however, of slight effect (Figure 8e).

b. With Accelerometer Control

1) $\omega_a = 55$ radians/sec: change of a_o exhibits practically no effect (Figure 10j).

2) $\omega_a = 12$ radians/sec: the change of a_o also shows only minor effects. Increasing a_o decreases the danger zone slightly

and causes a minor increase in stability. The danger zone was already three times as large as in case 1) and half as large as in the case without accelerometer control. The damping required is about ten times that of the case 1) and about twice as much as in the case with no accelerometer control.

3) Ideal accelerometer: the change of a_o has practically no influence.

6. Gain Value, $\lambda = g\, g_2$, of Accelerometer

a. ω_a = 55 radians/sec: for increasing gain value λ, the danger zone between the center of instantaneous rotation and the center of gravity decreases accompanied by increasing stability. At $\lambda = 1.5$ the optimum seems to be reached. For further increasing gain value λ the danger zone is in front of the center of instantaneous rotation and requires increased baffling (Figure 10k).

b. ω_a = 12 radians/sec: for increasing gain value λ the danger zone is increasing aft of the center of instantaneous rotation and requires excessively large baffling. Any accelerometer control with a low natural frequency has detrimental effects upon the stability (Figure 10m).

c. Ideal accelerometer: for increasing gain value λ, the danger zone between the center of instantaneous rotation and the center of gravity of the vehicle is decreased and the stability is increased. Here $\lambda = 1.0$ seems to be the optimum value, while for further increase of λ, the danger zone increases in front of the center of instantaneous rotation and requires more damping in order to maintain stability (Figure 9f).

7. Accelerometer Frequency ω_a

Increasing accelerometer frequency decreases the stability and increases the danger zone behind the center of instantaneous rotation for values of $\frac{\omega_a}{\omega_s} < 1$ i.e. for values of the accelerometer frequency below the sloshing frequency. For further increase of the accelerometer frequency, the stability enhances and the danger zone decreases. For ideal accelerometer control ($\omega_a \rightarrow \infty$), the danger zone is diminished to a small region about the center of instantaneous rotation, where practically no baffling is required to maintain stability (Figure 10n).

8. Accelerometer Damping ζ_a

a. $\omega_a = 55$ radians/sec: an increase of accelerometer damping ζ_a results in an increase of the danger zone aft the center of instantaneous rotation and a decrease in stability (Figure 10 o).

b. $\omega_a = 12$ radians/sec: Increase of the accelerometer damping increases the danger zone aft the center of instantaneous rotation and decreases the stability for subcritical and low supercritical damping. For supercritical damping $\zeta_a > 2$ further increase in damping has the opposite effect. The danger zone for corresponding damping values is larger than in the previous case $\omega_a = 55$ radians/sec for $\zeta_a < 3$ and vice versa for $\zeta_a > 3$. For low subcritical damping, the required baffling is approximately the same in both cases ($\omega_a = 55$ and $\omega_a = 12$ radians/sec); while for large subcritical damping, twice as much damping is needed in the tanks to maintain stability for the low accelerometer case. For low supercritical accelerometer damping, about four times as much baffling is needed; while for large supercritical damping only about twice as much baffling is required in the tanks compared to Case A (Figure 10p and 10q).

9. Accelerometer Locations X_a (or $\alpha = \dfrac{x_a}{|X_{cIR}|}$)

a. $\omega_a = 55$ radians/sec: accelerometer location behind the center of gravity has a detrimental effect on the stability and exhibits only a rather short region of stability immediately in front of the center of instantaneous rotation. This stability region increases towards the nose of the craft as the accelerometer location is moved from the aft of the vehicle towards the center of gravity. Accelerometer locations in front of the center of gravity exhibit only small danger zones between the center of instantaneous rotation and the center of gravity, where only slight baffling is required to maintain stability. (Figure 10n, wall friction is in many cases already sufficient)

b. $\omega_a = 12$ radians/sec: again, as in the low accelerometer frequency case, stability is endangered. Location of the accelerometer behind the center of gravity again exhibits detrimental effects upon the stability and a danger zone which reaches from the center of instantaneous rotation to the tail of the vehicle. Large baffling would be required to maintain stability. But even for an accelerometer location in front of the center of gravity, there is a need for small baffling. The further the accelerometer is shifted toward the nose, the less damping is required. The danger zone decreases also to one between the center of gravity and center of instantaneous rotation (Figures 10s and 10t).

c. Ideal accelerometer: for ideal accelerometer control the stability of the spacecraft is insensible to the location of the accelerometer (Figure 9g). This, however, as in all previous cases is only valid for the particular accelerometer gain value $\lambda = 1.0$. For other gain values $\lambda > 1$, accelerometer location in front of the center of gravity results in instability for the tanks in front of the center of instantaneous rotation, while for a location behind the center of gravity all tanks behind the center of instantaneous rotation exhibit instabilities, which decrease with a further shift of the location of the accelerometer toward the aft of the craft (Figure 9h). A change of accelerometer location toward the nose of the vehicle results in less baffling requirement in the tanks in front of the center of instantaneous rotation. Enhanced stability can always be obtained by changing the previous parameters and by proper choice of control values. The sloshing mass can be reduced by special selection of tanks for the propellant. Tanks with a large fineness ratio (fluid height over diameter ratio) exhibit small sloshing masses. A circular cylindrical tank compared with the same tank containing cross walls thus making four cylindrical quarter tanks, exhibits a ratio of the slosh masses of about 1: 3.3 which means that by introduction of quarter tanks, the sloshing mass can be reduced to one third. Besides this the slosh frequency is increasing thus shifting the natural liquid frequency into a better region (above the control frequency: $\omega_s > \omega_c$). For four cluster tanks with circular cross sections compared with four quarter tanks, the sloshing ratio is still 1:1.6, which means that by the introduction of quarter tanks instead of four cluster tanks of equal volume, the sloshing mass can be reduced to six tenths. It should be noted, however, that additional sloshing masses appear in the quarter tank arrangement, which have only a slightly different frequency, but can no longer be neglected. These frequencies are about 20% apart. The change of the control frequency and control damping is a matter of control system design (change of the gain value a_0 and a_1), of the selection of center of gravity (which reflects on the swivel point location X_E), the moment of inertia of the vehicle, and the longitudinal acceleration of the craft. The slosh frequency can be increased by subdivision of the tanks in the longitudinal direction. Large accelerometer frequency enhances the stability and the danger zone and thus requires less baffling for stability. Proper choice of accelerometer gain values and accelerometer location also play an important role.

VI. APPENDIX:

Mechanical Model

An equivalent mechanical model which describes the motion of the propellant in the tank can be seen in Figure 1. This model consists of vibrating mass points, springs and dampers, a fixed mass with a moment of inertia and a massless disc with a moment of inertia. It is so derived that it exerts the same forces and moments as the propellant and that it has the same natural frequency as the liquid. The complete analysis of presenting the fluid motion as mechanical model either with mass-spring-damper systems or pendulum systems is given in Reference 3 for cylindrical tanks with circular or annular cross sections. Part of the results will be summarized here.

A. <u>For a Tank with Circular Cross Section</u>

$$\omega_n^2 = \frac{k_n}{m_n}$$

$$\frac{m_n}{m} = \frac{2 \tanh(\epsilon_n \frac{h}{a})}{(\epsilon_n \frac{h}{a})(\epsilon_n^2 - 1)}$$ ratio of sloshing mass to liquid mass

$$\frac{h_n}{h} = \frac{1}{2}\left\{1 - \frac{4}{\epsilon_n \frac{h}{a}} \tanh\left(\frac{\epsilon_n}{2} \frac{h}{a}\right)\right\}$$

B. <u>For a Tank with Annular Cross Section</u>

$$\omega_{n-1}^2 = \frac{k_n}{m_n}$$

$$\frac{m_n}{m} = \frac{\bar{A}_{n-1}\left\{\frac{2}{\pi \xi_{n-1}} - k\, C_1 (k\, \xi_{n-1})\right\} \tanh\left(\xi_{n-1} \frac{h}{a}\right)}{(1 - k^2)\left(\xi_{n-1} \frac{h}{a}\right)}$$

$$\frac{h_n}{h} = \frac{1}{2}\left\{1 - \frac{4}{\xi_{n-1} \frac{h}{a}} \tanh\left(\frac{\xi_{n-1}}{2} \frac{h}{a}\right)\right\} \qquad n - 1$$

In Figures 2 through 6, the sloshing mass m_n and height ratios $\frac{h_n}{h}$ are shown versus the fluid height ratio $\frac{h}{a}$.

REFERENCES

1. Mario H. Rheinfurth: Control Feedback Analysis, ABMA Report No. DA-TR-2-60.

2. Helmut F. Bauer: Fluid Oscillations in a Circular Cylindrical Tank. ABMA Report No. DA-TR-1-58.

3. Helmut F. Bauer: Mechanical Analogy of Fluid Oscillations in Cylindrical Tanks with Circular and Annular Cross Section. Report No. MTP-AERO-61-4, NASA-Marshall Space Flight Center, January 12, 1961.

4. Helmut F. Bauer: Theory of the Fluid Oscillations in a Circular Cylindrical Ring Tank Partially Filled with Liquid. NASA Report No. TN D-557, December 1960.

5. Helmut F. Bauer: Theory of Fluid Oscillations in a Circular Cylindrical Quarter Tank Partially Filled with Liquid. (Unpublished.)

6. A. T. Fuller: Stability Criteria for Linear Systems and Reliability Criteria for RC Networks. Proc. of Camb. Phil. Soc. Vol. 53 (1957).

MECHANICAL MODEL FOR PROPELLANT SLOSHING

FIG. 1

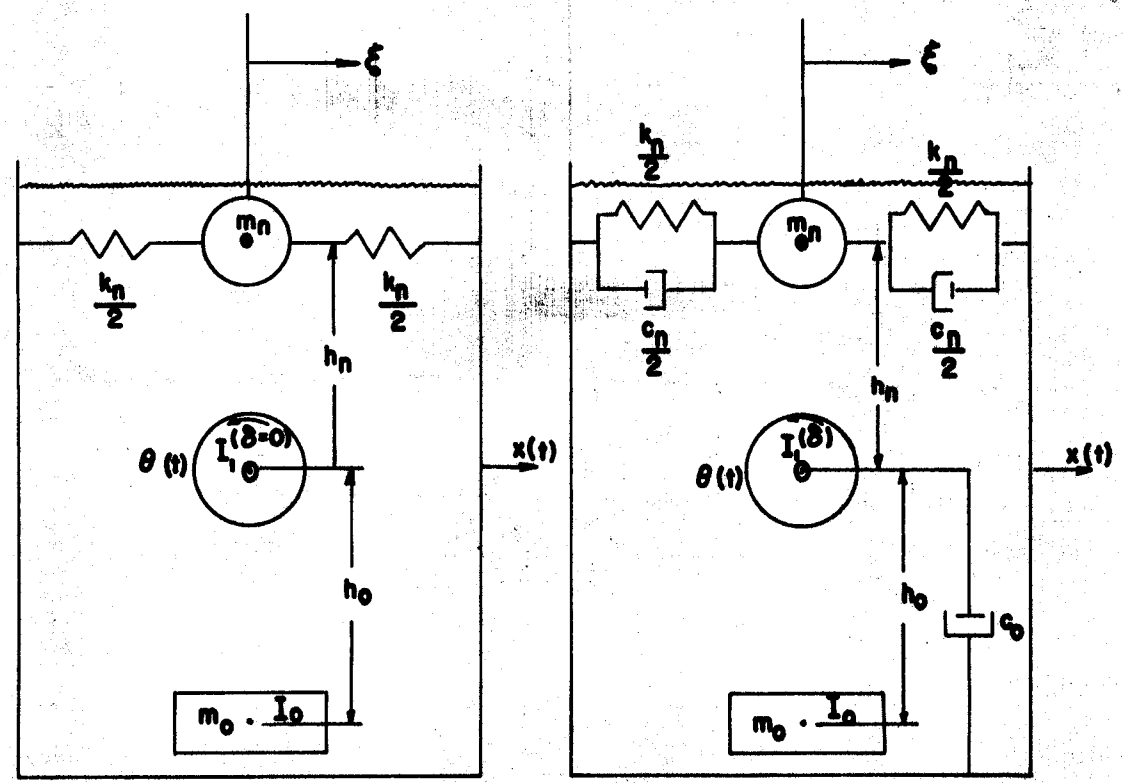

WITHOUT DAMPING

WITH DAMPING

FIG. 2

NATURAL FREQUENCIES OF LIQUID IN A CYLINDRICAL TANK

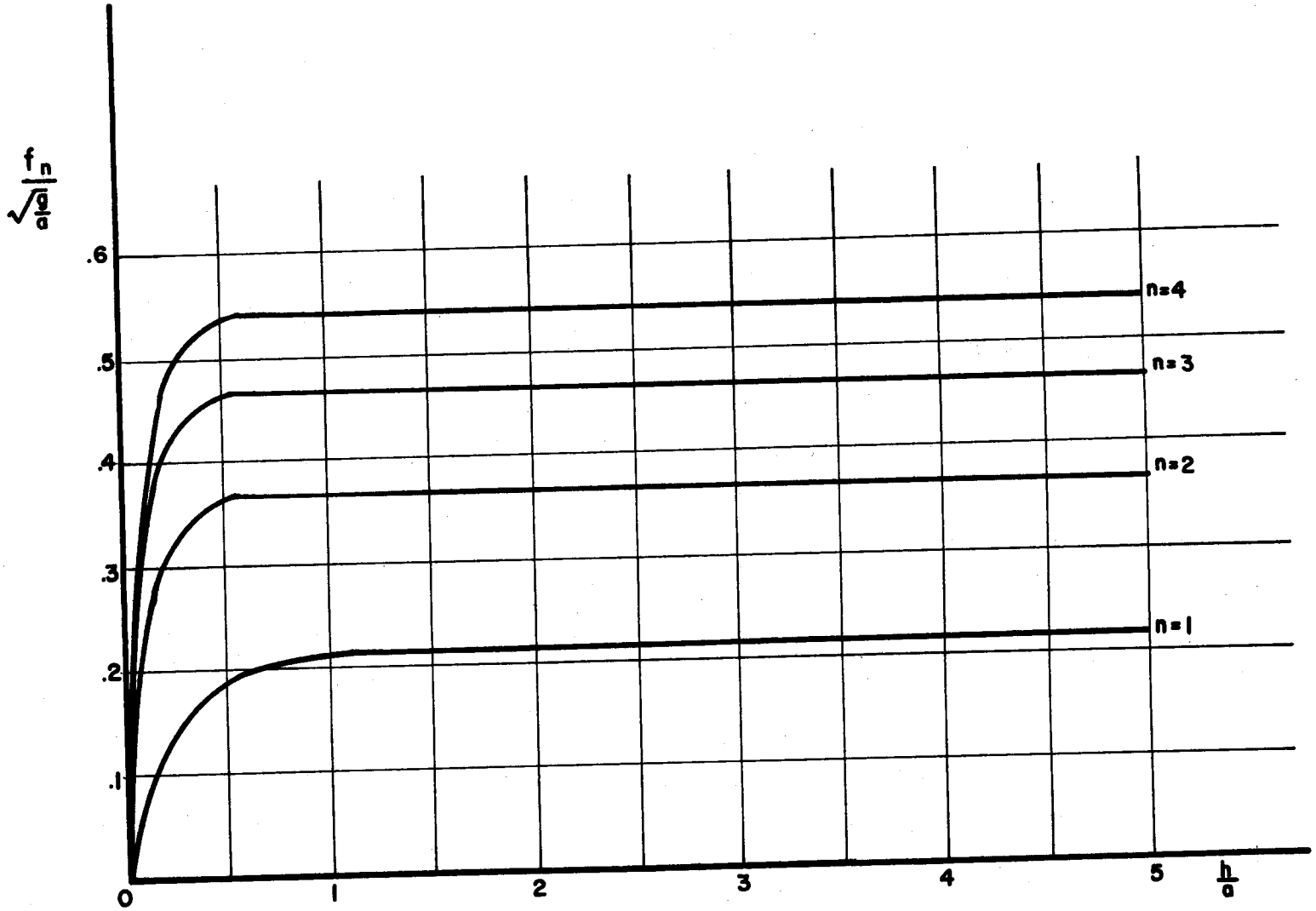

FIG. 2a

NATURAL FREQUENCIES OF PROPELLANT IN CIRCULAR CYLINDRICAL TANK WITH ANNULAR CROSS SECTION

VS

FLUID HEIGHT RATIO

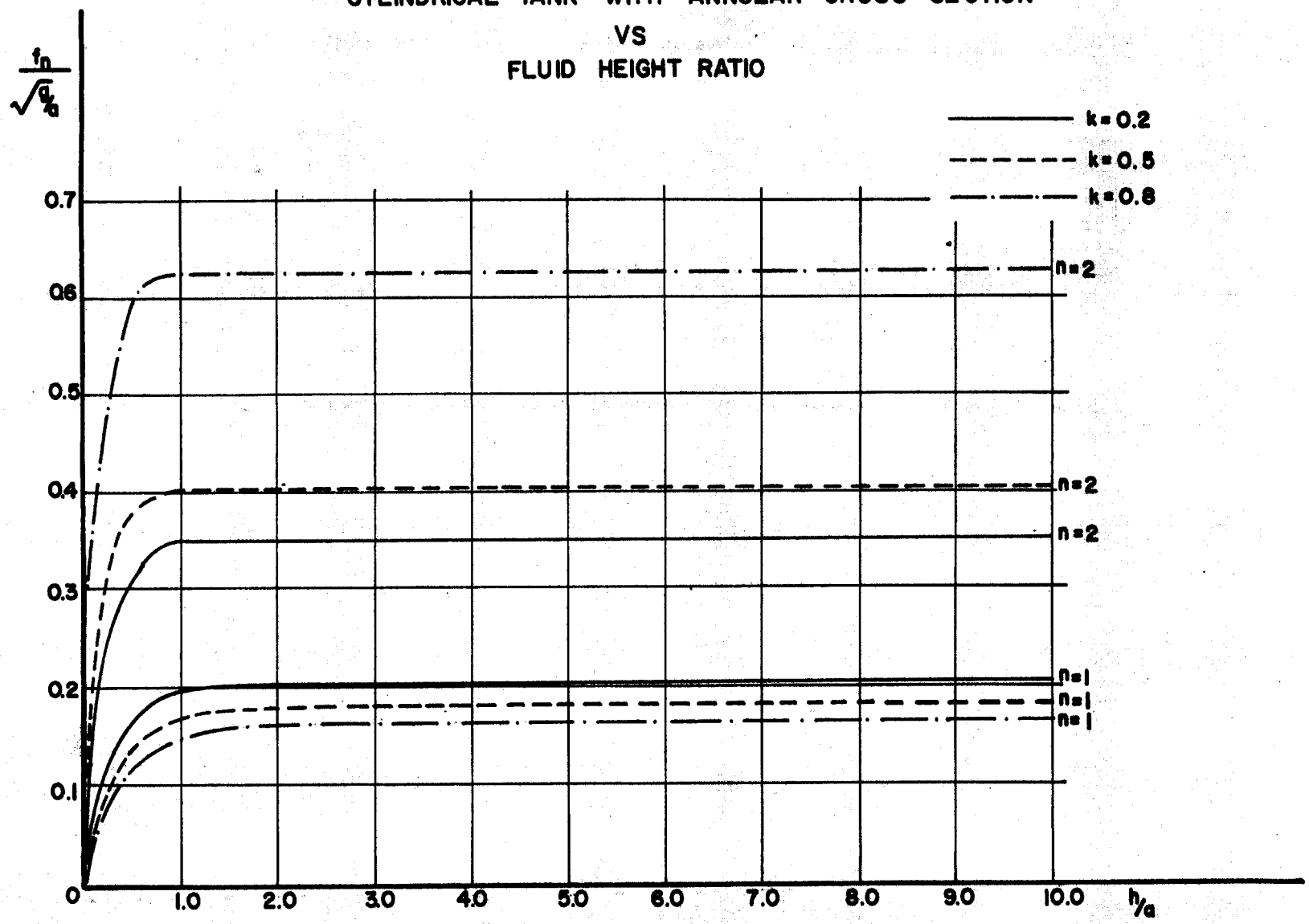

FIG. 3

NATURAL FREQUENCIES OF A LIQUID
IN A CYLINDRICAL QUARTER TANK
VS
FLUID HEIGHT RATIO

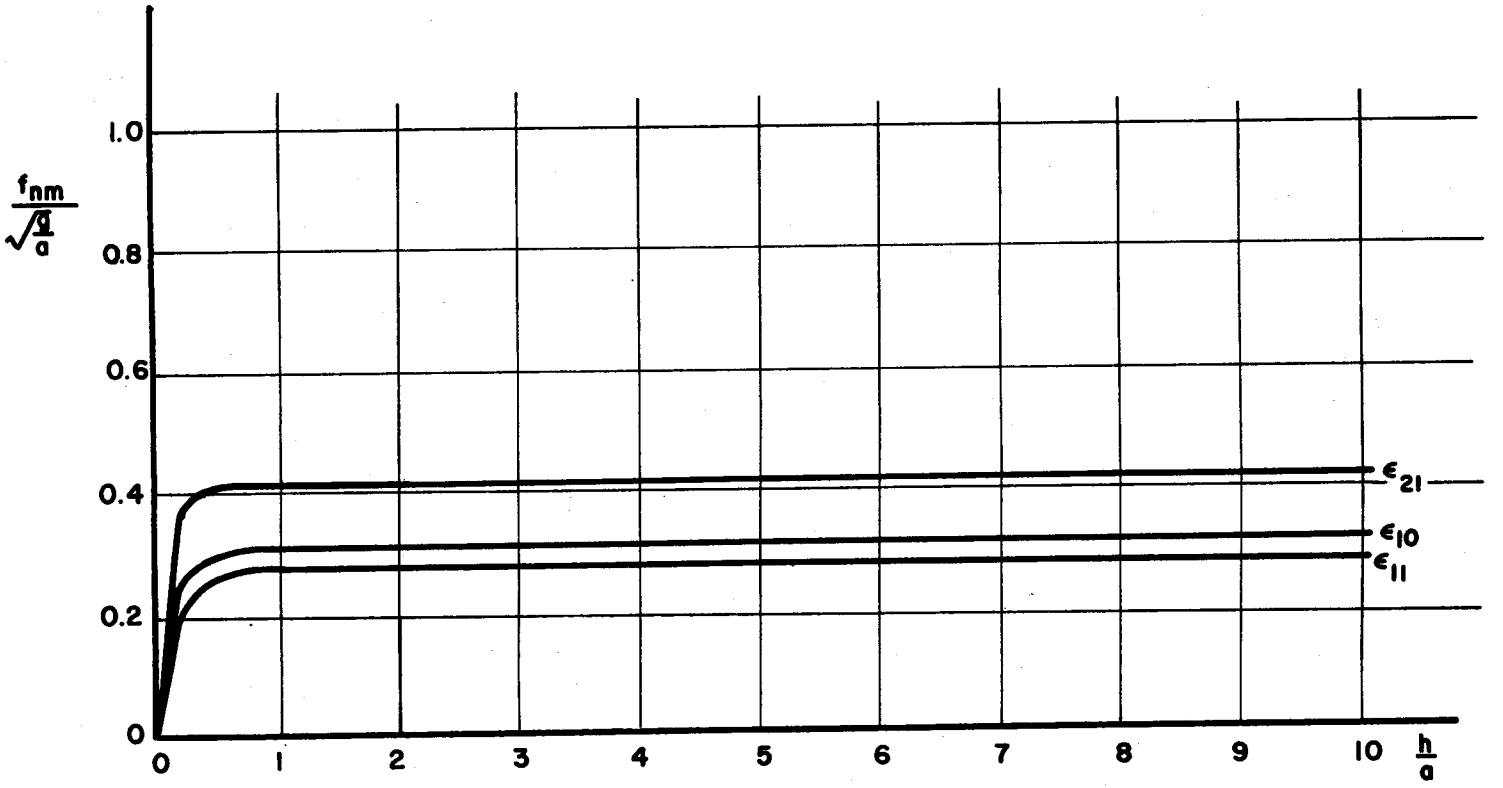

FIG. 14

SLOSHING MASS
VS
FLUID HEIGHT RATIO
FOR CYLINDRICAL TANK WITH
CIRCULAR CROSS SECTION

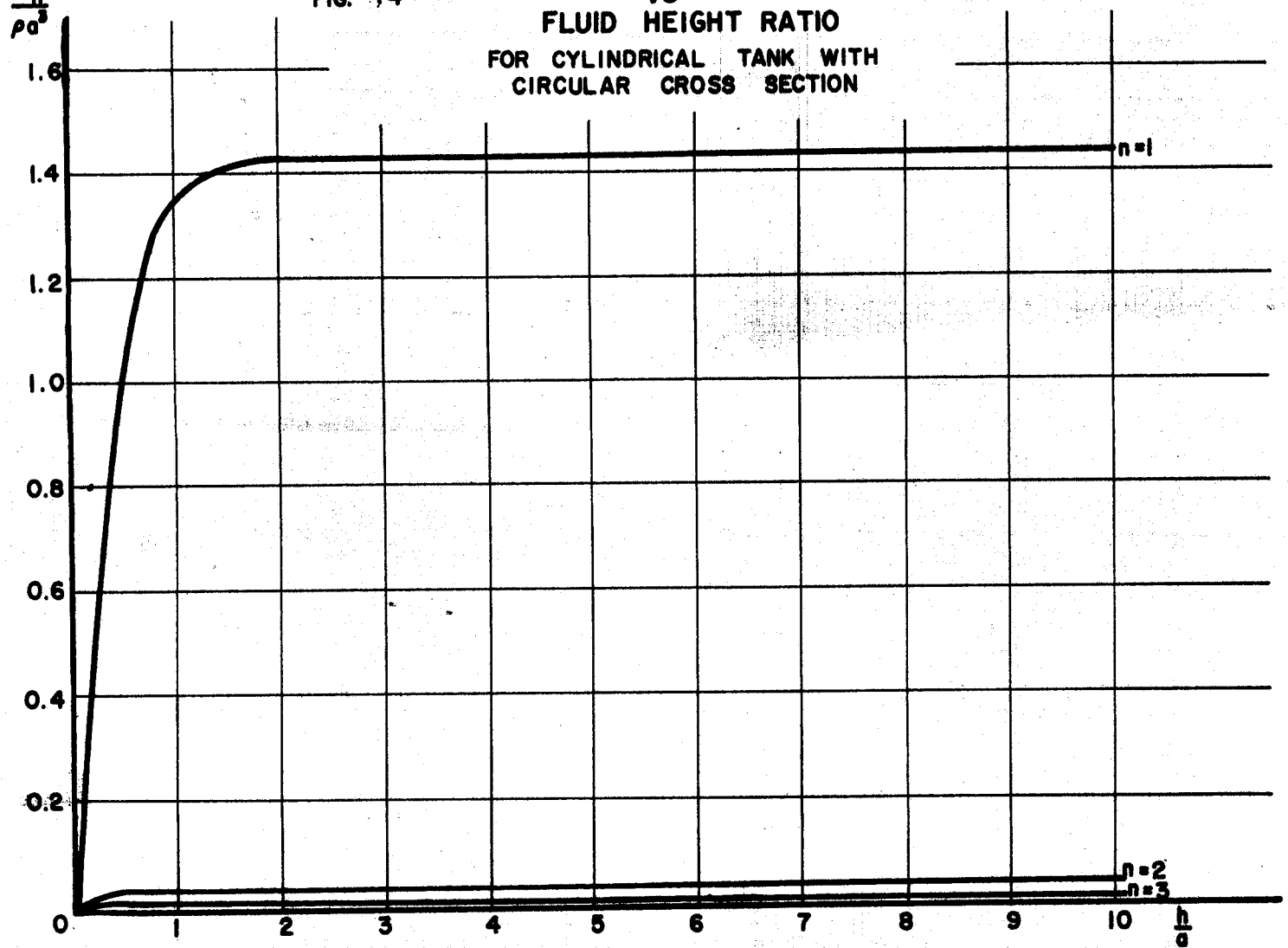

FIG. 5

SLOSHING MASS
VS
FLUID HEIGHT RATIO
FOR CYLINDRICAL TANK WITH
ANNULAR CROSS SECTION
K=0.5

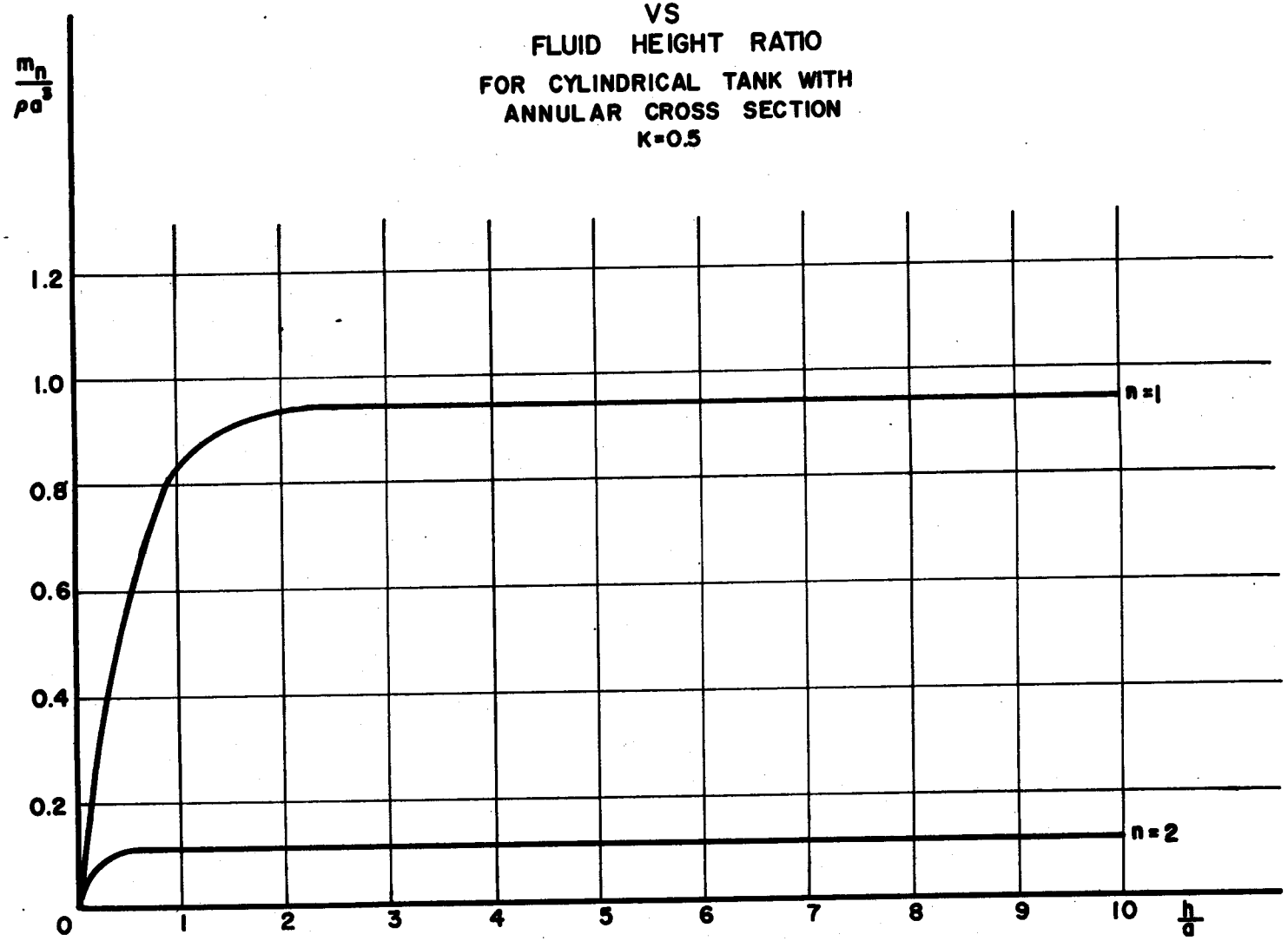

FIG. 6 SLOSHING MASS VS FLUID HEIGHT RATIO FOR FOUR CYLINDRICAL QUARTER TANKS

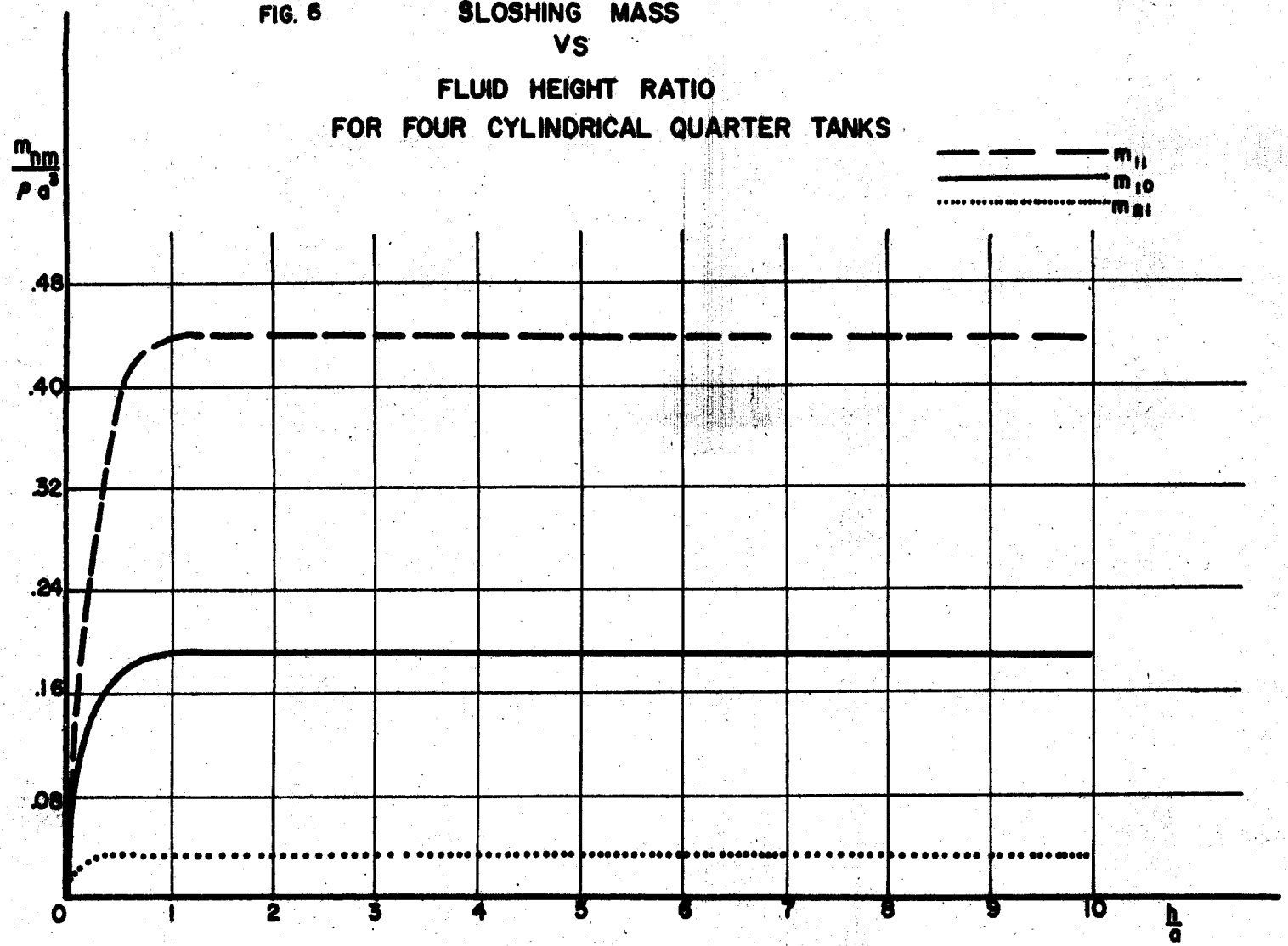

STABILITY BOUNDARY FOR RIGID ACCELEROMETER CONTROLLED SPACE VEHICLE (CASE A)

FIG. 7a

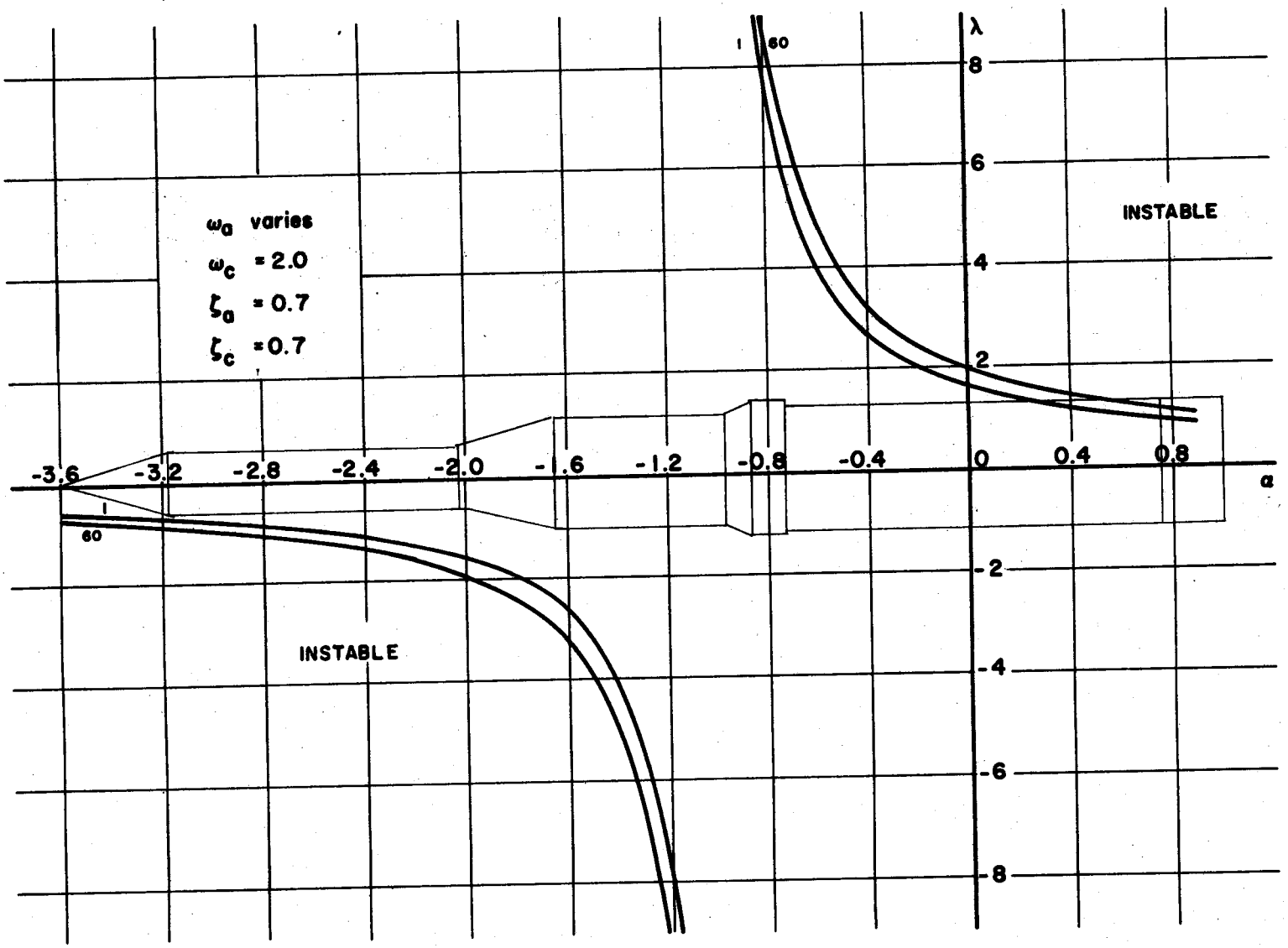

STABILITY BOUNDARY FOR RIGID
ACCELEROMETER CONTROLLED SPACE VEHICLE
(CASE A)

FIG. 7b

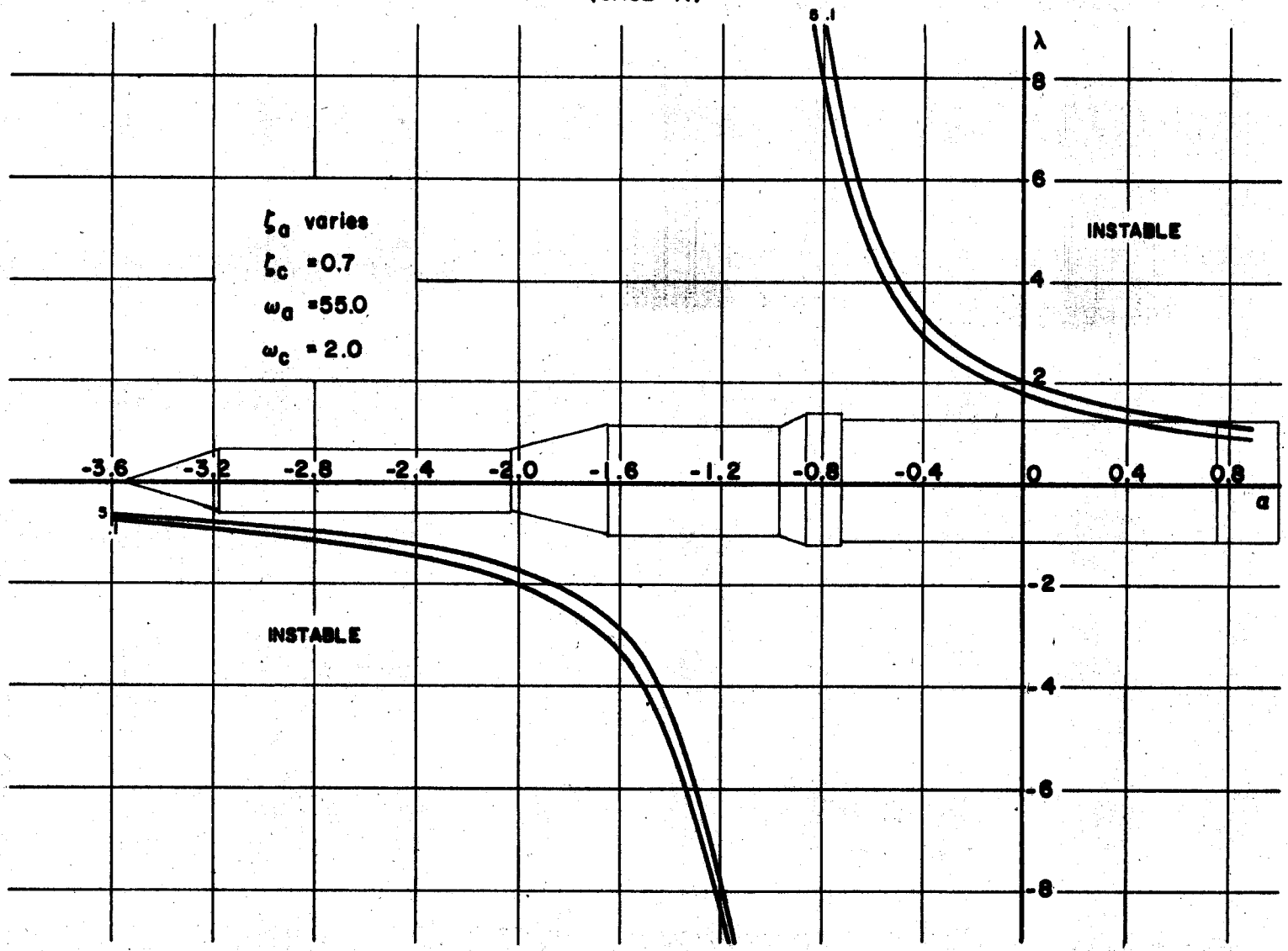

FIG. 7c

STABILITY BOUNDARY FOR RIGID ACCELEROMETER CONTROLLED SPACE VEHICLE (CASE A)

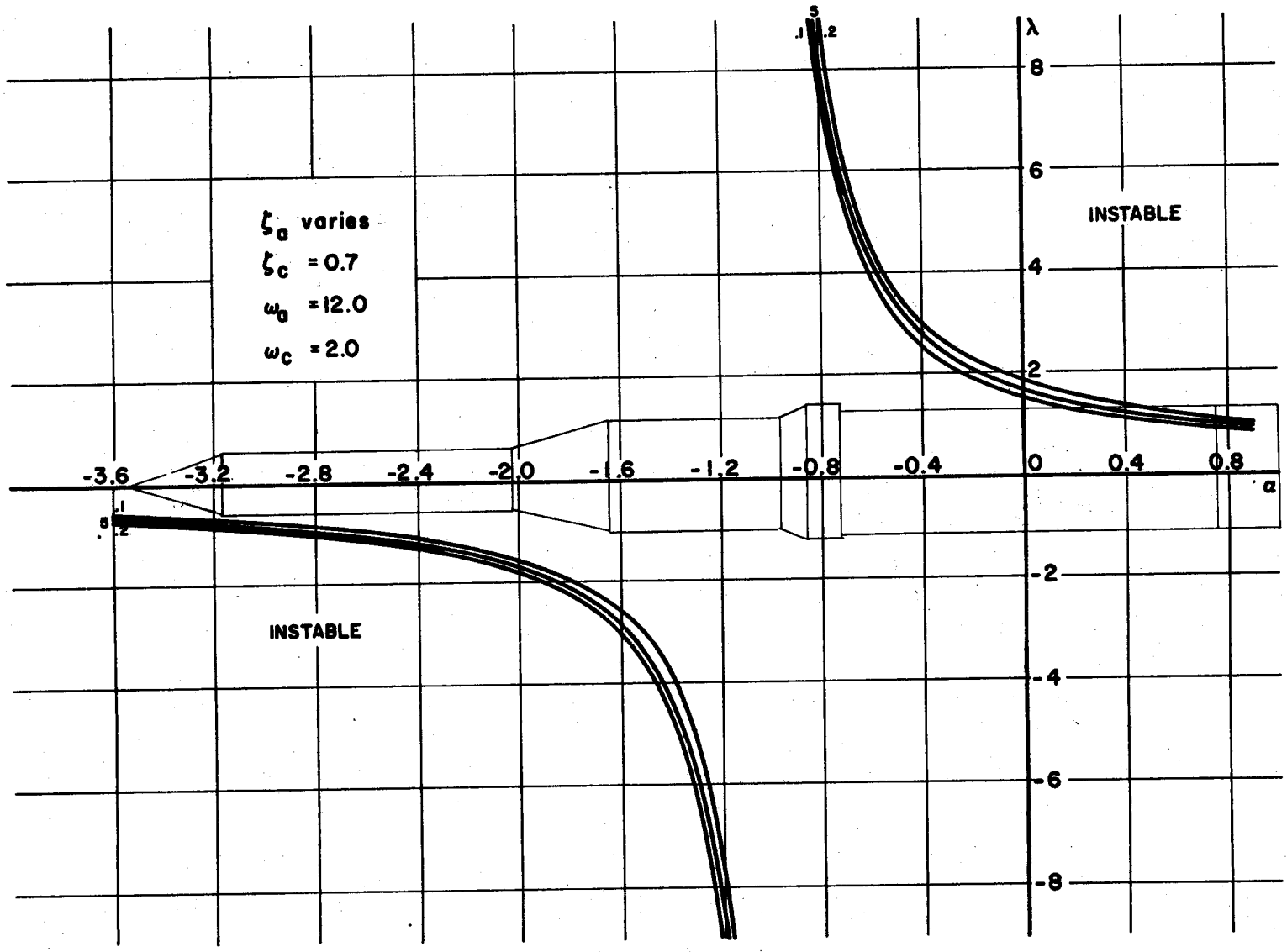

STABILITY BOUNDARY FOR RIGID
ACCELEROMETER CONTROLLED SPACE VEHICLE
(CASE A)

FIG. 7d

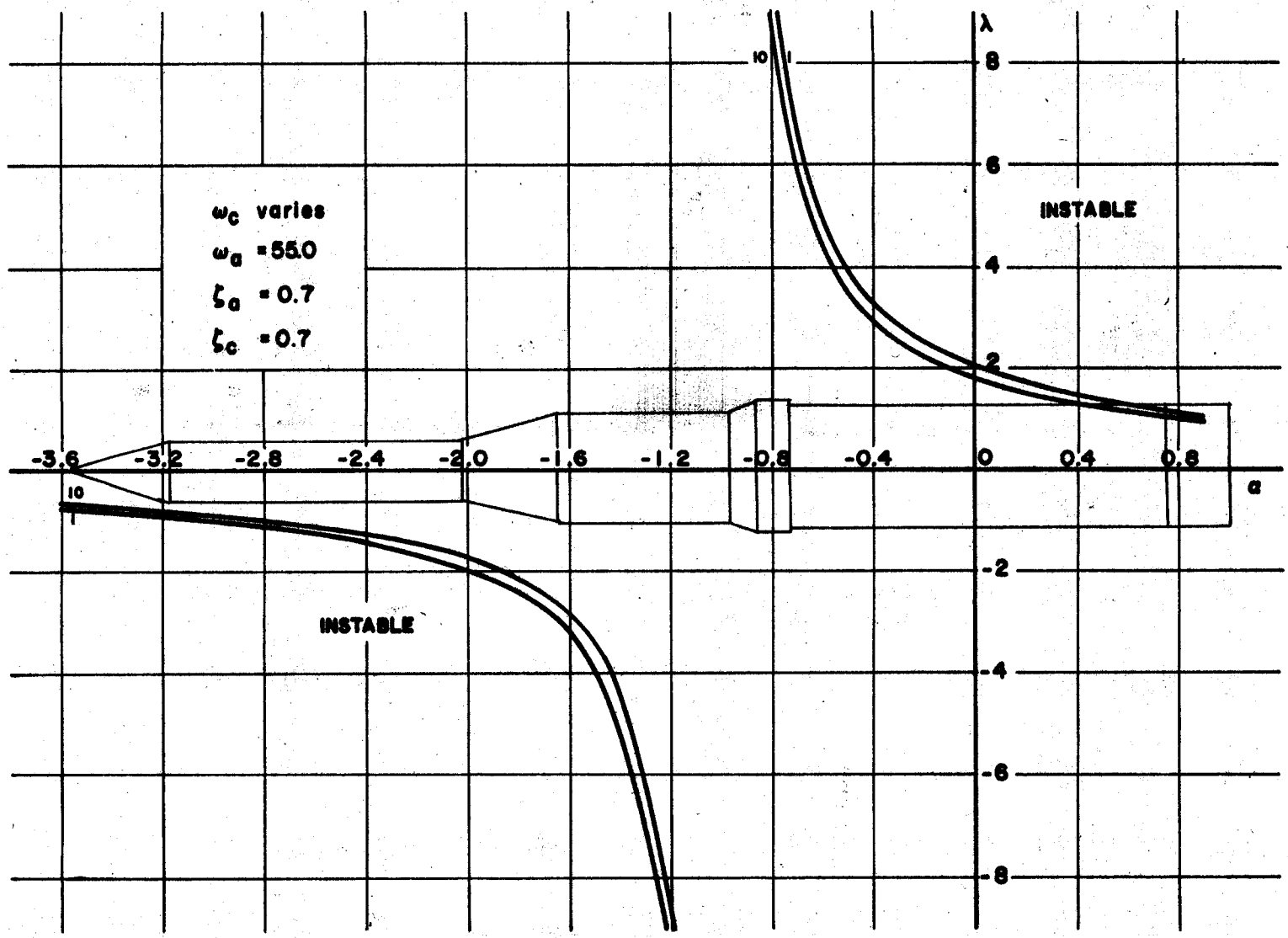

STABILITY BOUNDARY FOR RIGID ACCELEROMETER CONTROLLED SPACE VEHICLE (CASE A)

FIG. 7e

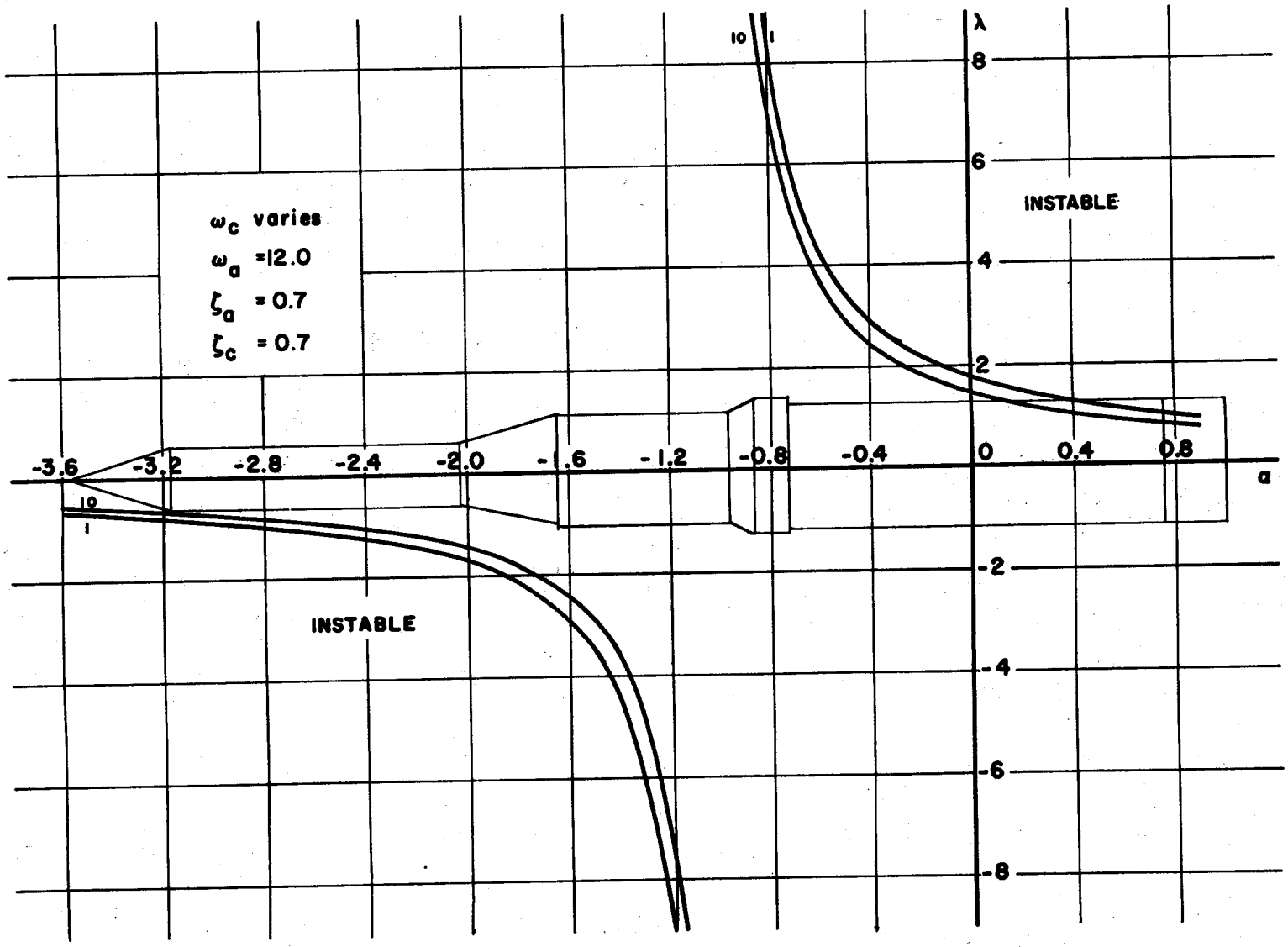

STABILITY BOUNDARY FOR RIGID
ACCELEROMETER CONTROLLED SPACE VEHICLE
(CASE A)

FIG. 71

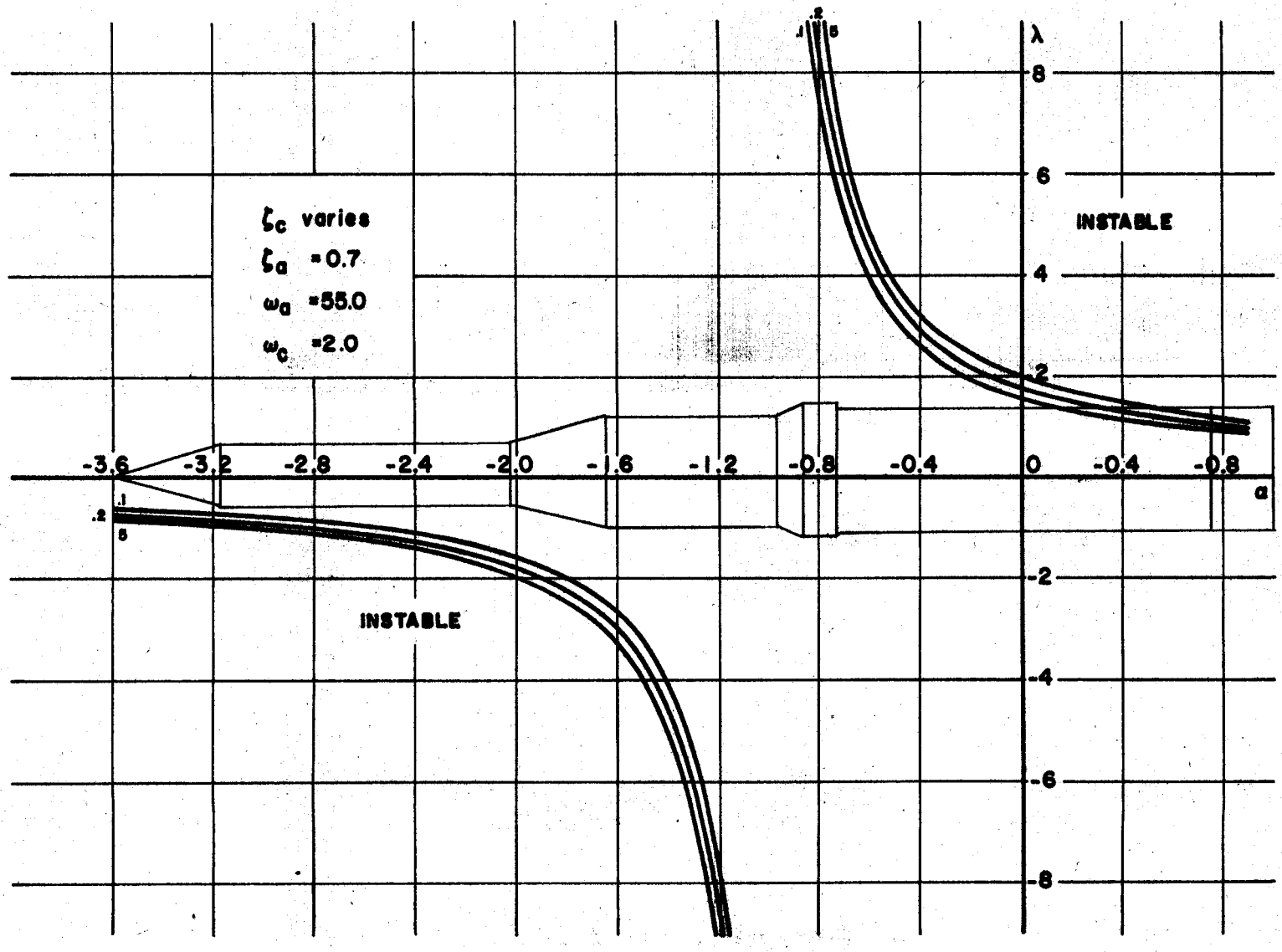

STABILITY BOUNDARY FOR RIGID
ACCELEROMETER CONTROLLED SPACE VEHICLE
(CASE A)

FIG. 7g

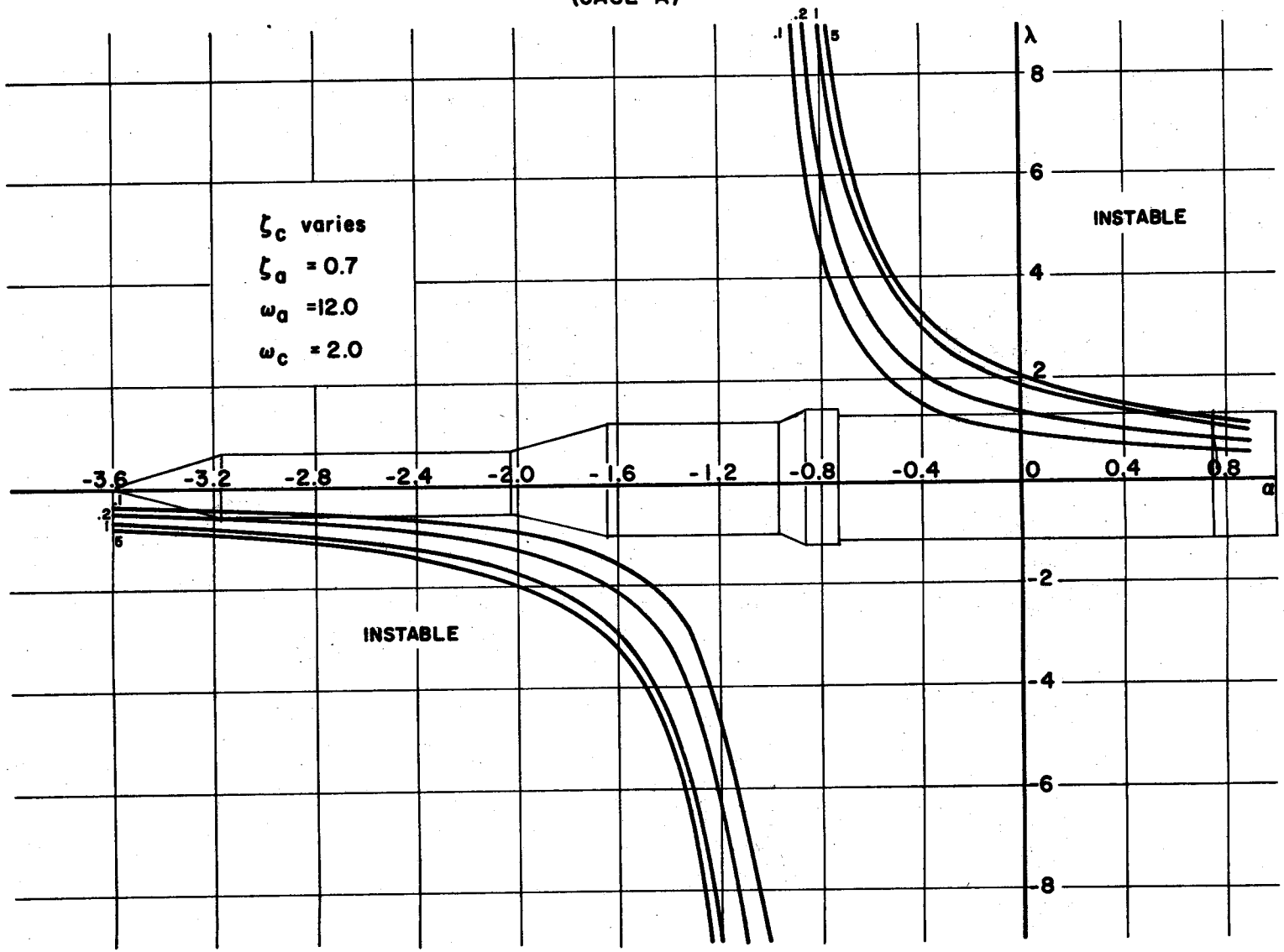

STABILITY BOUNDARY FOR RIGID SPACECRAFT FIG. 8a

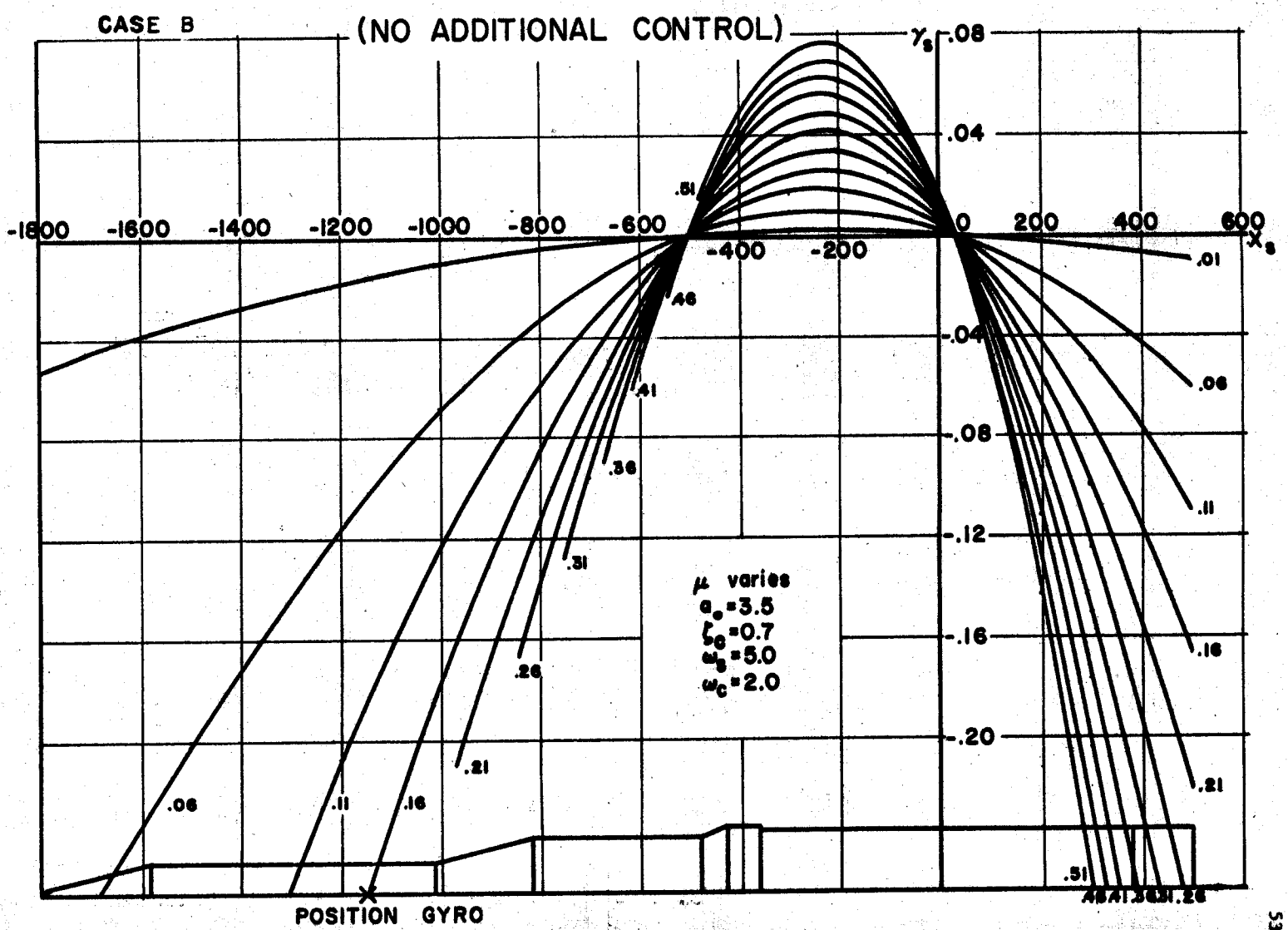

CASE B

FIG. 8b

STABILITY BOUNDARY FOR RIGID SPACECRAFT

(NO ADDITIONAL CONTROL)

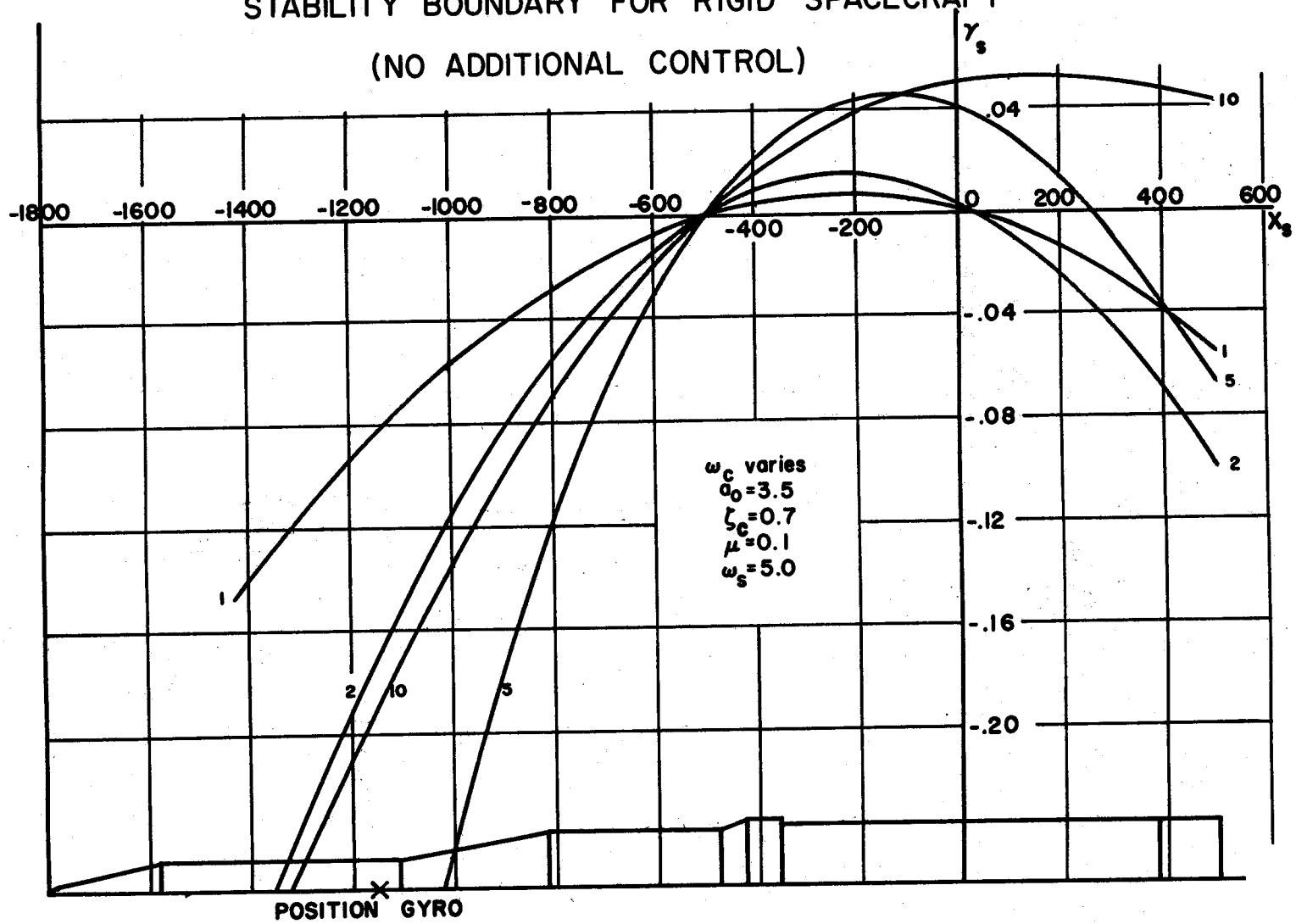

CASE B

STABILITY BOUNDARY FOR RIGID SPACECRAFT FIG. 8c

(NO ADDITIONAL CONTROL)

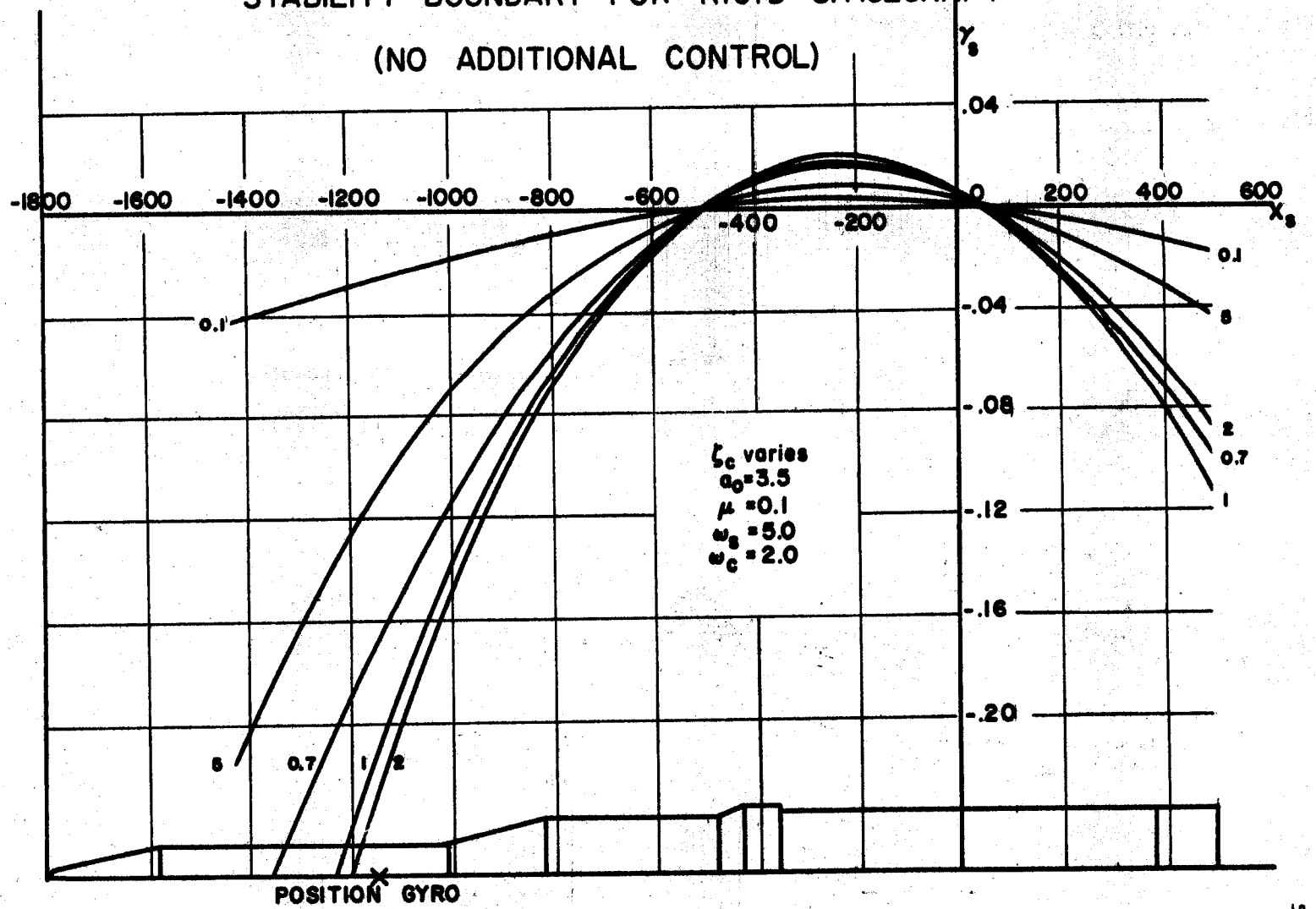

CASE B

FIG. 8d

STABILITY BOUNDARY FOR RIGID SPACECRAFT

(NO ADDITIONAL CONTROL)

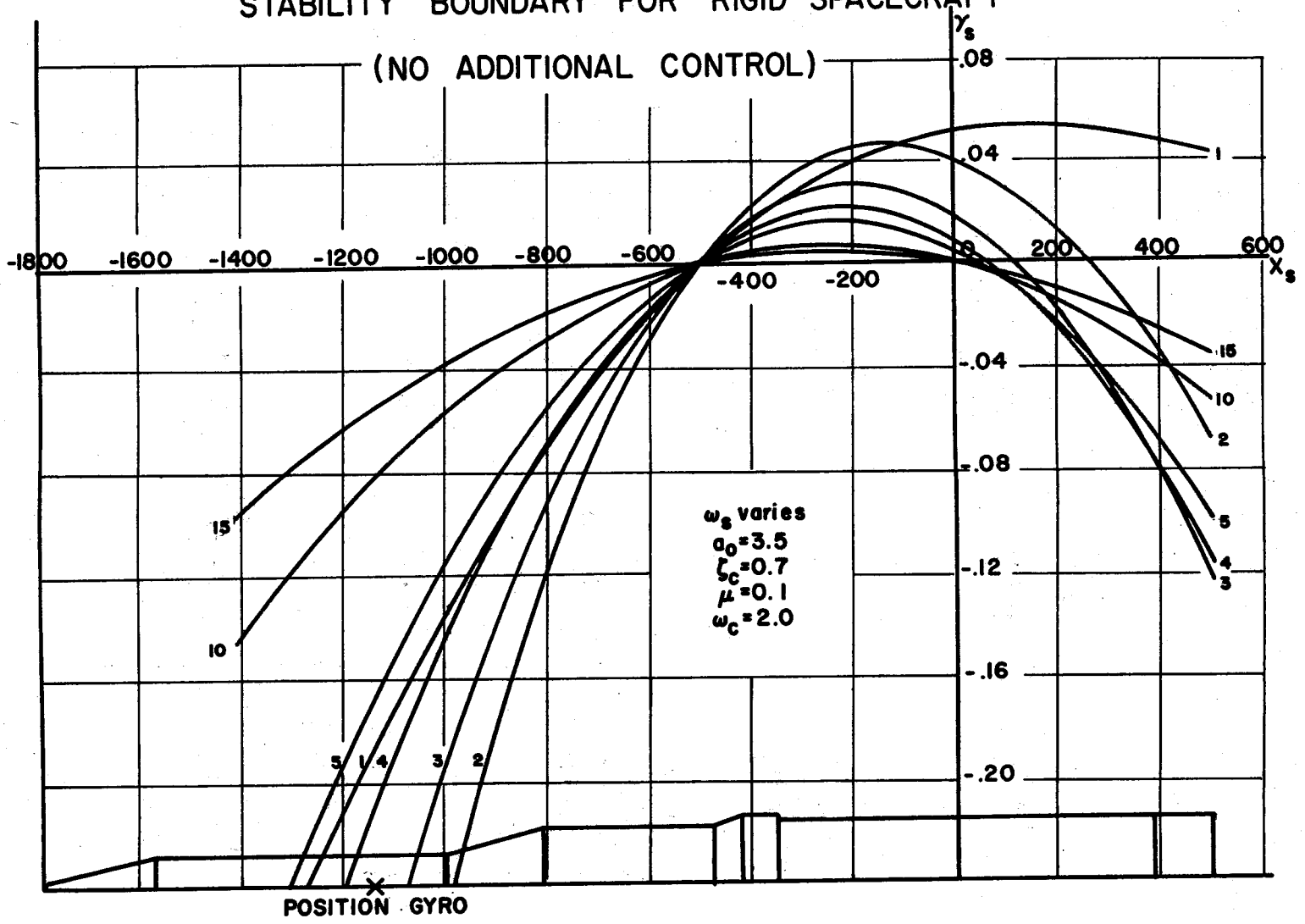

CASE B

STABILITY BOUNDARY FOR RIGID SPACECRAFT

(NO ADDITIONAL CONTROL)

FIG. 8e

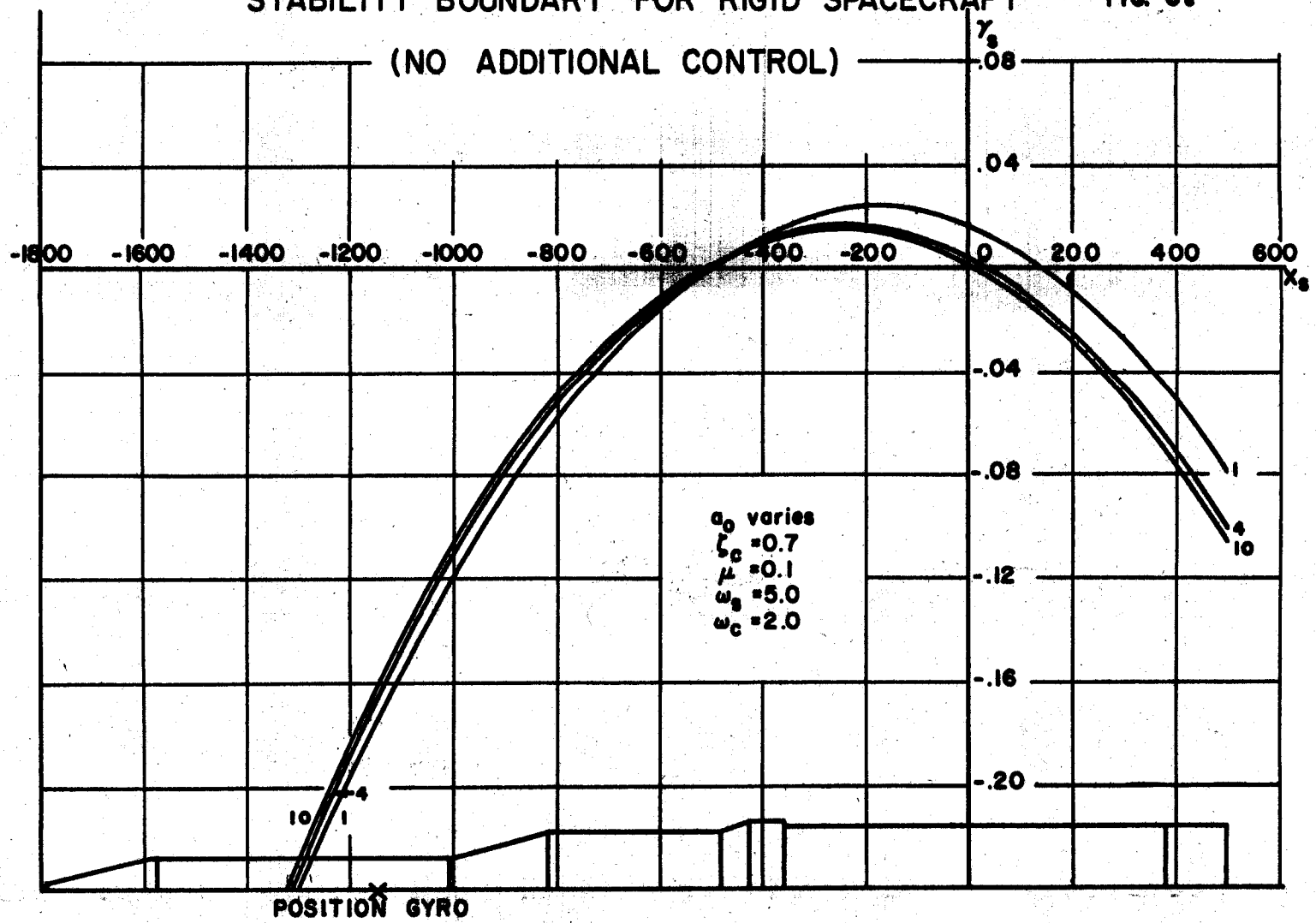

FIG. 9a

CASE C

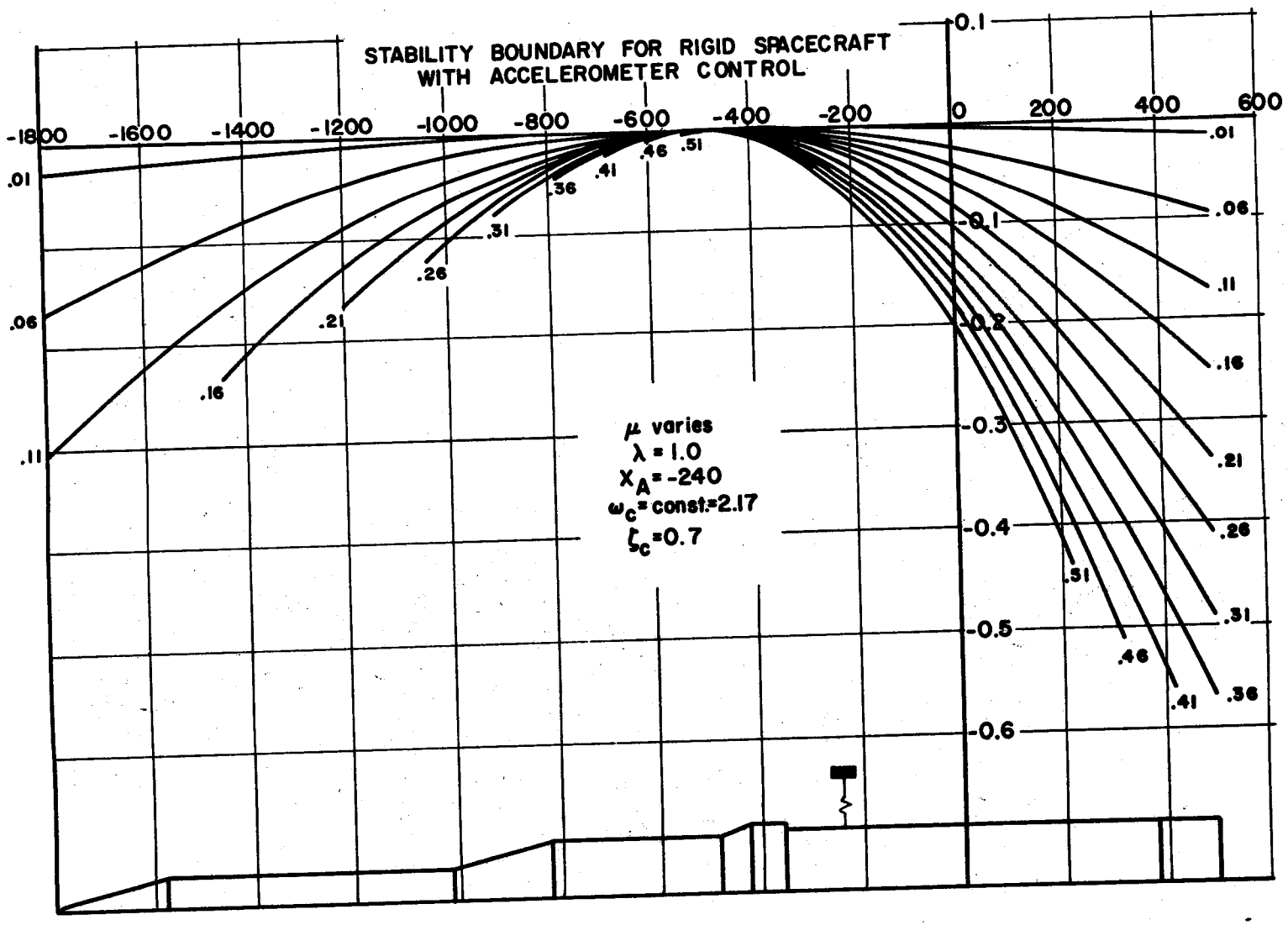
STABILITY BOUNDARY FOR RIGID SPACECRAFT
WITH ACCELEROMETER CONTROL
-1800
-1600
-1400
-1200
-1000
-800
-600
-400
-200
0
200
400
600
0.1
-0.1
-0.2
-0.3
-0.4
-0.5
-0.6
.01
.06
.11
.16
.21
.26
.31
.36
.41
.46
.51
μ varies
λ = 1.0
X_A = -240
ω_c = const.=2.17
ζ_c =0.7

FIG. 9b

CASE C

STABILITY BOUNDARY FOR RIGID SPACECRAFT WITH ACCELEROMETER CONTROL

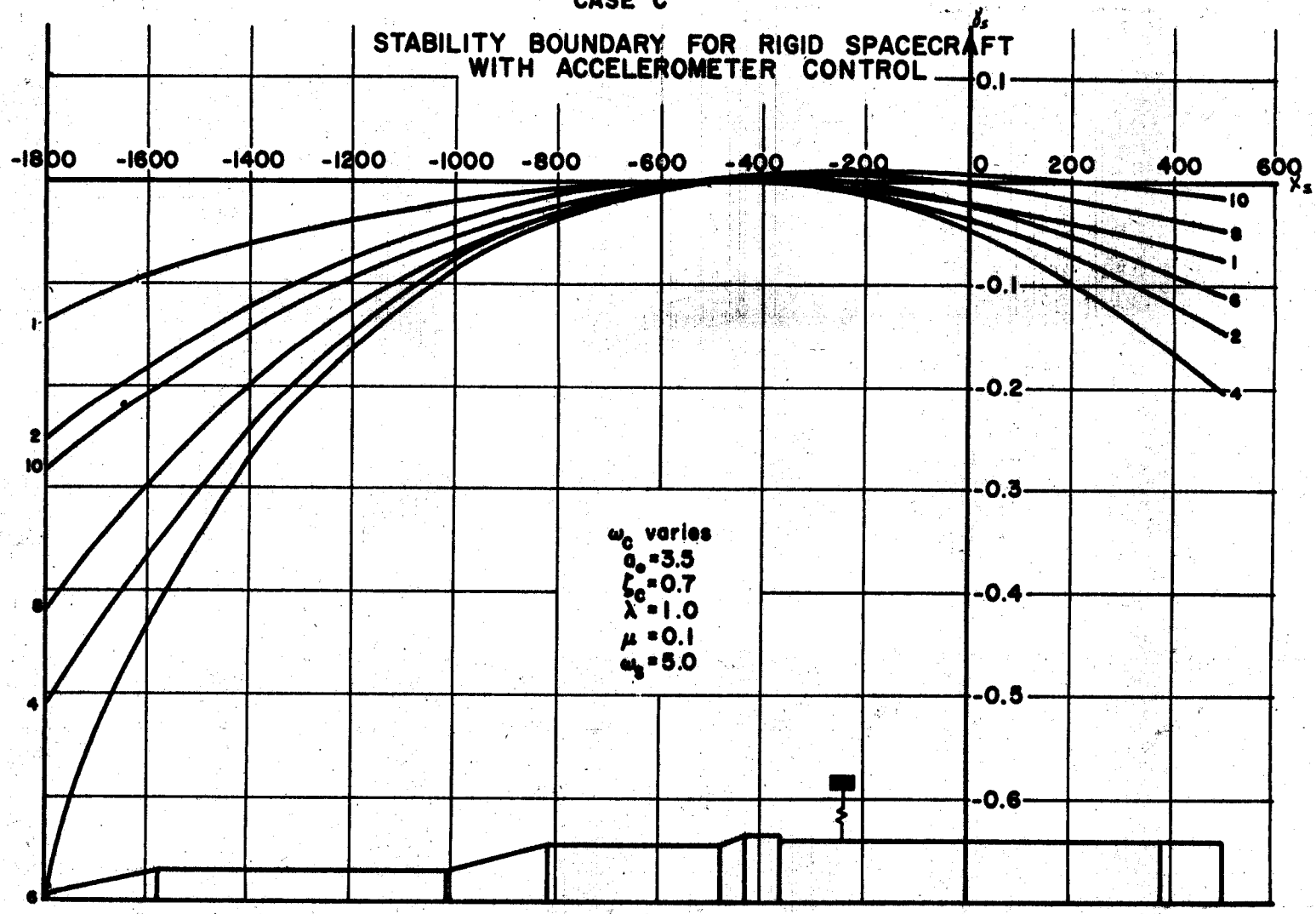

CASE C

FIG. 9c

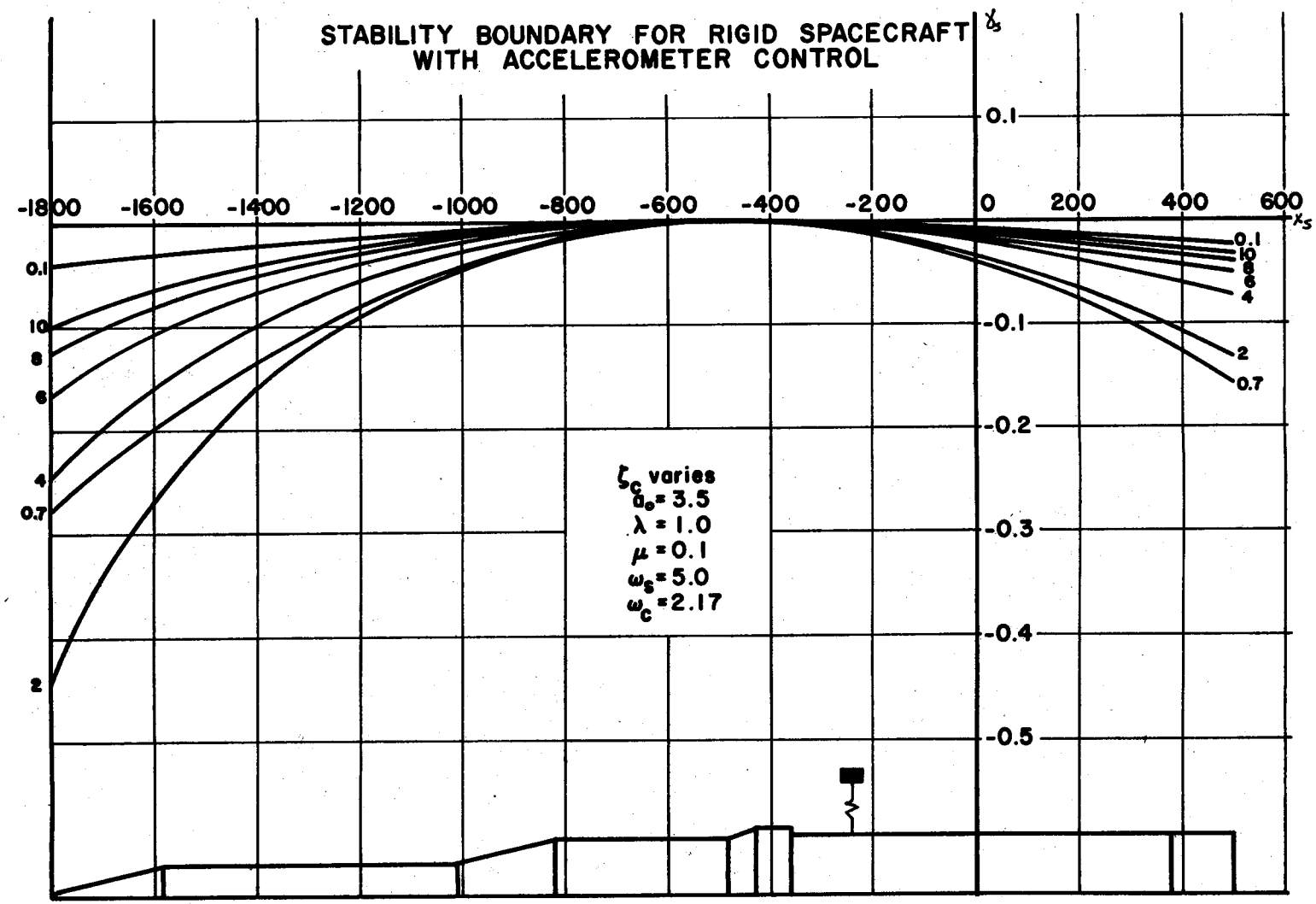
STABILITY BOUNDARY FOR RIGID SPACECRAFT
WITH ACCELEROMETER CONTROL
$\dot{x}_s$
x_s
-1800
-1600
-1400
-1200
-1000
-800
-600
-400
-200
0
200
400
600
0.1
-0.1
-0.2
-0.3
-0.4
-0.5
0.1
10
8
6
4
0.7
2
ζ_c varies
$a_o = 3.5$
$\lambda = 1.0$
$\mu = 0.1$
$\omega_s = 5.0$
$\omega_c = 2.17$

CASE C

FIG. 9d

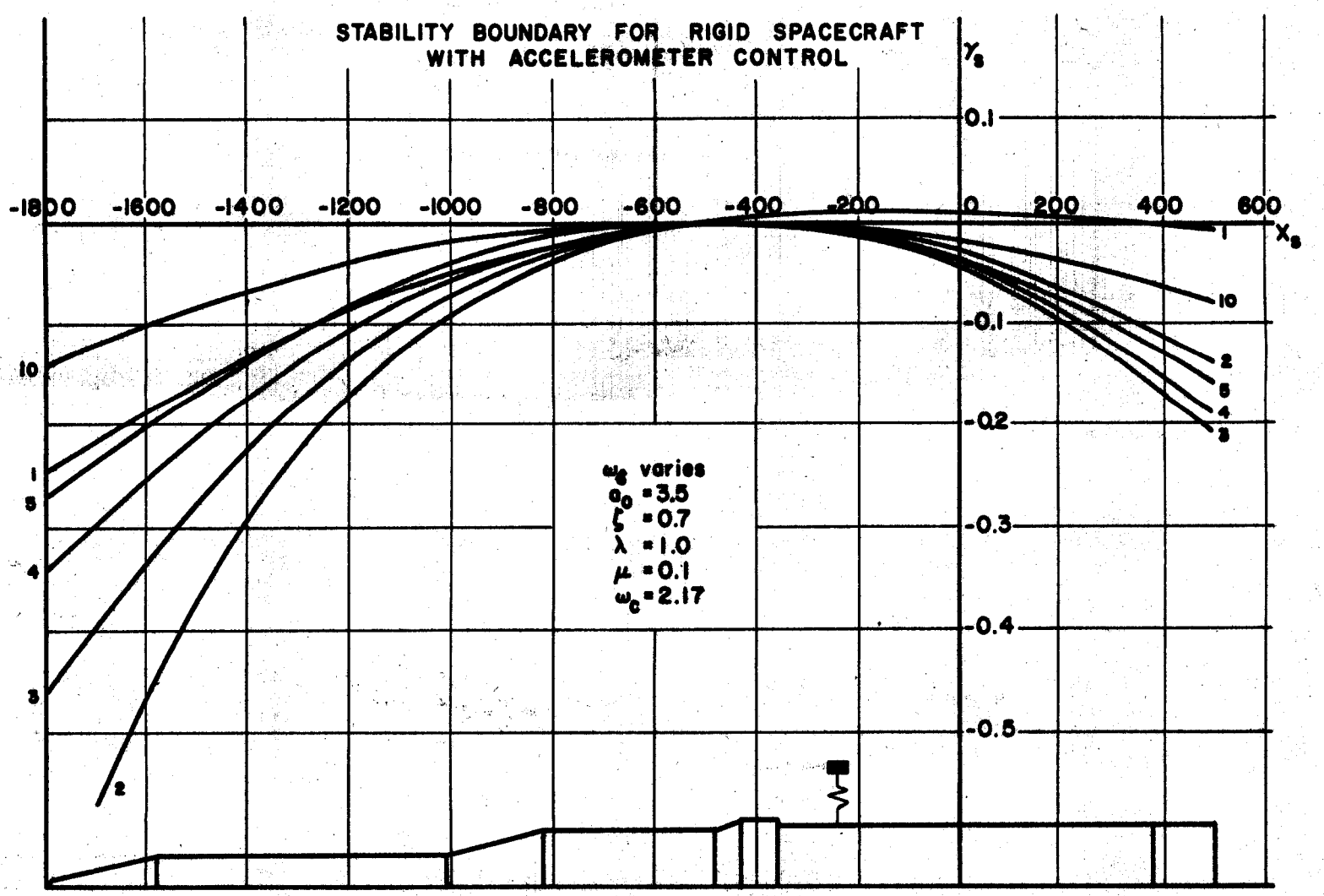
STABILITY BOUNDARY FOR RIGID SPACECRAFT
WITH ACCELEROMETER CONTROL
Y_s
X_s
0.1
-0.1
-0.2
-0.3
-0.4
-0.5
-1800
-1600
-1400
-1200
-1000
-800
-600
-400
-200
0
200
400
600
1
10
2
5
4
3
ω_s varies
a_0 = 3.5
ζ = 0.7
λ = 1.0
μ = 0.1
ω_c = 2.17

CASE C

FIG. 9e

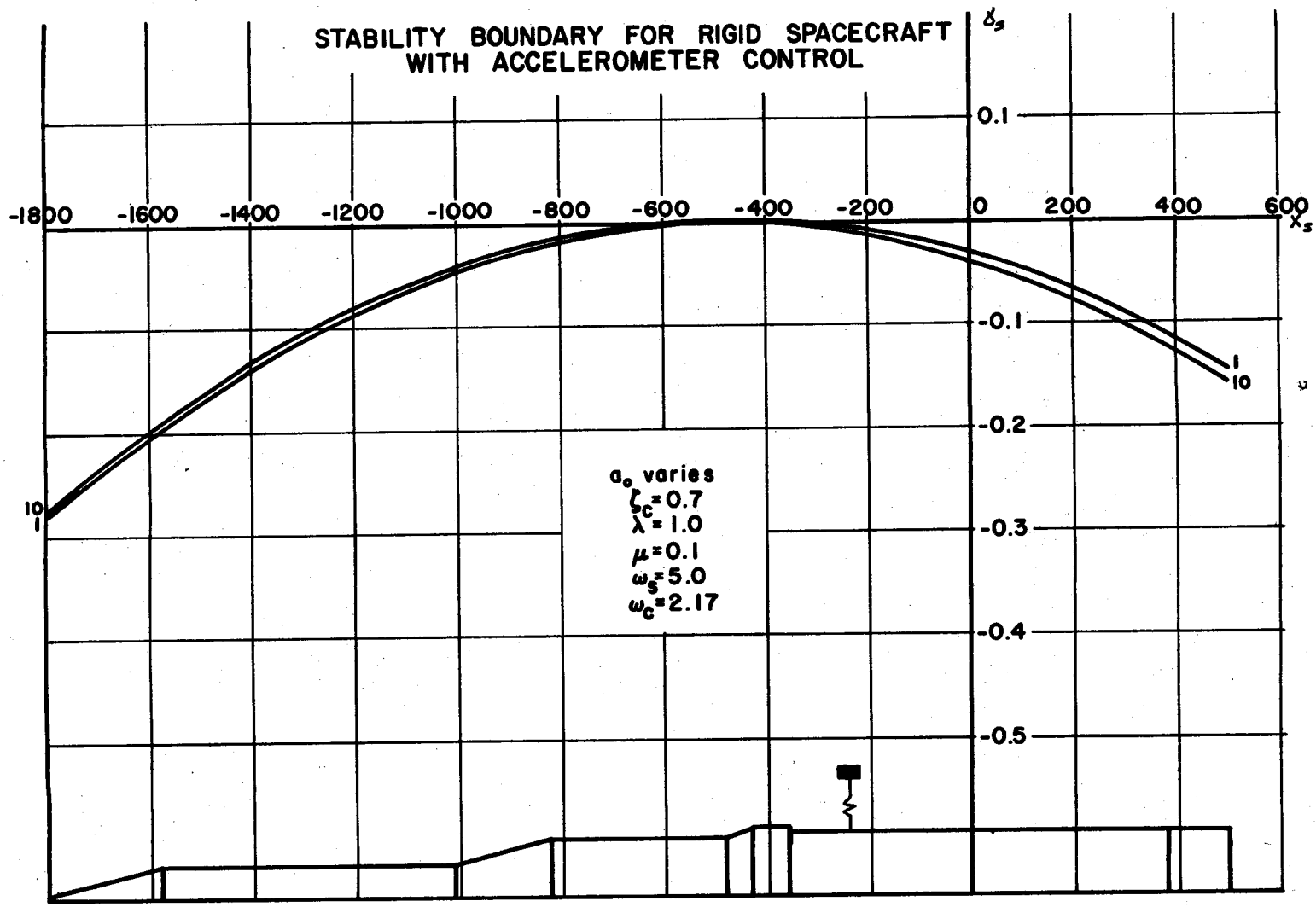
STABILITY BOUNDARY FOR RIGID SPACECRAFT
WITH ACCELEROMETER CONTROL
δ_s
0.1
-0.1
-0.2
-0.3
-0.4
-0.5
-1800
-1600
-1400
-1200
-1000
-800
-600
-400
-200
0
200
400
600
X_s
1
10
10
1
a_o varies
$\zeta_c = 0.7$
$\lambda = 1.0$
$\mu = 0.1$
$\omega_s = 5.0$
$\omega_c = 2.17$

CASE C

FIG. 9f

STABILITY BOUNDARY FOR RIGID SPACECRAFT WITH ACCELEROMETER CONTROL

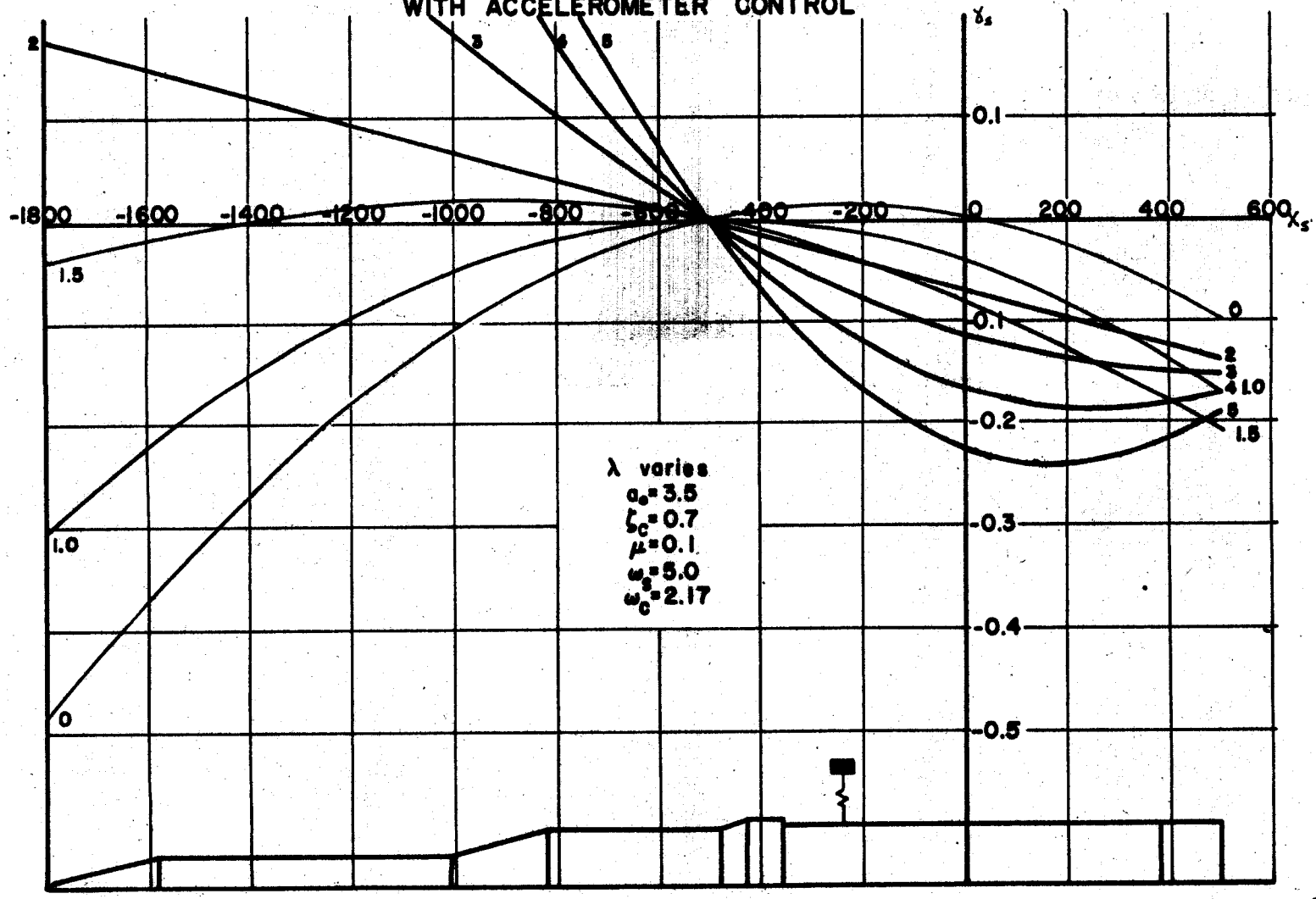

CASE C

FIG. 9g

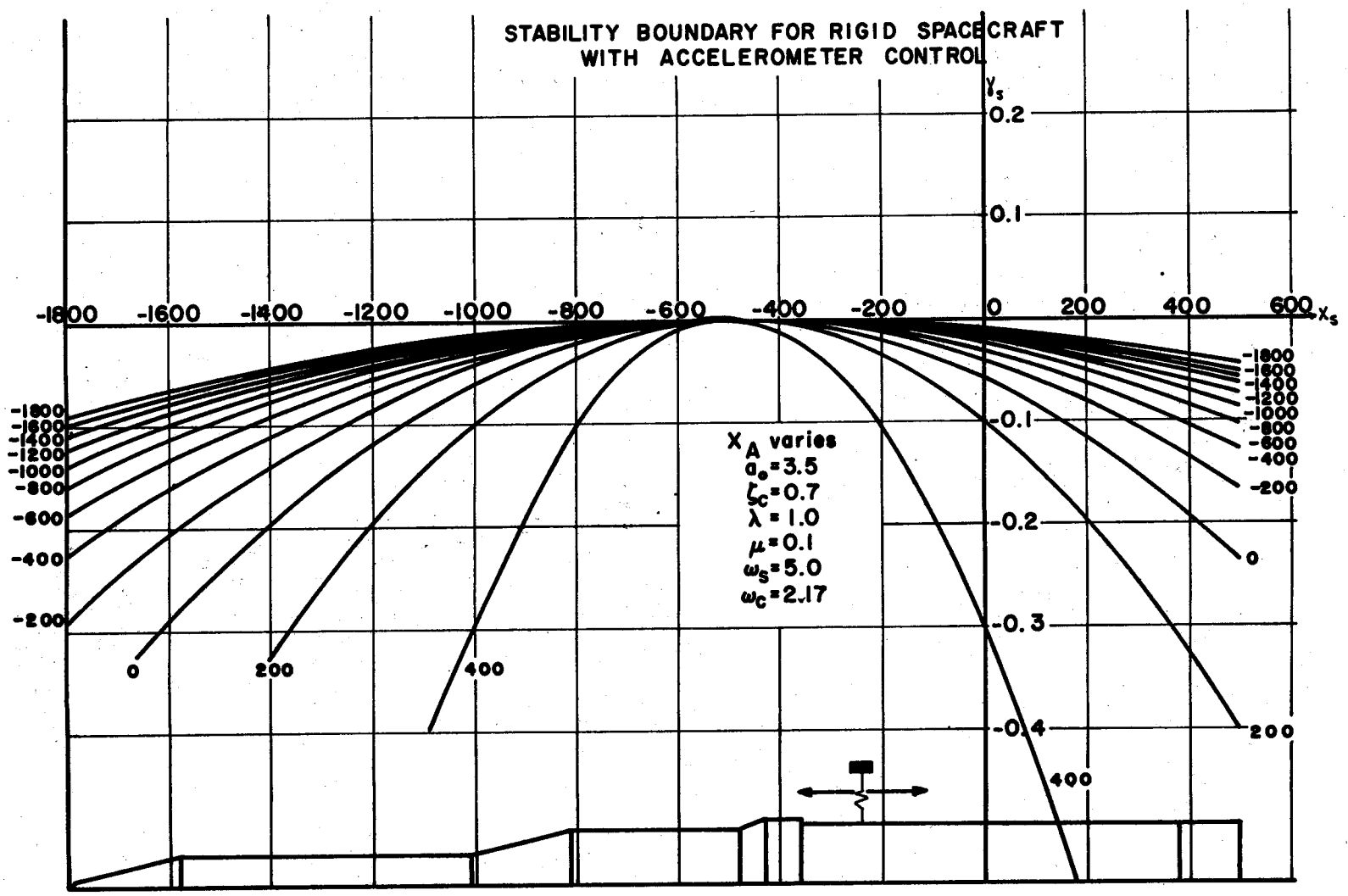
STABILITY BOUNDARY FOR RIGID SPACECRAFT
WITH ACCELEROMETER CONTROL
γ_s
0.2
0.1
-0.1
-0.2
-0.3
-0.4
-1800
-1600
-1400
-1200
-1000
-800
-600
-400
-200
0
200
400
600
X_s
X_A varies
a_e=3.5
ζ_c=0.7
λ=1.0
μ=0.1
ω_s=5.0
ω_c=2.17

CASE C FIG. 9h

STABILITY BOUNDARY FOR RIGID SPACECRAFT WITH ACCELEROMETER CONTROL

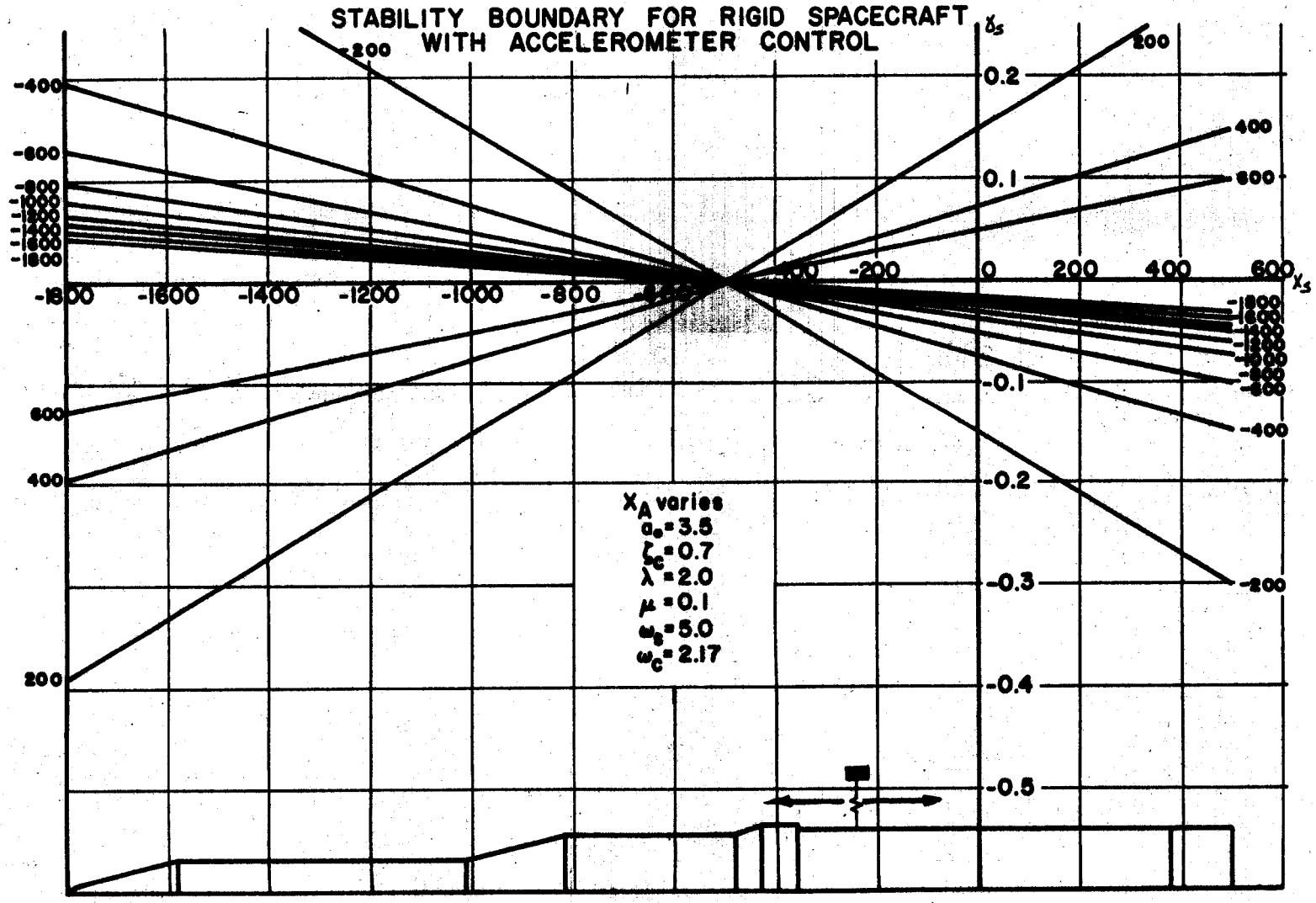

CASE D

STABILITY BOUNDARY FOR RIGID SPACECRAFT
WITH REAL ACCELEROMETER CONTROL

FIG. 10a

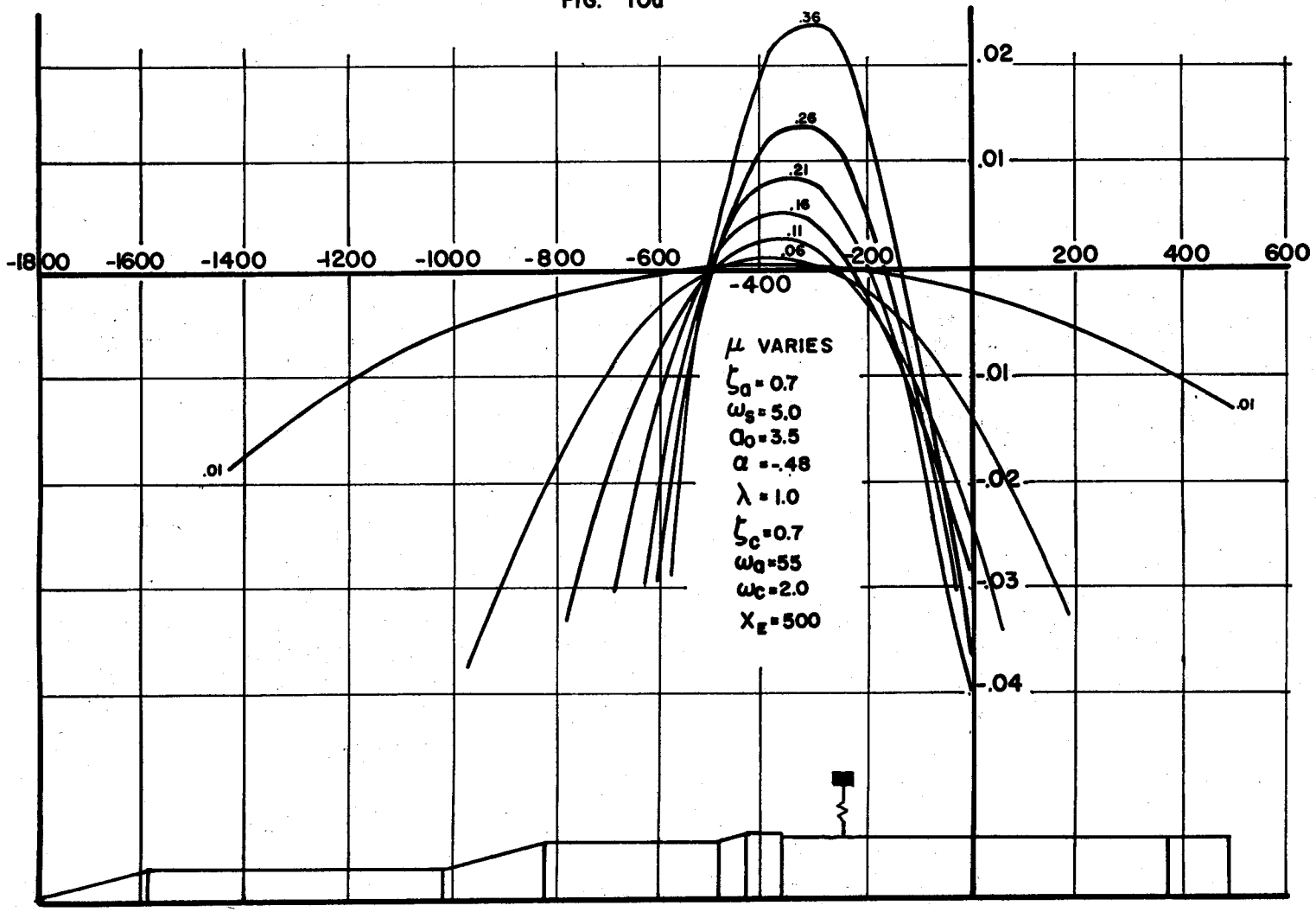

CASE D

STABILITY BOUNDARY FOR RIGID SPACE VEHICLE
WITH REAL ACCELEROMETER CONTROL

FIG. 10b

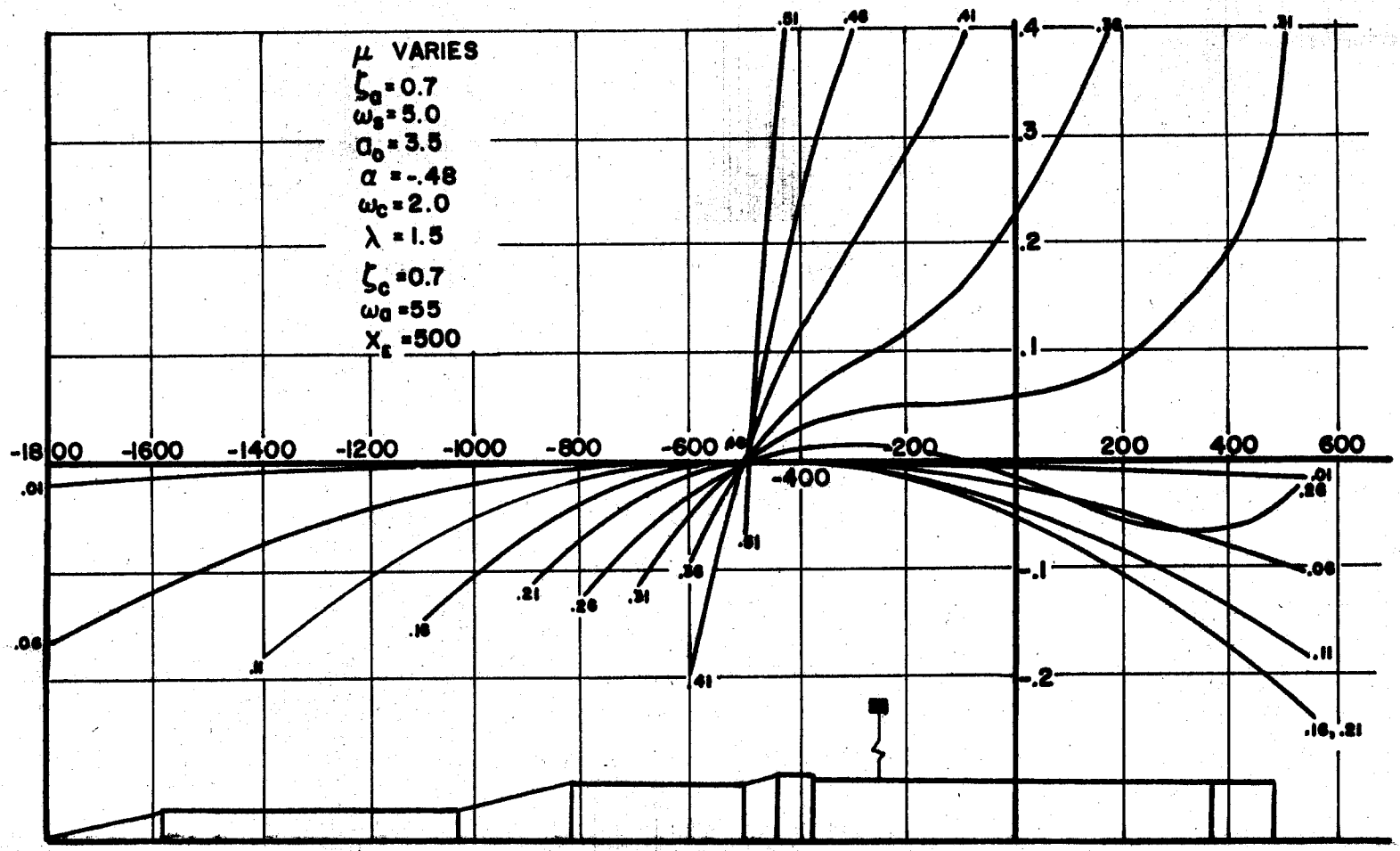

CASE D

STABILITY BOUNDARY FOR RIGID SPACECRAFT WITH REAL ACCELEROMETER CONTROL

FIG. 10c

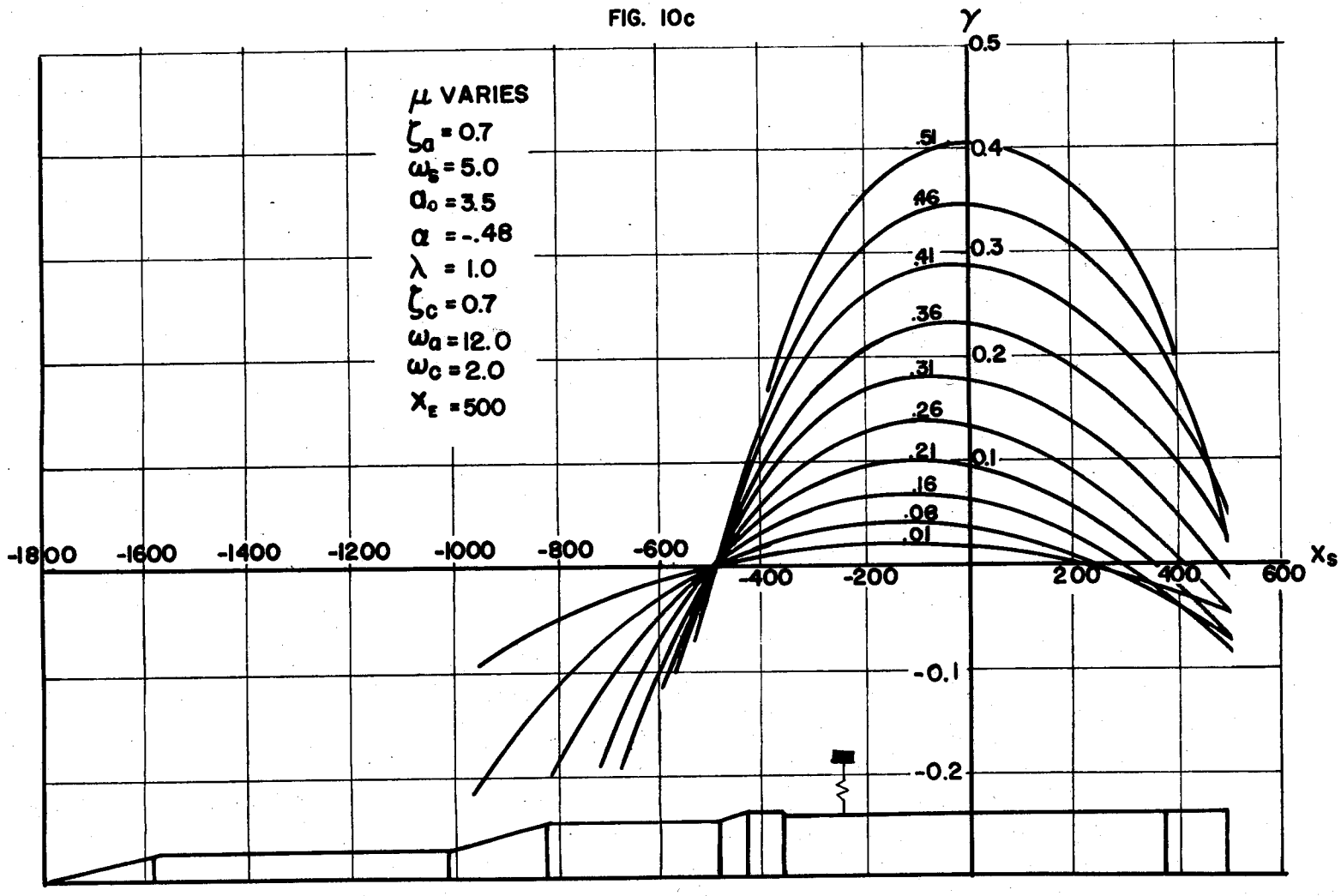

CASE D

STABILITY BOUNDARY FOR RIGID SPACECRAFT
WITH REAL ACCELEROMETER CONTROL

FIG. 10d

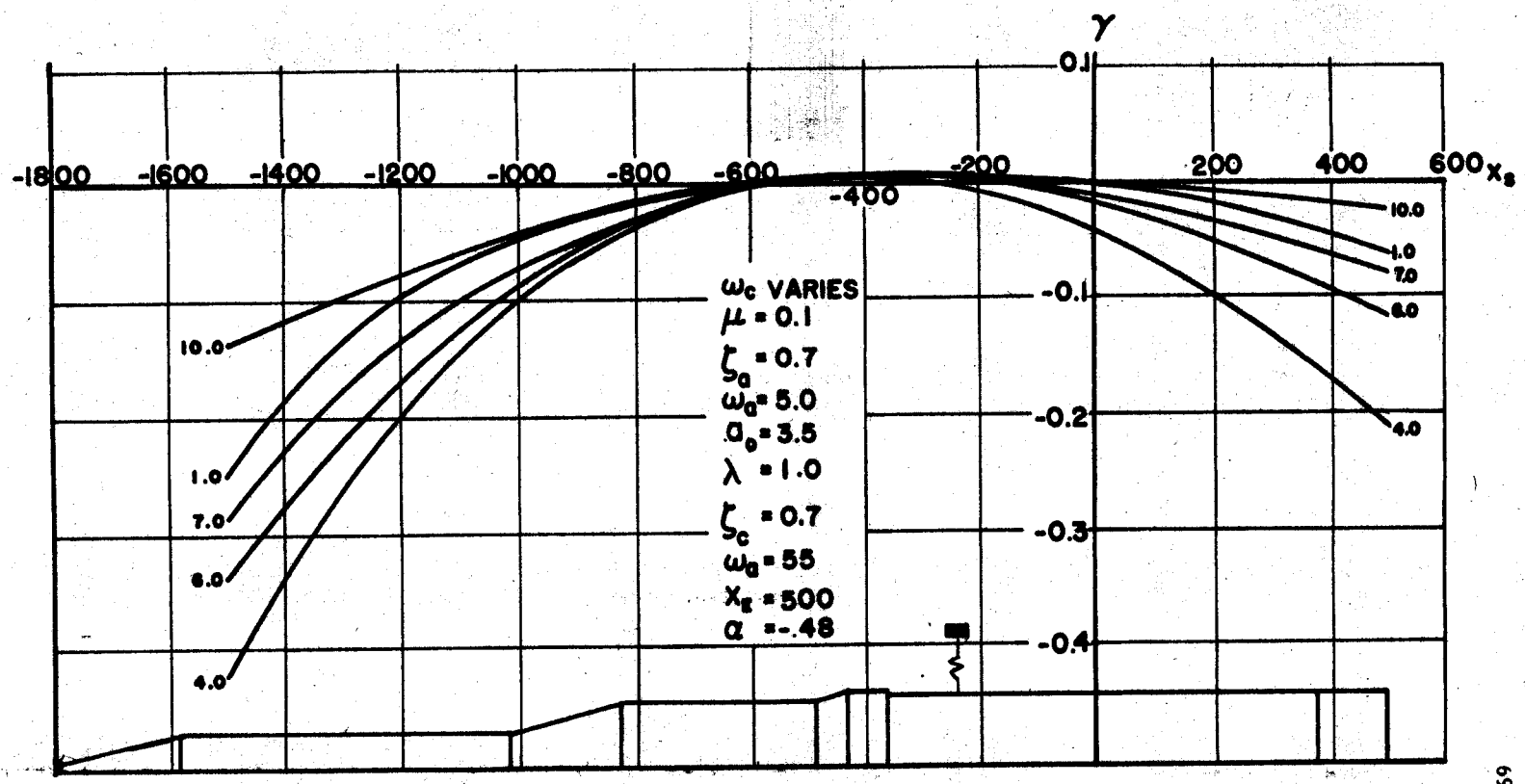

CASE D

STABILITY BOUNDARY FOR RIGID SPACECRAFT

WTIH REAL ACCELEROMETER CONTROL

FIG. 10e

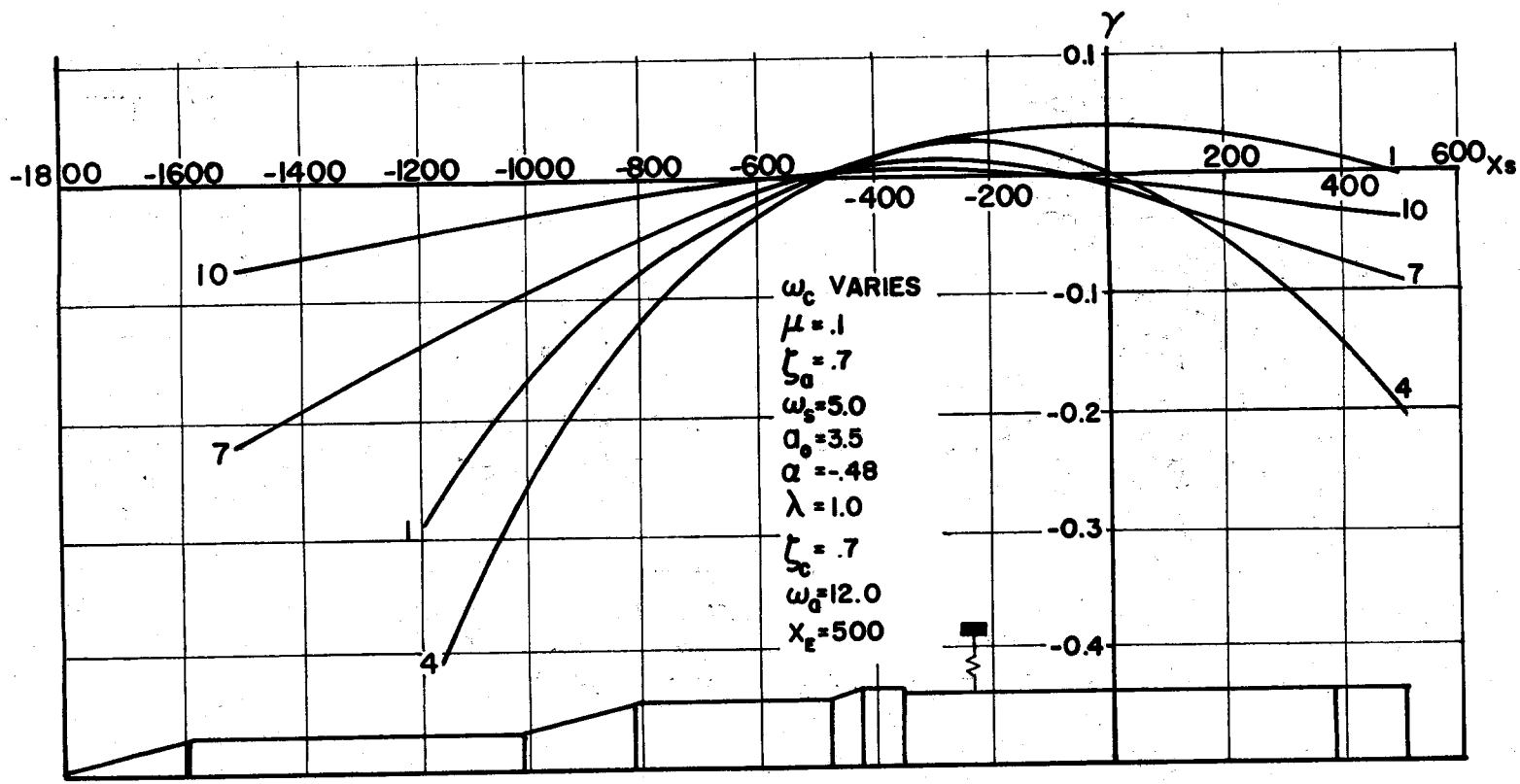

CASE D

STABILITY BOUNDARY FOR RIGID SPACECRAFT
WITH REAL ACCELEROMETER CONTROL

FIG. 10f

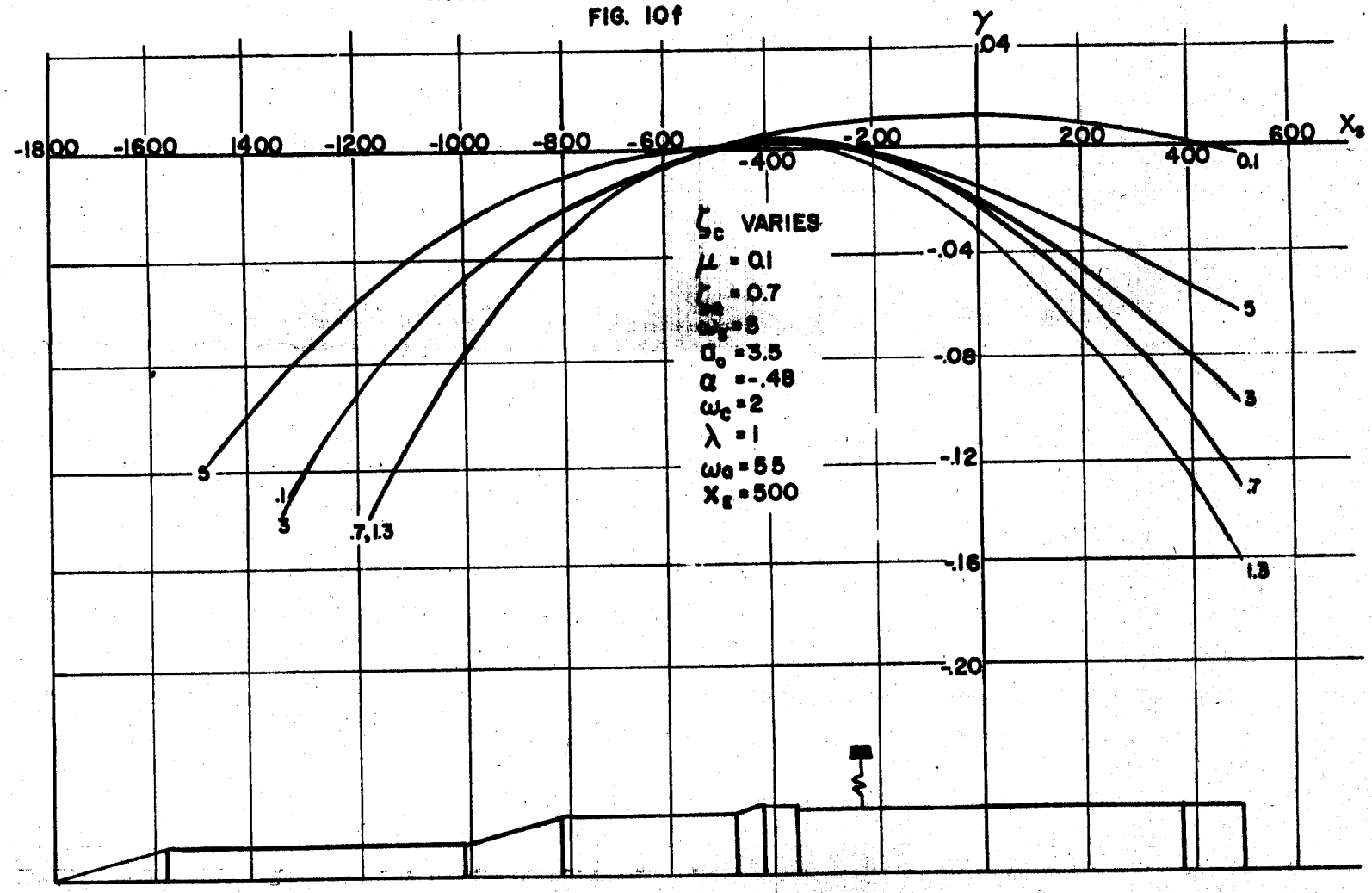

CASE D

STABILITY BOUNDARY FOR RIGID SPACECRAFT

WITH REAL ACCELEROMETER CONTROL

FIG. 10g

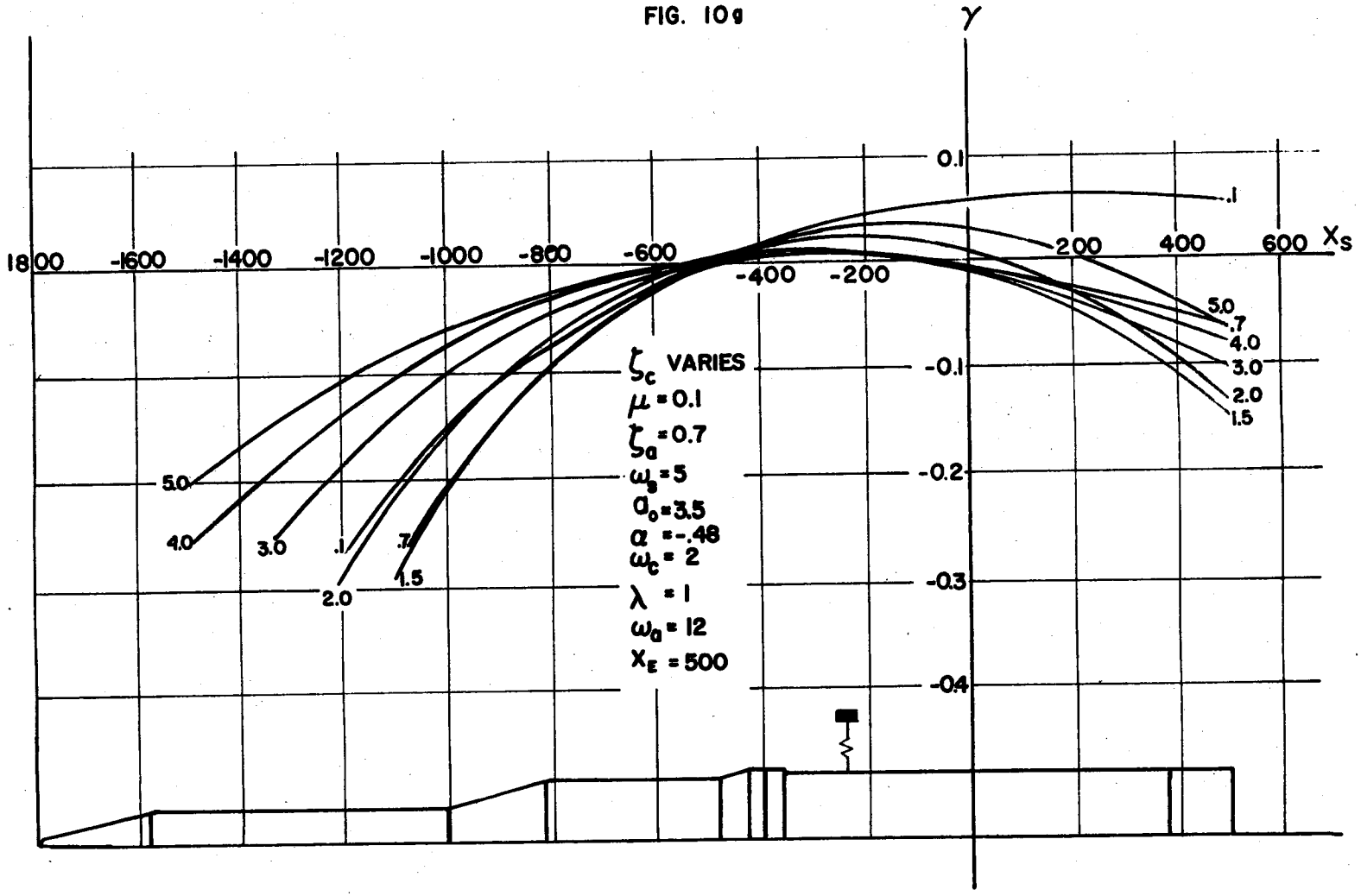

CASE D

STABILITY BOUNDARY FOR RIGID SPACECRAFT

WITH REAL ACCELEROMETR CONTROL

FIG. 10h

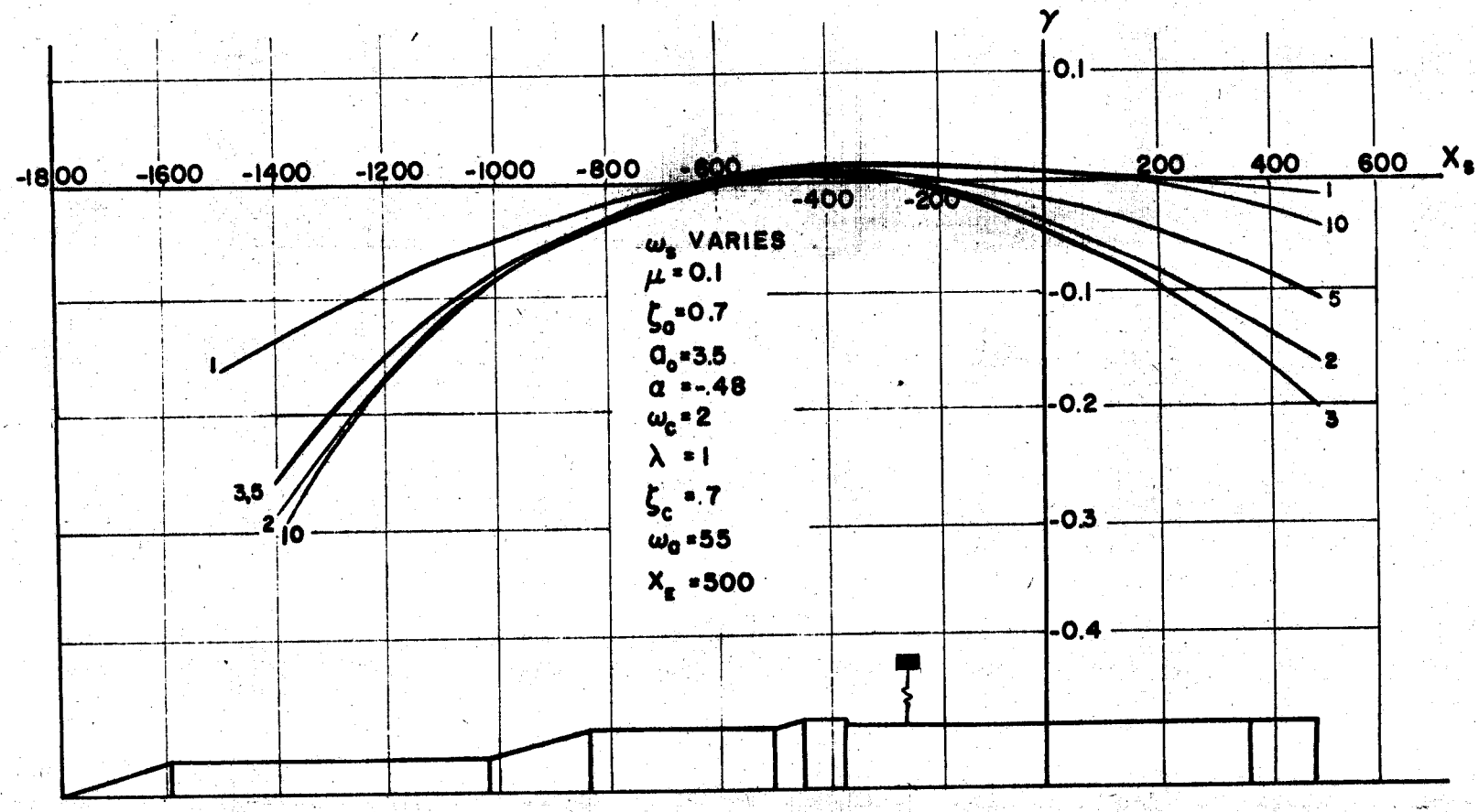

CASE D

STABILITY BOUNDARY FOR RIGID SPACECRAFT WITH REAL ACCELEROMETER CONTROL

FIG. 10i

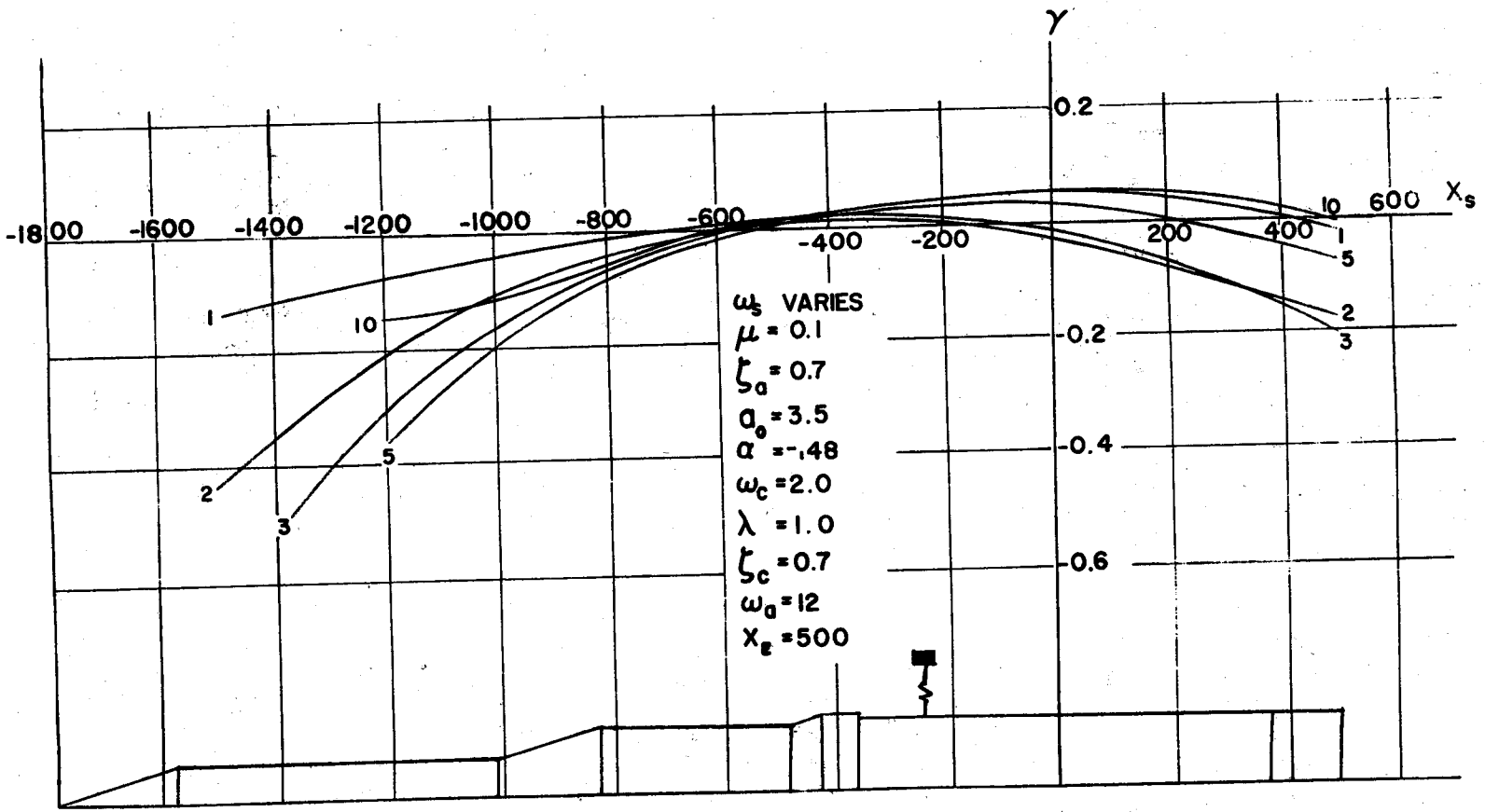

CASE D

STABILITY BOUNDARY FOR RIGID SPACECRAFT
WITH ACCELEROMETER CONTROL

FIG. 10j

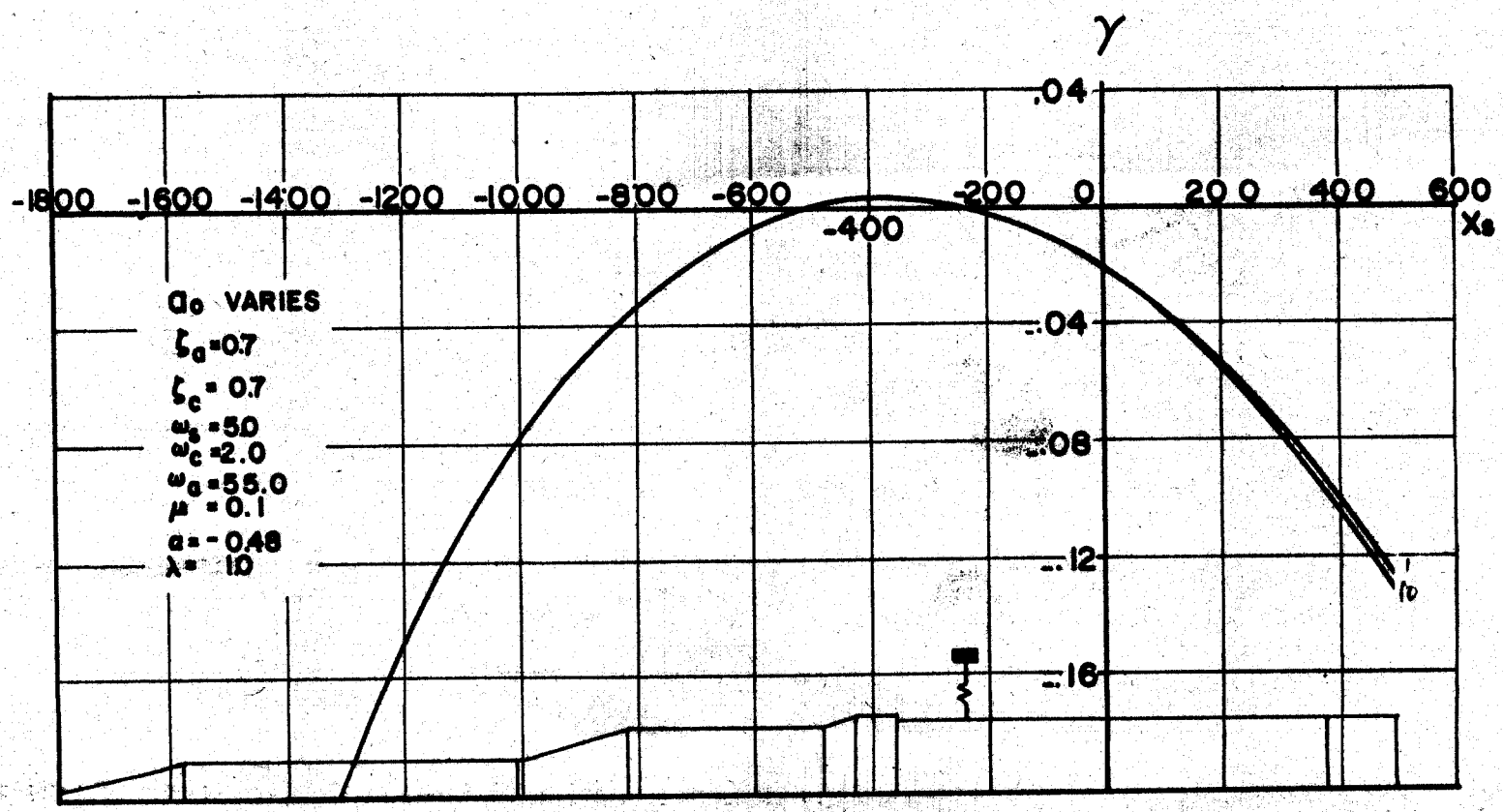

CASE D

STABILITY BOUNDARY FOR RIGID SPACECRAFT WITH REAL ACCELEROMETER CONTROL

FIG. 10k

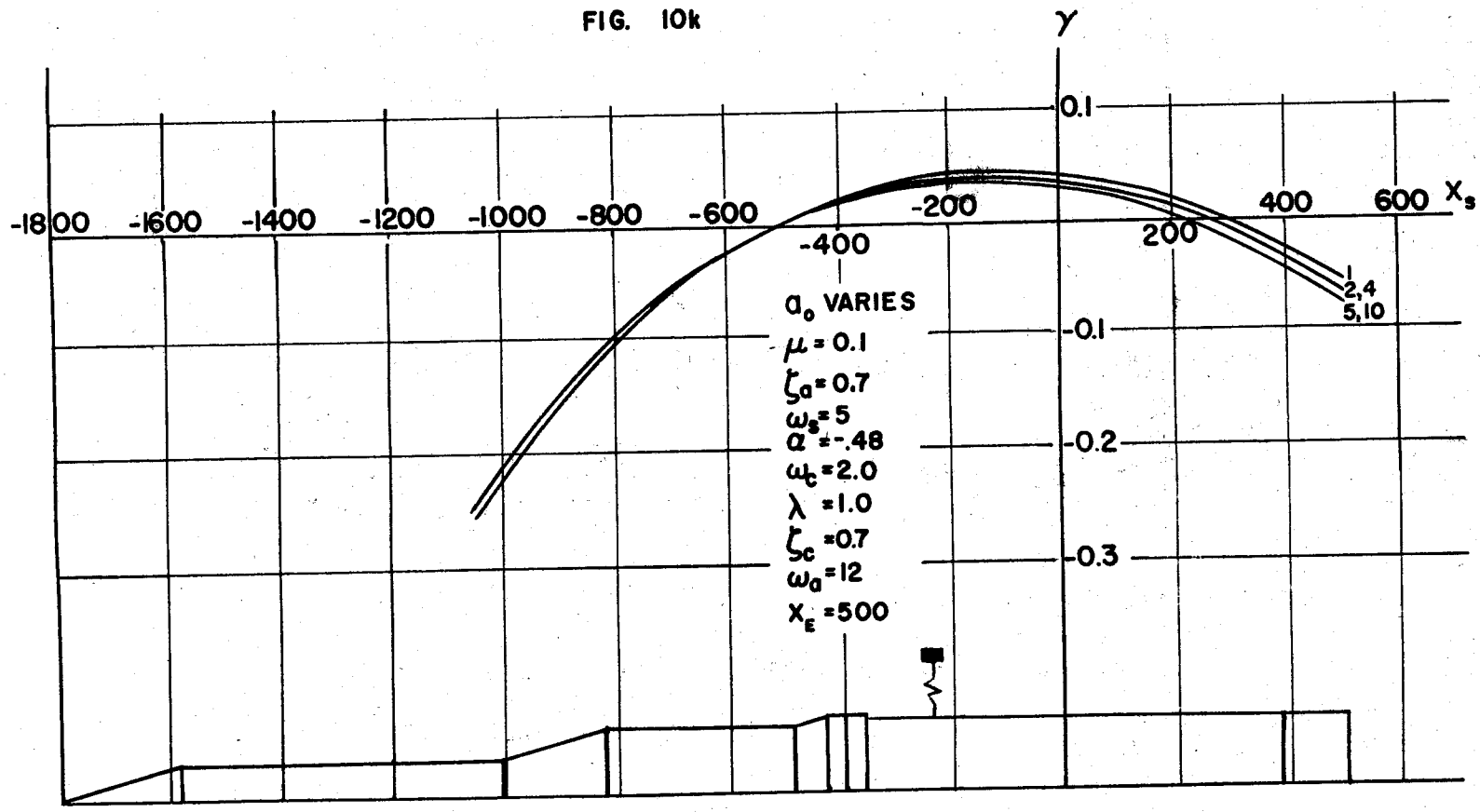

CASE D

STABILITY BOUNDARY FOR RIGID SPACECRAFT

WITH REAL ACCELEROMETER CONTROL

FIG. 10L

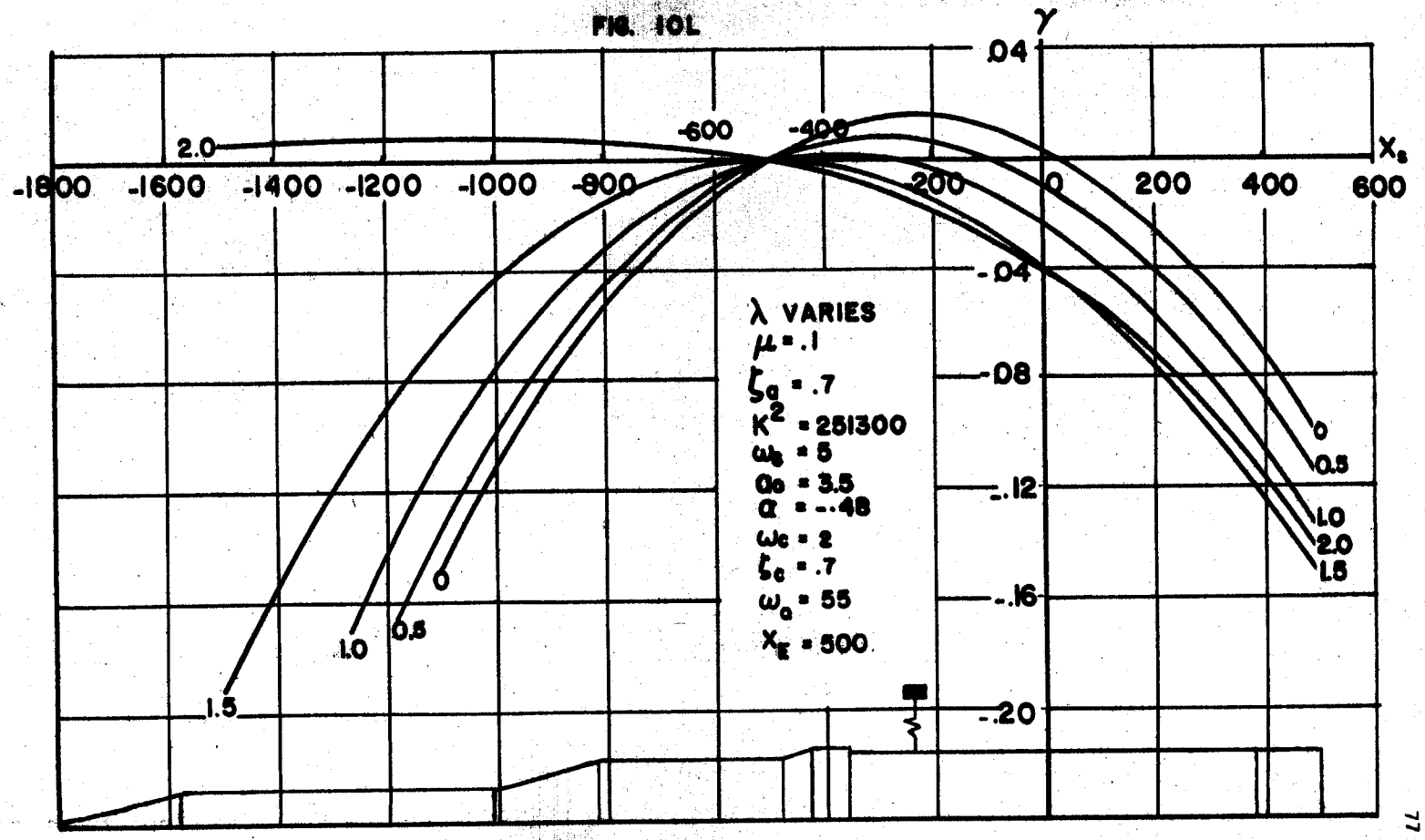

CASE D

STABILITY BOUNDARY FOR RIGID SPACECRAFT WITH REAL ACCELEROMETER CONTROL

FIG. 10m

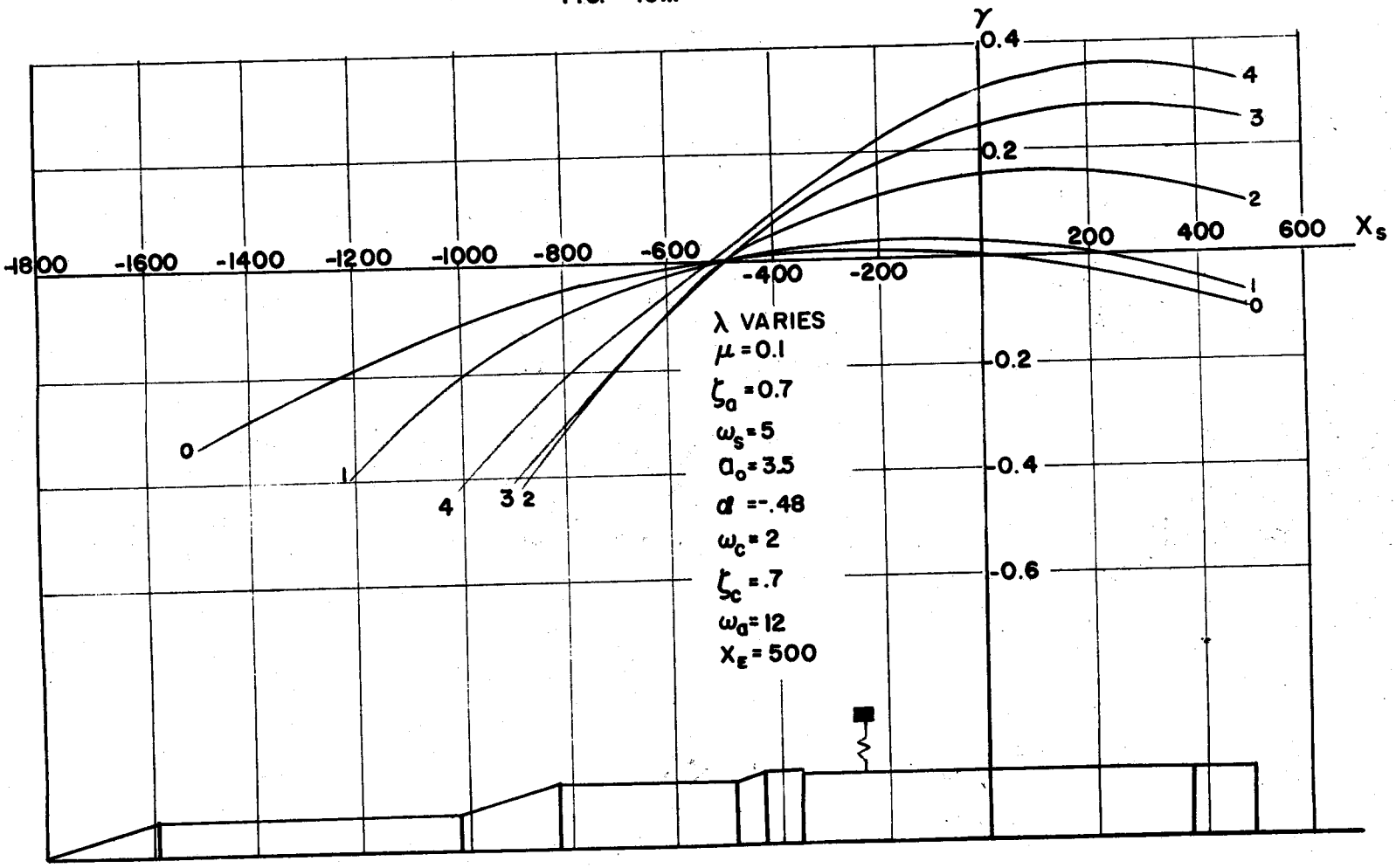

CASE D

STABILITY BOUNDARY FOR RIGID SPACECRAFT
WITH REAL ACCELEROMETER CONTROL

FIG. 10n

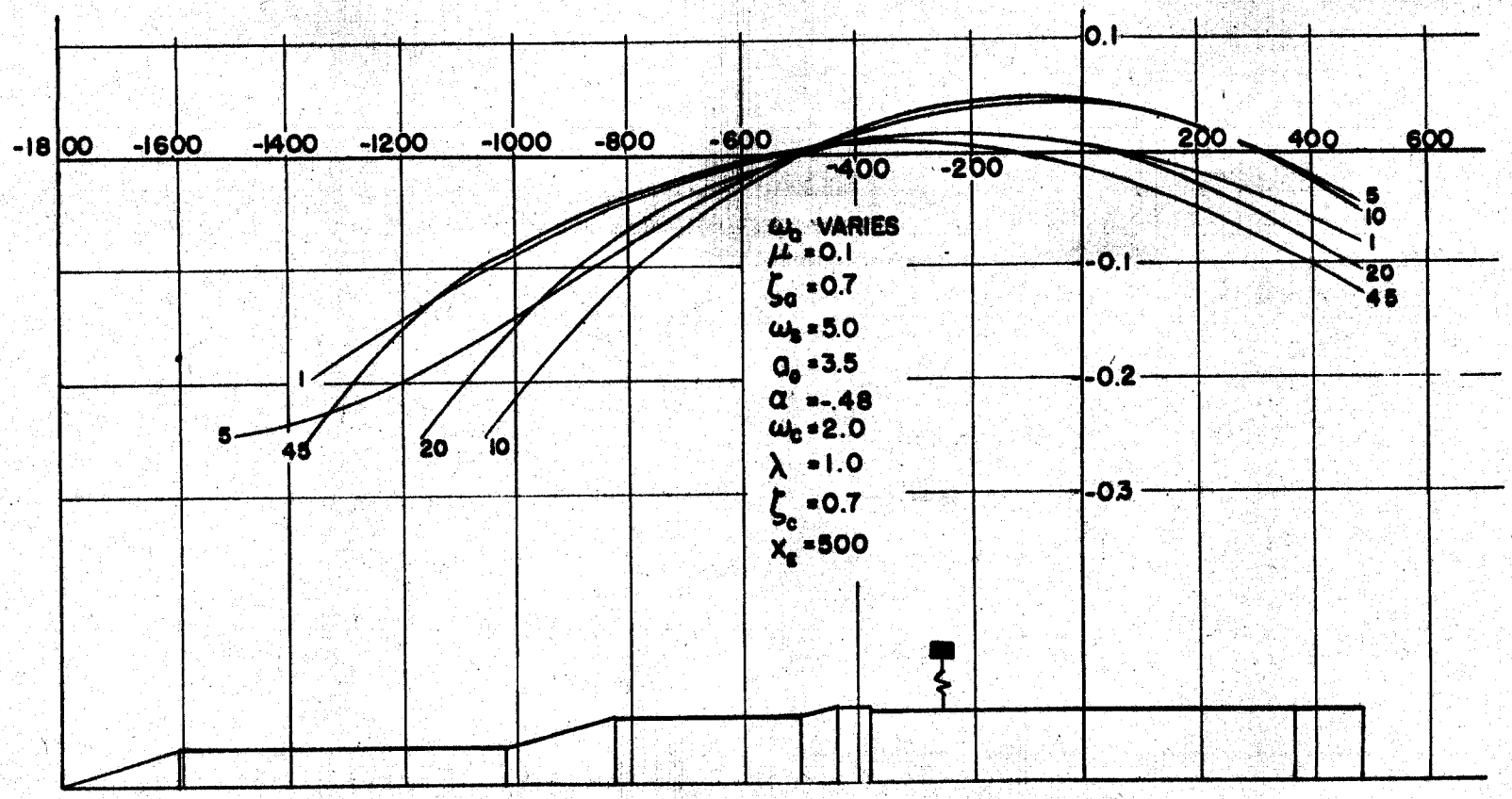

CASE D

STABILITY BOUNDARY FOR RIGID SPACECRAFT
WITH REAL ACCELEROMETER CONTROL

FIG. 10o

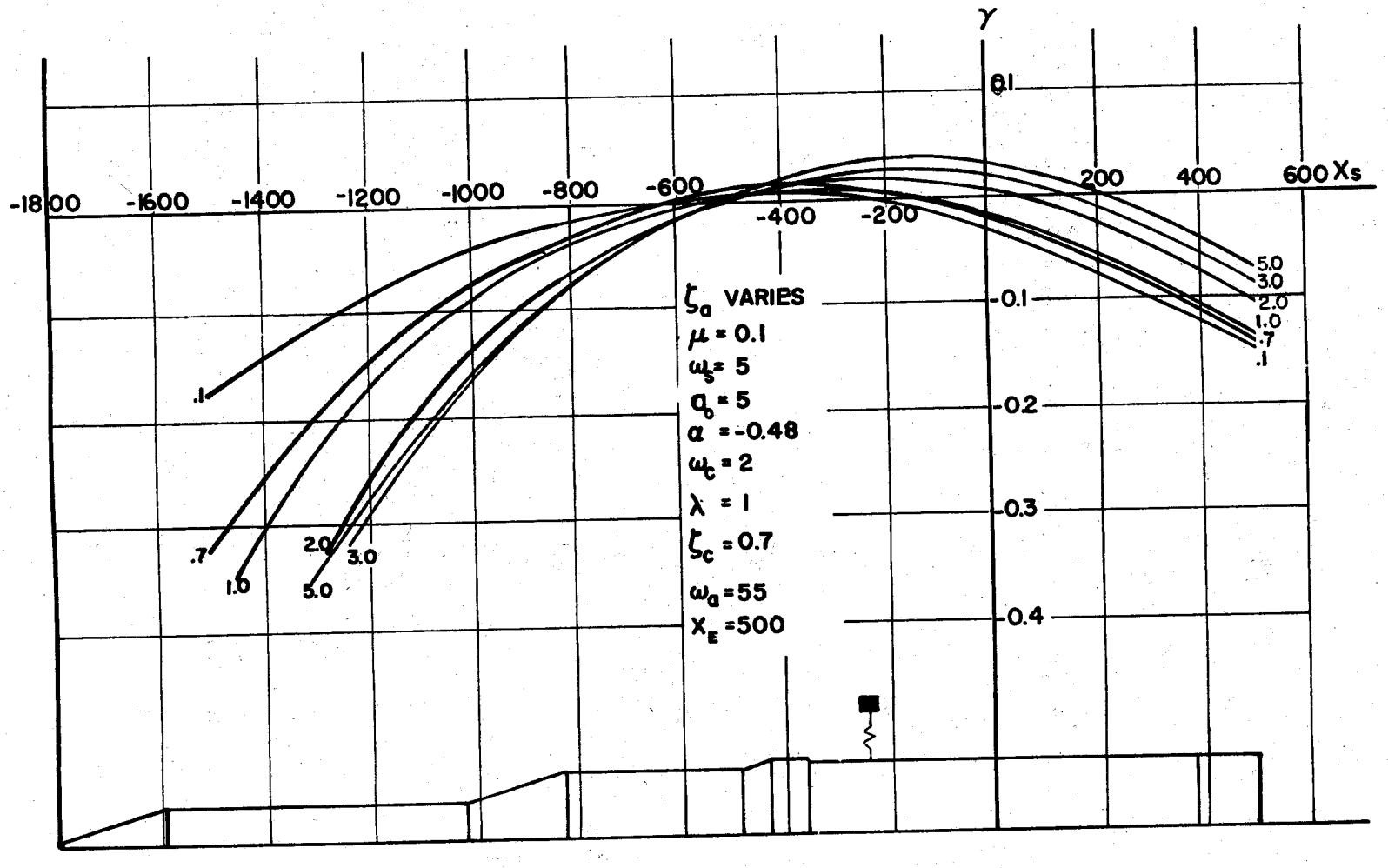

CASE D

STABILITY BOUNDARY FOR RIGID SPACECRAFT

WITH REAL ACCELEROMETER CONTROL

FIG. 10p

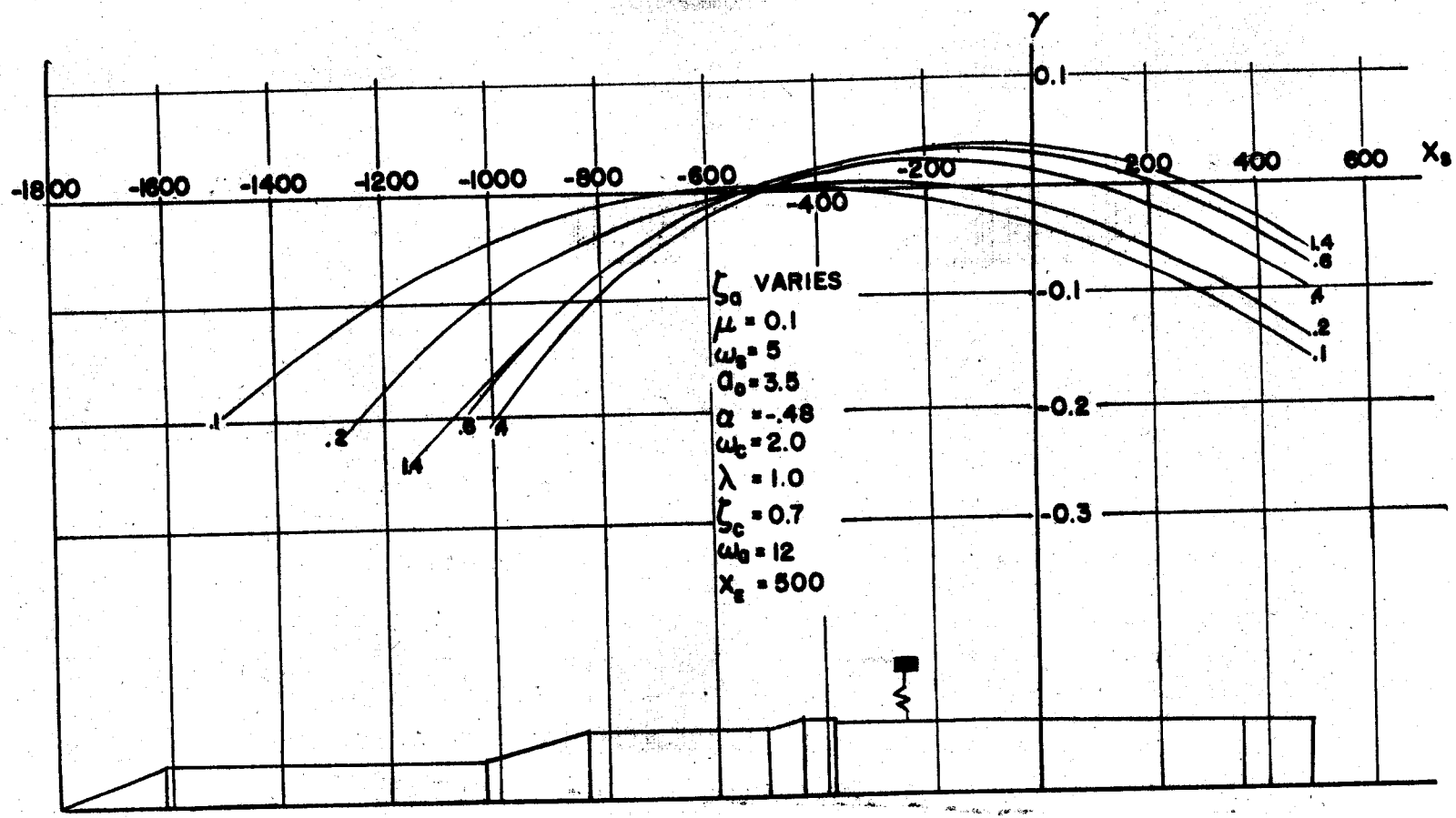

CASE D

STABILITY BOUNDARY FOR RIGID SPACECRAFT
WITH REAL ACCELEROMETER CONTROL

FIG. 10q

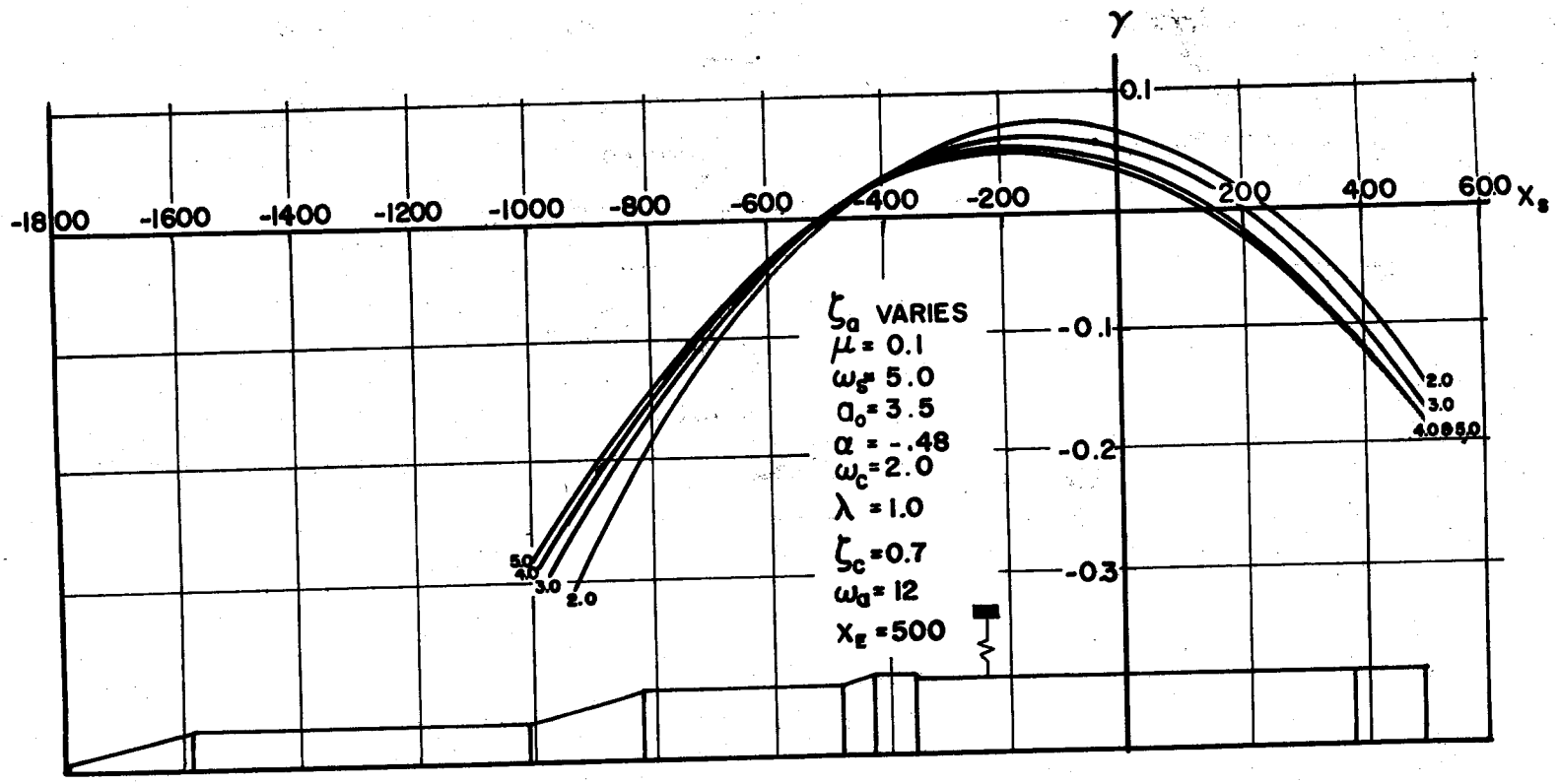

STABILITY BOUNDARY FOR RIGID SPACECRAFT
WITH REAL ACCELEROMETER CONTROL

CASE D

FIG. 10r

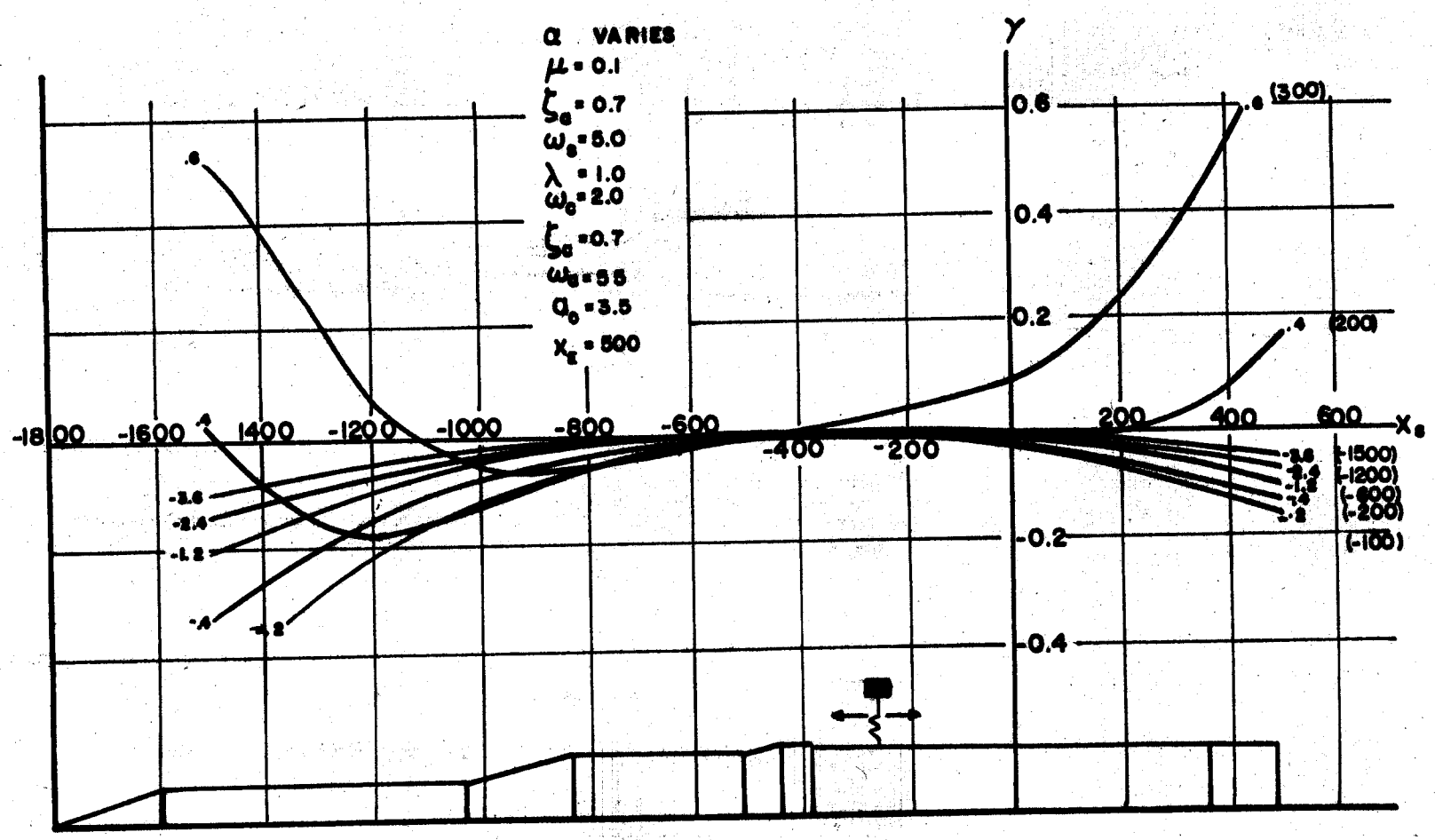

STABILITY BOUNDARY FOR RIGID SPACECRAFT
WITH REAL ACCELEROMETER CONTROL
CASE D

FIG. 10s

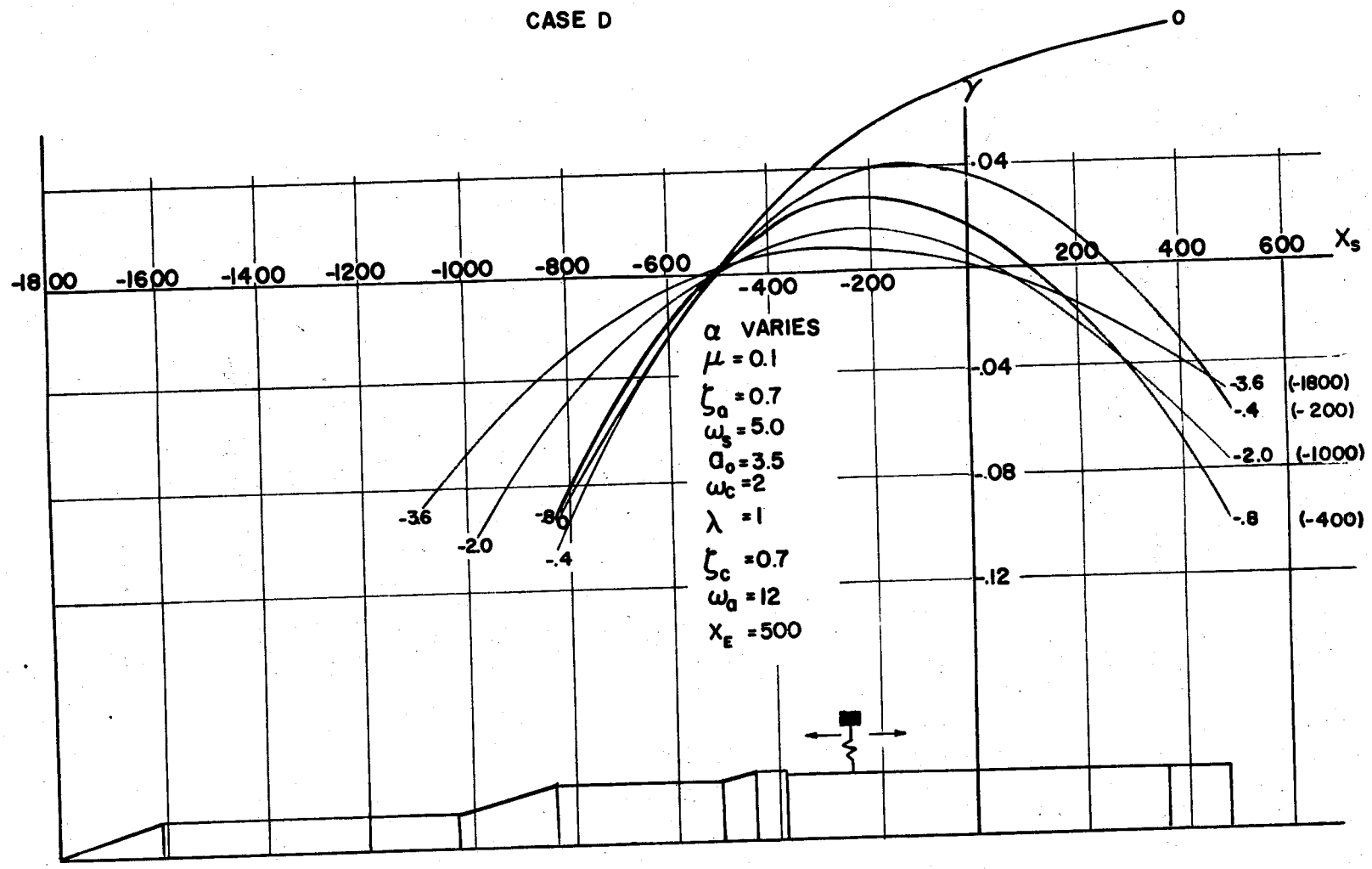

STABILITY BOUNDARY FOR RIGID SPACECRAFT

WITH REAL ACCELEROMETER CONTROL

CASE D

FIG. 10f

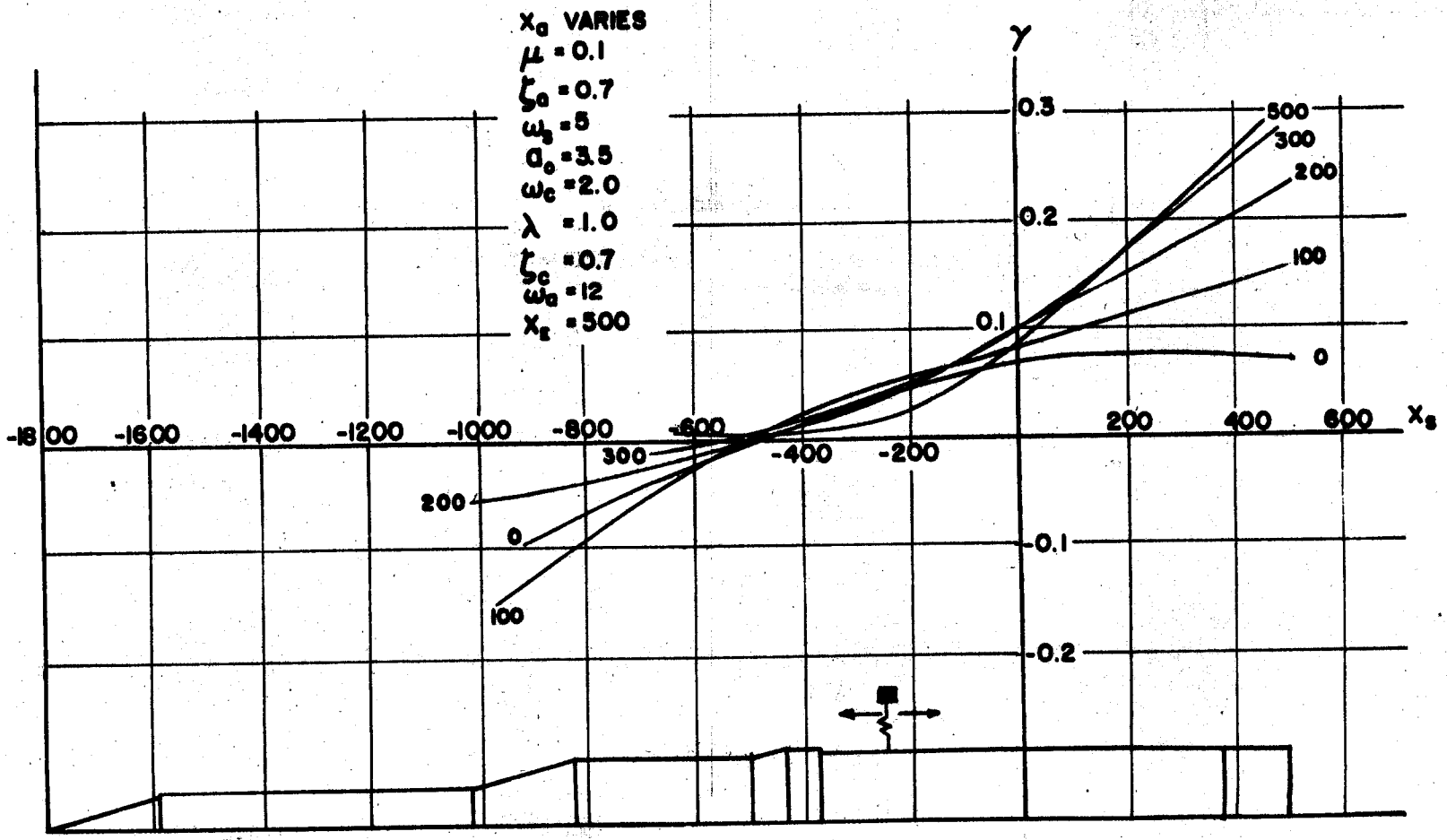

ORIGINATOR:

HELMUT F. BAUER
Chief, Flutter & Vibration Section

APPROVAL:

HELMUT J. HORN
Chief, Dynamics Analysis Branch

E. D. GEISSLER
Director, Aeroballistics Division

INTERNAL DISTRIBUTION:

Director, MSFC
Deputy Director, MSFC

Saturn Systems Office
Dr. O. H. Lange

Computation Division
Dr. Hoelzer
Dr. Fehlberg
Dr. Schulz-Arenstorff
Miss Morgan

Fabrication & Assembly Engr Div
Director
Mr. H. Wuenscher

Guidance and Control Division
Director
Mr. Hosenthien (3)
Mr. B. Moore
Mr. Digesu
Mr. Blandon

Launch Operations Directorate
Director
Dep Director
Dr. A. H. Knothe

Research Projects Division
Director
Mr. Miles
Mr. J. Dowdy

Test Division
Director
Dep Director
Mr. Kramer
Dr. Sieber
Mr. Haukohl
Mr. Schuler

Structures & Mechanics Division

Director	Mr. Hunt
Dep Director	Mr. Voss
Mr. Hellebrand	Mr. Bergeler
Mr. Kroll	Mr. Neighbors
Mr. Paul	Mr. Goerner
Mr. Palaoro	Mr. Engler
Mr. Heusinger	Mr. Thomae
Mr. Schulze	
Mr. M. Nein	

Aeroballistics Division
Director
Dep Director
Mr. Horn
Mr. Dahm
Mr. Reed
Dr. Speer
Mr. Rheinfurth (5)
Mr. Ryan (5)
Mr. Hart
Mr. Golmon
Mr. Stone
Mr. Baker
Mrs. Chandler
Mr. Larsen
Mr. Beard
Mr. Pack
Mr. Kiefling
Mr. Bauer (25)
Dr. Sperling
Mr. Hays
Mr. Franke
Mr. Asner
Mr. Wells

Publications Engr Section (1)

M-MS-IPL (8)

M-PAT

M-MS-H

EXTERNAL DISTRIBUTION:

Dynamic Loads Division
Langley Research Center, NASA
Langley Field, Virginia
Attn: Mr. E. Garrick
Mr. H. Runyan
Mr. Regier
Mr. Brooks

NASA - Ames
Moffett Field, California
Attn: Mr. Erickson (3)

JPL
4800 Oak Grove Drive
Pasadena, California
Attn: Mr. Alper (2)

NASA - Lewis
2100 Brookpark Road
Cleveland 35, Ohio
Attn: Mr. Sanders (2)

Boeing Aircraft
P. O. Box 3707
Seattle 24, Washington
Attn: Dr. Hua Lin
Mr. Hunter

Douglas Missile and Space Division
2000 Ocean Park Blvd.
Santa Monica, California
Attn: Mr. D. L. Pitman (3)
Mr. W. T. Hunter
Mr. D. W. Goldberg
Mr. W. S. Hayes
Mr. K. W. Kiser (3)
Mr. R. E. Holmen
Mr. W. Weymeyer

Space Technology Laboratory
P. O. Box 95001
Los Angeles 45, California
Attn: Dr. Robert M. Cooper
Library (2)

General Electric Company
3198 Chestnut Street
Philadelphia 4, Pennsylvania
Attn: Mr. H. Saunders